Mercury Cycling in the Marine Environment: Insights from Hg stable isotopes

by

Gretchen E. Gehrke

A dissertation submitted in partial fulfillment
of the requirements for the degree of
Doctor of Philosophy
(Geology)
in the University of Michigan
2011

Doctoral Committee:

Professor Joel D. Blum, Chair
Professor G. Allen Burton
Professor Gerald J. Keeler (Deceased)
Professor Robert M. Owen
Assistant Professor Niladri Basu

Acknowledgements

I would like to thank several people and organizations for making this dissertation research possible. First and foremost, I would like to thank my advisor, Joel Blum. His unwavering support of me as a scientist and as a person has allowed me the freedom and confidence to explore and grow. He has been my foundation. I would also like to thank my laboratory colleagues because the BEIGL group functions as a team. Their friendship has been vital, and their collaboration for methods development has been crucial for the work presented in this dissertation. To that end, I would like to thank Marcus Johnson especially. His indefatigable work ethic and commitment to quality data are the cornerstone of the Blum laboratory.

For intellectual support and inspiration, I would like to thank my committee and other members of the faculty, especially Phil Meyers. For financial support, I would like to thank the U.S. EPA for the STAR Fellowship that provided me three years of funding, and the Consortium for Ocean Leadership for the Schlanger Fellowship that provided me one year of funding. I would also like to thank the Geological Sciences Department for generously providing the First Year Fellowship funding. For emotional connection and the true essence of life, I'd like to thank my friends and family.

Table of Contents

List of Figures

List of Tables

Chapter 1

Introduction

Mercury (Hg) is a globally distributed trace metal with natural and anthropogenic sources to Earth's surface. In the surface environment, Hg actively cycles among atmospheric, terrestrial, and marine reservoirs. As Hg is mobilized, its atomic and molecular transformations can fractionate Hg stable isotopes, and the resultant isotope ratios can be used to distinguish different reservoirs of Hg and identify processes that have influenced Hg transport. This doctoral dissertation analyzes and assesses Hg concentrations and Hg stable isotopes to investigate the sources and geochemical cycling of Hg in the marine environment.

The second chapter of this dissertation, which was published in *Geochimica et Cosmochimica Acta* (Gehrke et al., 2009), investigates the influences of primary productivity and water column oxygen depletion on the cycling of natural marine Hg. Deep Sea sediments from the mid-Pleistocene (c.a. 955 ka) Mediterranean Sea before, during, and after a sapropel-forming climate excursion were analyzed for Hg, Ni, Cu, Zn, Mo, Ba, Re, U concentrations, and Hg stable isotopes. Sediment Hg concentrations have a depth-profile pattern of enrichment similar to Ni and Re, and increase by a factor of 6 from ~65 ng/g in background sediments to ~385 ng/g in sapropel sediments. However, the Hg isotopic compositions of background

sediments and sapropels are indistinguishable, with sapropel $\delta^{202}Hg$ = -0.91 ± 0.15‰ and $\Delta^{199}Hg$ = 0.11 ± 0.03‰. The consistency of Hg isotopic composition between background sediments and sapropels provides evidence that the source of Hg to Mediterranean Sea sediments was the same (i.e. seawater) throughout the sequence, and elevated Hg concentrations in sapropels were prompted by changes in the marine chemistry. Using sediment Hg accumulation rates and estimated seawater Hg fluxes, this chapter proposes that seawater Hg was nearly completely transferred to the seafloor during sapropel deposition and demonstrates that marine Hg cycling is largely controlled by dissolved (and particulate) organic matter.

The third chapter, which has been submitted to *Chemical Geology* (Gehrke et al., 2011b), seeks to determine whether Industrial Era changes in water column chemistry or changes in Hg emissions and discharge fluxes have altered the Hg composition of Baltic Sea sediments. Specifically, the study utilizes sediment Hg isotope compositions to discern whether the 3-fold surface sediment Hg enrichment is due to greater deposition of ambient marine Hg through eutrophication, or Hg enrichment due to additional anthropogenic Hg source contributions. Pre-Industrial sediments have $\delta^{202}Hg$ values of -1.04 ± 0.17‰, which is within error of mid-Pleistocene Mediterranean Sea sediments, and likely represents the Hg isotopic composition of natural marine Hg. Baltic Sea surface sediments have higher $\delta^{202}Hg$ values of -0.65±0.07‰, which likely reflect input of an additional Hg source with higher $\delta^{202}Hg$ values than marine Hg. A mixing curve between a marine Hg end-member source ($\delta^{202}Hg \approx$ -1.1‰), and an anthropogenic Hg end-member source ($\delta^{202}Hg \approx$ -0.5‰) describes the Baltic Sea sediment data well (r^2 = 0.62), and

suggests that surface sediments receive a significant contribution (up to 90%) of anthropogenic Hg. This chapter suggests that Hg enrichment in surface sediments is due to the combination of enhanced deposition and preservation due to eutrophication and additional anthropogenic input of Hg to the marine reservoir.

In San Francisco Bay, high Hg concentrations in modern sediments and fish have indicated substantial anthropogenic Hg input to the SF Bay surface environment. The fourth chapter of this dissertation, published in *Geochimica et Cosmochimica Acta* (Gehrke et al., 2011a), utilizes Hg isotope analyses to distinguish sources of Hg to tidal surface sediments in SF Bay. The Hg isotopic compositions of surface tidal sediments in twenty locations throughout SF Bay have a south-to-north spatial gradient, with δ^{202}Hg values ranging from -0.30‰ in the south to -0.99‰ in the northern Bay. This spatial gradient demonstrates two regional sources of Hg, rather than several localized sources, dominate Hg input to SF Bay sediments. Fluvial sediments downstream of historic Hg and placer Au mines have δ^{202}Hg values of ~ -0.3 and ~ -0.9‰, respectively, which suggests that historic Hg and Au mining continue to be the dominant contributors of Hg to SF Bay.

Using a similar study plan to that of Chapter 4, the fifth chapter of this dissertation, published in *Environmental Science & Technology* (Gehrke et al., 2011c), examines the primary sources of Hg to the aquatic food web in SF Bay. The δ^{202}Hg values of sentinel fish range from 0.60 to -0.25‰, with a distinct spatial gradient that resembles that of SF Bay sediments. Co-located fish and surface sediments (described in Chapter 4) have highly correlated δ^{202}Hg values ($r^2 = 0.83$), that are offset by ~0.7‰. This strongly suggests that surface sediments are the primary

source of Hg to the small fish food web in SF Bay, and the incorporation of that Hg into the food web is modified by photochemical and microbial Hg degradation.

Utilizing the knowledge about Hg isotope systematics garnered in Chapters 2-5, the sixth chapter in this dissertation explores the global Hg cycle under a significantly different climate regime, the Paleocene-Eocene Thermal Maximum (PETM). Deep sea marine sediments deposited ~15 kyr prior to the PETM have the lowest δ^{202}Hg values ever measured, δ^{202}Hg = -4.51‰. The sediment δ^{202}Hg values then rapidly increased over ~20 kyr to δ^{202}Hg values more typical of marine sediments, -1.1 to -0.3‰, and remained in that range for at least 80 kyr. This wide range and rapid excursion of δ^{202}Hg values indicates that there was a significant change in the Hg cycle through the PETM interval. In order to elucidate that change, analyses of early-and mid-Paleocene deep sea sediments are necessary, as well as Hg isotope analyses of continental shelf and terrestrial sediments of the Paleocene and Eocene epochs.

This dissertation utilizes Hg stable isotopes to examine the behavior of Hg in the marine environment, explore environmental controls on Hg cycling, and assess the effects of anthropogenic Hg inputs. The work described here has helped develop reliable measurement of Hg isotopes and pioneers the application of Hg isotope analyses to marine sediments.

References:

Gehrke, G. E., Blum, J. D., and Marvin-DiPasquale, M., 2011a. Sources of mercury to San Francisco Bay surface sediment as revealed by mercury stable isotopes. *Geochimica Et Cosmochimica Acta* **75**, 691-705.

Gehrke, G. E., Blum, J. D., and Meyers, P. A., 2009. The geochemical behavior and isotopic composition of Hg in a mid-Pleistocene western Mediterranean sapropel. *Geochimica Et Cosmochimica Acta* **73**, 1651-1665.

Gehrke, G. E., Blum, J. D., and Slomp, C. P., 2011b. Mercury Concentration and Isotopic Composition in Modern and Pre-Industrial Baltic Sea Sediments. *Chemical Geology* ***submitted***.

Gehrke, G. E., Blum, J. D., Slotton, D. G., and Greenfield, B. K., 2011c. Mercury Isotopes Link Mercury in San Francisco Bay Forage Fish to Surface Sediments. *Environmental Science & Technology* **45**, 1264-1270.

Chapter 2

The geochemical behavior and isotopic composition of Hg in a mid-Pleistocene Western Mediterranean sapropel

Authors: Gretchen E. Gehrke, Joel D. Blum, Philip A. Meyers

Citation: Gehrke, G.E., Blum, J.D., Meyers, P.A., 2009. The geochemical behavior and isotopic composition of Hg in a mid-Pleistocene western Mediterranean sapropel. *Geochimica Et Cosmochimica Acta* **73**, 1651-1665.

Abstract

The concentrations of mercury (Hg) and other trace metals (Ni, Cu, Zn, Mo, Ba, Re, U) and the Hg isotopic composition were examined across a dramatic redox and productivity transition in a mid-Pleistocene Mediterranean Sea sapropel sequence. Characteristic trace metal enrichment in organic-rich layers was observed, with organic-rich sapropel layers ranging in Hg concentration from 314 to 488 ng/g (avg = 385), with an average enrichment in Hg by a factor of 5.9 compared to organic-poor background sediments, which range from 39 to 94 ng/g Hg (avg = 66). Comparison of seawater concentrations and sapropel accumulations of trace metals suggests that organic matter quantitatively delivers Hg to the seafloor. Near complete scavenging of Hg from the water column renders the sapropel Hg isotopic

composition representative of mid-Pleistocene Mediterranean seawater. Sapropels have an average δ^{202}Hg value of -0.91 ± 0.15‰ (n = 5, 1 SD) and Δ^{199}Hg value of 0.11 ± 0.03‰ (n = 5, 1 SD). Background sediments have an average δ^{202}Hg of -0.76 ± 0.16‰ (n = 5, 1 SD) and Δ^{199}Hg of 0.05 ± 0.01‰ (n = 5, 1 SD), which is indistinguishable from the sapropel values. We suggest that the sapropel isotopic composition is most representative of the mid-Pleistocene Tyrrhenian Sea.

1. Introduction

Mercury (Hg) is a globally distributed trace metal, the mobility and bioavailability of which are highly dependent upon its redox state and speciation. Hg has two common oxidation states, Hg(0) and Hg(II), with distinctly different physiochemical properties. Hg(0) exists primarily as a gaseous species and readily evades from aqueous media, whereas Hg(II) exists as highly particle-reactive gaseous, aqueous, and solid species. Dissolved Hg(II) has especially strong affinities for sulfides (e.g. Dyrssen and Wedborg, 1991) and organic matter (e.g. Benoit et al., 2001; Haitzer et al., 2002). The extreme toxicity of Hg warrants thorough investigation into its biogeochemical transformations, especially in the marine environment where it biomagnifies in food webs. The global ocean is the largest reservoir of Hg in the actively cycling environment, and marine organisms present the primary source of human exposure to toxic Hg species. It is, therefore, important to better understand the effects of primary productivity and water column redox conditions on marine Hg behavior.

Significant variations in seawater chemistry have occurred in the Mediterranean Sea since the Pliocene (e.g. Calvert and Pederson, 1993), making it an ideal location to study the behavior of natural Hg under differing marine conditions. The Mediterranean Sea is a semi-restricted basin, sufficiently isolated that it experiences dramatic changes in productivity and water column redox conditions in response to small climatic variations. Marine sediment sequences in the Mediterranean reflect the wide range of redox conditions under which they were deposited. Mediterranean sediments are generally characterized by organic-poor (<0.3% total organic carbon (TOC)), carbonate-rich marls (Calvert et al., 1992), representative of oxic, oligotrophic conditions. However, these typical organic-poor background sediments are interspersed with discrete dark-colored sapropel layers (> 1 cm thick) containing at least 2% (Kidd et al., 1978) and up to 30% TOC (Bouloubassi et al., 1999). These sapropel sediments are formed under oxygen-limited water column conditions due to climate-driven amplified rates of surface primary productivity and resulting water column oxygen consumption (e.g. Rohling and Bryden, 1994; Meyers and Bernasconi, 2005; Brumsack, 2006). Transitions between sapropels and background sediments are rapid, with TOC dropping from >4% to ~0.2% within hundreds of years (e.g. Meyers and Bernasconi, 2005), indicating a sensitive water column response to climate variations. Rapid transitions that capture both end-members of extreme marine conditions (i.e. sapropel and non-sapropel forming conditions) present an opportunity to study biogeochemical responses to varied redox and productivity conditions at a single location.

Trace metals often accumulate in marine sediments deposited under reducing conditions, and sapropels are characteristically enriched in them (e.g. Warning and Brumsack, 2000; Rinna et al., 2002; Arnaboldi and Meyers, 2006). Trace metals are routinely characterized by their sensitivity to biogeochemical conditions that promote their accumulation in sediments; two general categories are redox-sensitive metals and productivity-sensitive metals. Redox-sensitive trace metals, including Mo, Re, and U, generally behave conservatively in seawater and precipitate or are scavenged under strongly reducing conditions (e.g. Tribovillard et al., 2006). Oxidized Mo, Re, and U species diffuse from overlying seawater into pore waters and precipitate or adsorb onto mineral surfaces below the sediment-water interface under sufficiently reducing conditions (Crusius et al, 1996; Böning et al., 2004; McManus et al., 2005). Additionally, suboxic conditions can promote accumulation of Mo and U associated with organic and particulate matter (e.g. Zheng et al., 2002; McManus et al., 2005). Productivity-sensitive trace metals such as Ni, Cu, and Zn, are incorporated into organic matter via planktonic uptake or sequestration by humic and fulvic acids, and are exported to underlying waters in association with this organic matter (e.g. Whitfield, 2001; Böning et al., 2004). Delivery of the productivity-sensitive metals Ni, Cu, and Zn to marine sediments requires the conservation of their carrier organic matter through the water column. Ba also is a productivity-sensitive trace metal and has been employed as a qualitative indicator of export productivity (Dymond et al., 1992). Delivery of Ba to sediments is a function of decaying organic matter and suspended silica, the formation of microcrystalline barite, and delivery of barite to depth (Bishop, 1988).

Ba accumulation in sediments can depend on delivery of biological barite, barite precipitation from free Ba and SO_4^{2-}, and Ba mobilization during sulfate reduction (e.g. Torres et al., 1996). Trace metals are often subject to multiple deposition and fixation processes. As stated above, dissolved Mo and U species directly respond to bottom water chemistry, but Mo and U can also be delivered to depth in association with organic matter. Preservation of senescing organic matter can promote elevated sediment concentrations of Mo and U (e.g. Zheng et al., 2002; McManus et al., 2005). Sediment accumulation of Ni, Cu, and Zn is sensitive to both surface water productivity and prevailing bottom water redox conditions. Ni, Cu, and Zn are associated with organic matter in the water column and also respond to the availability of free sulfides, which can fix them in sediments (e.g. Jacobs et al., 1985; Calvert and Pederson, 1993).

Mercury is a redox and productivity sensitive trace metal that has been studied very little in marine sediments compared to the other metals mentioned above. This study seeks to place the marine geochemical behavior of Hg within the context of these other metals. We aim to identify viable mechanisms of natural Hg accumulation in sediments by investigating Hg (and other trace metal) concentrations in sapropels and background sediments that preserve a pre-anthropogenic record of Hg behavior with changing redox and productivity. We analyzed a section of Core 974C-6H from the Tyrrhenian Basin (TB) containing an interrupted sapropel deposited around insolation cycle 90 (i90) *circa* 955 ka (Lourens et al., 1992), which will be referred to as the i90 TB sapropel. We refer to sediments deposited before the initial sapropel layer as background sediments and

the sediments deposited between the i90 TB sapropel layers as interruption sediments. Meyers and Bernasconi (2005) characterized the C and N concentrations and isotopic composition of this sapropel layer. We analyzed sediment concentrations of Hg, a suite of other trace metals (Ni, Cu, Zn, Mo, Ba, Re and U), and major elements (Mg, Al, Si, K, Ti, Mn, and Fe).

This study also reports the Hg isotopic composition of these sapropel and background sediments. Hg has seven naturally occurring stable isotopes, ranging from 196 to 204 amu. Fractionation of the stable isotopes of Hg has been demonstrated for geological (Smith et al., 2005), biological (Kritee et al., 2007), and photochemical (Bergquist and Blum, 2007) processes. Quantitative sequestration of Hg by organic matter during periods of high productivity (e.g. Han et al., 2006) suggests that sapropels may record the ambient seawater Hg isotope composition. We analyzed the i90 TB sapropel Hg isotopic composition and provide the first report of a marine Hg isotopic composition.

2. Methods and Materials

2.1 Sampling

A site description and sampling protocol employed in collection of the samples studied here are provided in Meyers and Bernasconi (2005). Briefly, core samples were obtained from Ocean Drilling Program (ODP) Hole 974C in the Tyrrhenian Basin (40º21' N, 12º09' E) (Figure 2.1) during ODP Leg 161 in 1995 (Comas et al., 1996). Aliquots of a 3-m sediment sequence were freeze-dried and homogenized with an agate mortar and pestle. A sub-set of samples were selected

for Hg and trace metal analysis that consisted of an interrupted sapropel (see Meyers and Bernasconi, 2005) deposited during insolation cycle 90 (ca 955 ka), background sediments deposited prior to the i90 sapropel and sediments deposited during the interruption of sapropel i90 TB.

2.2 Trace metal concentration analysis

Sediment samples and standard reference materials weighing ~100 mg were digested using a MARS 5.0 microwave digestion apparatus in 250 ml Teflon vessels with 1 ml hydrochloric acid (Fisher, Trace Metal Grade), 3 ml nitric acid (Fisher, Trace Metal Grade) and 6 ml of 18 MΩ deionized water. Samples and standards were digested at 1200 watts for 40 minutes, reaching 4.1 MPa for the final 15 minutes. This digestion is referred to as an "aqua regia digest." Organic matter, sulfides, and mafic silicate minerals were fully digested, but some quartz, feldspar and clay minerals remained as an insoluble residue. Residues of a subset of samples and standards that had undergone the aqua regia digests were further digested following a modification of the digestion procedure detailed by Stancin et al. (2006). Briefly, dried sample and standard residues were completely digested in 0.5 ml nitric acid (Fisher, Trace Metal Grade) and 4.5 ml hydrofluoric acid (Fisher, Optima) for 48 hrs at 120°C, followed by 0.5 ml perchloric acid (Fisher, Optima) at 160°C for 8 hours, and 3 ml hydrochloric acid (Fisher, Trace Metal Grade) at 100°C for 8 hours. Solutions produced by this digestion method are referred to as "hydrofluoric-perchloric digests." Dried hydrofluoric-perchloric digests were re-dissolved in 3 ml 3N nitric acid (Fisher, Optima) for ICP-MS analysis.

Trace metal concentrations of aqua regia and hydrofluoric-perchloric digest solutions were determined by magnetic sector inductively coupled plasma mass spectrometry (ICP-MS) using a Finnigan Element 2 after 1:100 dilution in 18 MΩ deionized water. Concentrations of Ni, Cu, Zn, Mo, Ba, Re and U were determined using four to five point calibration curves of High-Purity single element Certified Reference Material (CRM) standards. Replicate analyses yielded an analytical uncertainty of ± 4% (1 SD) for each element, except for U which was ± 5% (1 SD). The recovery of each trace metal from the aqua regia digest and the hydrofluoric-perchloric digest of the subset of samples are presented in Table 2.1a.

The labile fraction of each metal was recovered from the aqua regia digests of each sample and the insoluble fraction of metals was recovered from the hydrofluoric-perchloric digestion of aqua regia insoluble residues. Total metal contents were calculated from the sum of the two sequential digestions. Analyses of total digests of NIST Estuarine Sediment 1646a and USGS Marine Mud Mag-1, presented in Table 1b, agreed with certified and recommended (but uncertified) values to within ±15%, with the exception of Zn in NIST 1646a, which differed by 21%. Analyses of Mo differed by as much as 46% from uncertified, suggested values. The aqua regia digest recovered greater than 90% of the total Ni, Cu, Zn, and Mo for each sample and from 54 to 92% of Ba, Re, and U (Table 2.1a). Near total recovery of Ni, Cu, Zn, and Mo indicates that organic matter and sulfides were fully digested in aqua regia at high temperature and pressure. Reactive Re and U are likely present in marine sediments as sulfides or carbonates (e.g. Tribovillard, 2006), and are also recovered in the aqua regia digest. Reactive Ba is likely present

as barite, which may not have been completely digested. Non-biogenic Ba and the Re and U that were not recovered in the aqua regia digest are likely associated with the detrital fraction and are present in minerals that are inclusions in silicate minerals and rock fragments that were not digested in aqua regia.

Mercury concentrations of sample digests were determined by Au-trap atomic absorption spectroscopy (AAS) with a Nippon Instruments MA 2000. Five ml solutions were acidified with 250 µl 50% H_2SO_4, reduced with 250 µL of 20% $SnCl_2$, and purged onto a gold trap. Reagent preparation followed EPA Method 1631 E (2002). Hg was desorbed from the Au-trap at 650 ºC and concentrations were determined by comparing sample absorbance to a five-point calibration curve with $r^2 = 0.9997$. Analyses of a reference solution (NIST 3133) were performed for every two samples. Replicate analyses of samples and NIST 3133 yielded an analytical uncertainty of ± 3% (1 SD). Replicate analyses of the aqua regia digest of quality control standards (IRMM BCR062) agreed with reference Hg concentrations within 4%, indicating quantitative Hg recovery.

2.3 Major element concentration analysis

Samples and reference standards (USGS Sco-1, USGS MAG-1) weighing ~50 mg were mixed with ~1 g of a $Li_2B_4O_7$-$LiBO_2$-LiBr flux and heated to 900 ºC for 10 minutes in Pt crucibles using a Claisse M4 fluxer. Molten flux-sample mixtures were added to 50 g of 5% (wt/wt) nitric acid (Fisher, Trace Metal Grade) and fully digested. Samples were then diluted 1:5 in 2% (wt/wt) nitric acid (Fisher, Trace Metal Grade). Concentrations of Mg, Al, Si, K, Ti, Mn, and Fe were analyzed on a

Perkin Elmer Optima 3300 DV Inductively Coupled Plasma Optical Emission Spectrometer (ICP-OES) using an eight-point calibration curve. The following High-Purity CRM standards were used for quality control: River Sediment B, Soil A, SM2251-002, and VHG Labs CRM SM90C-100 Comprehensive Mix B. Analyses of reference standards verified complete digestion and replicate analyses yielded an analytical uncertainty of ± 4% (1 SD).

2.4 Mercury isotope analysis

Mercury isotopic analyses were carried out using methods described previously (Lauretta et al., 2001; Smith et al., 2005; Kritee et al., 2007; Blum and Bergquist; 2007; Bergquist and Blum, 2007). Briefly, homogenized samples were combusted in a two-stage furnace at 1000 ºC to separate Hg from the sediment matrix for isotopic analysis. Mercury was volatilized as Hg(0), transported in a stream of air or Ar, and then trapped as Hg(II) by bubbling through an oxidizing 1% $KMnO_4$ solution. Procedural blanks and sample recoveries were determined for each sample and standard. Following combustion, Hg isotopic compositions were determined using a Nu Instruments multi-collector inductively coupled plasma mass spectrometer (MC-ICP-MS). Before analysis $KMnO_4$ was reduced with NH_2OH and solutions were diluted to ~10 ng/g Hg. Using continuous-flow analyses Hg(II) was reduced by $SnCl_2$ and Hg(0) was separated from the solution matrix using a frosted-tip gas-liquid separator and introduced to the MC-ICP-MS. Instrumental mass-bias was corrected using an internal thallium (Tl) spike (NIST 997) introduced as an aerosol to the gas flow, as well as by sample-standard bracketing using a NIST

3133 solution matched in concentration and matrix to each sample. On-peak zero corrections were applied to all masses. Mass dependent Hg isotope compositions are reported in delta notation as δ^{202}Hg in permil (‰), referenced to NIST 3133 (Blum and Bergquist, 2007). δ^{202}Hg values are calculated as:

$$\delta^{202}Hg = 1000*\{[(^{202}Hg/^{198}Hg)_{sample}]/[(^{202}Hg/^{198}Hg)_{3133}]-1\}.$$

Mass independent Hg isotope fractionation is reported as Δ^{199}Hg and Δ^{201}Hg in permil (‰) referenced to NIST 3133 (Blum and Bergquist, 2007). Δ^{199}Hg and Δ^{201}Hg and are calculated as:

$$\Delta^{199}Hg = \delta^{199}Hg_{measured} - (\delta^{202}Hg_{measured}*0.252)$$

$$\Delta^{201}Hg = \delta^{201}Hg_{measured} - (\delta^{202}Hg_{measured}*0.752)$$

Typical internal precision of at least ±0.03‰ (2SE) was achieved on a daily basis for all isotope ratios. The average isotopic composition and external reproducibility of our laboratory standard (elemental Hg from Almadèn, Spain) was –0.54 ± 0.08‰ (*n* = 25, 2SD) for δ^{202}Hg, -0.04 ± 0.04‰ (*n* = 25, 2SD) for Δ^{201}Hg, and –0.01 ± 0.05‰ (*n* = 22, 2SD) for Δ^{199}Hg (Blum and Bergquist, 2007).

3. Results

3.1 Recovery of trace metal digestions

The labile fraction of each metal was recovered from the aqua regia digests of the samples. Data on trace metal recovery is presented in Tables 2.1a and 2.1b and discussed in Section 2.2. Organic matter, sulfides, and carbonates were fully digested in aqua regia at high temperature and pressure. The metals that were not recovered in the aqua regia digest are likely associated with the detrital fraction of

the sediments. This manuscript focuses on water column and sediment biogeochemical influences on trace metal accumulation in sediments rather than clastic detrital trace metals. Therefore, we suggest that the most relevant trace metal and Hg concentrations to this study are those recovered from the aqua regia digest, and it is these concentrations that we utilize in the following discussion.

3.2 Hg and trace metal concentrations in Tyrrhenian Basin sediments

Mercury concentrations are significantly higher in sapropels than in background sediments deposited prior to sapropel i90 TB. Background sediments have Hg concentrations ranging from 39 to 94 ng/g (average = 66 ng/g) and an average Hg/Al ratio of $7.8*10^{-7}$. The older, less organic-rich sapropel unit contains Hg concentrations ranging from 144 to 208 ng/g (average = 159 ng/g) and an average Hg/Al ratio of $1.9*10^{-6}$. The younger, more organic-rich sapropel unit contains higher Hg concentrations ranging from 314 to 488 ng/g (average = 385 ng/g) and an average Hg/Al ratio of $4.6*10^{-6}$. The two sapropel units are separated by sediment containing background levels of TOC (~0.2%) which was deposited during a brief return to typical Mediterranean conditions during i90 (see section 4.2; Meyers and Arnaboldi, 2005). Sediments deposited during the interruption between the two sapropel layers return to background levels of Hg, with Hg concentrations ranging from 55 to 78 ng/g (average = 64 ng/g) and with an average Hg/Al ratio of $9.5*10^{-7}$. Figure 2.2 displays Hg concentration as a function of TOC in the 974C 6H5 core section. There are three distinct ranges of TOC content, corresponding to background and interruption sediments, the partially developed

lower sapropel layer, and the fully developed upper sapropel layer. Enrichment factors (EF) express the ratio of the average element/Al concentration in the sapropel sediments to the background sediments.

$$EF_{metal} = (metal/Al)_{sapropel}/(metal/Al)_{background\ sediment}$$

The i90 TB upper and lower sapropel layers have EF_{Hg} of 5.9 and 2.4, respectively. Sapropel i90 TB is enriched in all trace metals analyzed, with the magnitude of EF ranging from EF_{Zn} = 2.0 to EF_{Mo} = 75 for the upper sapropel, and ranging from EF_{U} = 1.2 to EF_{Re} = 8.1 for the lower sapropel. Trace metal concentrations and trace metal/Al ratios are presented in Table 2.2a and 2.2b, respectively, and average trace metal/Al ratios are presented in Table 2.3. Figure 2.3 shows trace metal/Al ratios through the sediment sequence. Background sediments contain Ni/Al, Cu/Al, Zn/Al and Mo/Al ratios within a factor of 2 of average shale concentrations, and lower Ba/Al and Re/Al ratios [Ba: $35*10^{-4}$ (background) versus $66*10^{-4}$ (average shale); Re: $0.38*10^{-7}$ (background) versus $1.1*10^{-7}$ (average shale)] (Wedepohl 1971, 1991). The U/Al ratio determined is lower than that of average shales [$0.21*10^{-4}$ (background) versus $0.42*10^{-4}$ (average shale)], likely due to incomplete aqua regia digestion of the silicate fraction containing a significant U concentration (Wedepohl 1971, 1991).

Tyrrhenian Basin interruption layer sediment Ni/Al, Zn/Al, and Hg/Al ratios are close to the values of background sediments. In contrast, ratios of Mo/Al, Re/Al, and U/Al do not return to background levels within the interruption layer. All Cu/Al ratios are elevated compared to background levels, but decline through the interruption layer (Figure 2.3). Ba/Al ratios are elevated at the onset of the

interruption but steadily decrease to background levels. One interruption layer sample has an anomalously high Zn/Al ratio which has been included in Table 2.2a and 2.2b, Table 2.3, and EF calculations, but has been excluded from Figure 2.3 and Hg correlation coefficient calculations.

3.3 Major element concentration ratios in Tyrrhenian Basin sediments

Concentrations and ratios of major element (Mg, Si, K, Ti, Mn and Fe) to Al concentrations are given in Table S2.1 and Table S2.2. The i90 TB sapropel and background sediments have indistinguishable ratios of Mg/Al [0.26 ± 0.004 (1 SD) and 0.28 ± 0.003 (1 SD)], Si/Al [2.63 ± 0.01 (1 SD) and 2.87 ± 0.11 (1 SD)], K/Al [0.31 ± 0.01 (1 SD) and 0.33 ± 0.01 (1 SD)], and Ti/Al [0.049 ± 0.001 (1 SD) and 0.051 ± 0.002 (1 SD)]. The two sapropel i90 TB layers have distinct ratios from the ratios in interruption and background sediments in the redox-sensitive elements Mn and Fe. The upper sapropel unit is depleted in Mn and enriched in Fe compared to background sediments {Mn/Al = [0.0094 ± 0.0004 (1 SD) versus 0.019 ± 0.003 (1 SD); Fe/Al [0.66 ± 0.06 (1 SD) versus 0.52 ± 0.02 (1 SD)]}.

3.4 Sediment Hg isotopic composition

Sapropel i90 TB sediments have δ^{202}Hg values ranging from -0.61 to -1.11‰, with an average value of -0.91 ± 0.15‰ (n = 5, 1 SD), and background and interruption sediments have δ^{202}Hg values ranging from -0.57 to -0.97‰, with an average value of -0.76 ± 0.16‰ (n = 5, 1 SD). Sapropel layers have Δ^{201}Hg values ranging from 0.01 to 0.10‰, with an average value of 0.04 ± 0.03‰ (1 SD), and

background and interruption sediments have Δ^{201}Hg values ranging from -0.04 to +0.05‰, with an average value of -0.02 ± 0.02‰ (1 SD). Finally, sapropel i90 TB sediments have Δ^{199}Hg values ranging from 0.09 to 0.17‰, with an average value of 0.11 ± 0.03‰ (1 SD), and background and interruption sediments have Δ^{199}Hg values ranging from 0.04 to 0.07‰, with an average value of 0.05 ± 0.01‰ (1 SD). There is no discernable difference in the Hg isotopic composition of sapropel and background sediments, despite the 6-fold difference in Hg concentration. Table 2.4 lists the isotopic compositions for samples analyzed.

4. Discussion

4.1 Variation of Hg concentrations across a redox and productivity boundary

Organic-poor background sediments and organic-rich sediments (sapropel layers) contain significantly different Hg concentrations. Pleistocene background sediments in Section 974C-6H5 contain Hg concentrations ranging from 39 to 94 ng/g, which are consistent with the 15 to 70 ng/g range of values for modern uncontaminated Mediterranean sediments (Leonardo et al., 2006). Hg concentrations in sapropel sediments are, however, significantly higher than in background and interruption sediments. Each of the sapropel layers is enriched in Hg, with the lower unit ranging from 144 to 208 ng/g Hg and the upper unit ranging from 314 to 488 ng/g Hg, which corresponds to enrichment above background sediment concentrations by factors of 2.4 and 5.9, respectively. Modern marine sediments containing greater than ~100 ng/g Hg are often assumed to be affected by pollution (Camargo, 2002), yet high levels of Hg in the Pleistocene marine

sediments demonstrates that Hg can be concentrated to high levels without anthropogenic inputs.

The source of detrital material to the Tyrrhenian Basin likely did not change during sapropel formation. Changes in detrital provenance may be identified by immobile major element concentration ratios. Previous studies have observed increases in Mg/Al, Si/Al and K/Al and distinct decreases in Ti/Al in Eastern Mediterranean sapropels compared to background sediments and have attributed these variations to a larger contribution of sediment delivered by the Nile River, clays in certain deep water currents, and a smaller contribution of dust from the Sahara Desert during sapropel deposition (e.g. Wehausen and Brumsack, 2000; Bottcher et al, 2003). Sapropel i90 TB and background sediments have indistinguishable concentration ratios of Mg/Al (0.26 ± 0.004 and 0.28 ± 0.003 (1 SD)), Si/Al (2.63 ± 0.01 and 2.87 ± 0.11 (1 SD)), K/Al (0.31 ± 0.01 and 0.33 ± 0.01 (1 SD)) and Ti/Al (0.049 ± 0.001 and 0.051 ± 0.002 (1 SD)), indicating the same detrital sediment source during both sapropel and non-sapropel forming times (Table S2.2). The six-fold increase in Hg concentration, reaching 488 ng/g Hg in the i90 TB sapropel, cannot be explained by a change in detrital provenance and is thus attributable solely to depositional and preservation processes.

4.2 Paleoproductivity and redox conditions of the i90 TB sapropel

4.2.1 Sapropel i90 TB formation

It is well documented that sapropels are deposited during periods of enhanced primary productivity (e.g. Rohling and Bryden., 1994; Meyers and

Arnaboldi, 2005; Meyers and Bernasconi, 2005). Amplified rates of primary production in the Tyrrhenian Basin during i90 have been proposed by Meyers and Arnaboldi (2005) and Meyers and Bernasconi (2005) on the basis of carbon concentration and isotopic data. At ODP Site 974C, increased organic carbon accumulation rates correlate with systematically higher values of $\delta^{13}C$, which shift from -26‰ to -21‰ during i90 (Meyers and Arnaboldi, 2005; Meyers and Bernasconi, 2005). Excursions towards higher $\delta^{13}C$ values suggest elevated marine primary productivity rates during sapropel formation.

This study provides further evidence of amplified primary productivity rates in the Tyrrhenian Basin during i90. Sediment enrichment in Ba is often used as a marine productivity proxy (e.g. Dymond et al., 1992; Francois et al., 1995) and sapropels are commonly enriched in Ba (e.g. Warning and Brumsack, 2000; Rinna et al., 2002; Gallego-Torres et al., 2007). The lower and upper i90 TB sapropel units are significantly enriched in Ba above background levels, with EF_{Ba} = 3.0 and 3.3, respectively (Table 2.3, Figure 2.3). Sapropel i90 TB has high concentrations of multiple metals associated with biological uptake and organic scavenging, with EF_{Ni} = 4.7, EF_{Cu} = 3.1, and EF_{Zn} = 2.0 (Table 2.3). The accumulation of Ni, Cu, and Zn in sapropels is likely promoted both by organic matter delivery and the presence of sulfides, which can fix these metals in sediments (e.g. Calvert and Pederson, 1993; Morse and Luther, 1999; Al-farawati and van den Berg, 1999; Whitfield, 2001; Böning et al., 2004). Sapropel i90 TB also has higher Fe/Al ratios than background sediments (0.66 ± 0.06 (1 SD) versus 0.52 ± 0.02 (1 SD)), likely resulting from increased sediment organic matter and free sulfide availability in sapropels.

Raiswell and Berner (1985) and Canfield et al. (1996) recognized reduction of organic matter as a limiting factor for pyrite precipitation under normal marine conditions. During sapropel deposition, elevated organic carbon rain rates and sulfide availability (discussed below) likely facilitate pyrite formation.

While increased primary productivity during sapropel events was a regional phenomenon occurring throughout the Mediterranean Sea, hydrographic conditions influenced water column ventilation within localized basins (Arnaboldi and Meyers, 2007). The water column redox condition of the Tyrrhenian Sea during the i90 sapropel was unknown prior to this study. Sapropel i90 TB is enriched in the redox-sensitive trace metals Mo, Re and U, with EF_{Mo} = 75, EF_{Re} = 64 and EF_{U} = 8.2, for the upper sapropel layer. Sapropel i90 TB also has distinct ratios of the redox-sensitive major elements Mn and Fe. The sapropel has lower Mn/Al ratios than background sediments (0.0094 ± 0.0004 (1 SD) versus 0.019 ± 0.003 (1 SD)) which suggests the reduction of Mn-oxides during sapropel deposition. Higher Fe/Al ratios in the sapropel likely result from pyrite formation, which is promoted by sustained exposure to hydrogen sulfide (e.g. Canfield et al., 1996). Fixation of Ni (EF_{Ni} = 4.7), Zn (EF_{Zn} = 2.0), and Mo (EF_{Mo} = 75) in sediments is facilitated by oxygen-depleted conditions and sulfide availability (Jacobs et al., 1985; Calvert and Pederson, 1993; Morse and Luther, 1999; Helz et al., 2004). Enrichment in sulfide-forming (Ni, Cu, Zn, Mo) and redox-sensitive (Mo, Re, U) trace metals, lower Mn/Al ratios, and higher Fe/Al ratios in the i90 TB sapropel indicate low-oxygen and possibly sulfidic conditions at the time of its formation.

Direct comparison of the lower and upper i90 TB sapropel layers suggest more strongly reducing conditions during deposition of the upper layer. The lower and upper i90 TB sapropel units are nearly equally enriched in Ba (EF_{Ba} = 3.0 versus 3.3) though primary productivity was more enhanced during deposition of the upper sapropel (Meyers and Bernasconi, 2005). Barite is stable under suboxic conditions but can be mobilized under sulfate-reducing conditions, which is what may have occurred during sapropel i90 TB deposition (Torres et al., 1996). The lower sapropel unit is significantly less enriched than the upper sapropel unit in redox-sensitive metals including Mo (EF_{Mo} = 6.7 versus 75), Re (EF_{Re} = 8.1 versus 64) and U (EF_{U} = 1.2 versus 8.2). Both the lower and upper i90 TB sapropel contain higher Re/Mo ratios compared to the seawater value of $0.8*10^{-3}$, but the Re/Mo ratio decreases from $5.3*10^{-3}$ in the lower unit to $3.8*10^{-3}$ in the upper unit, suggesting more sulfidic conditions (Crusius et al., 1996). It is possible that the water column was suboxic during formation of the lower i90 TB sapropel, whereas anoxic bottom water developed during formation of the upper sapropel layer.

4.2.2 Oxidative interruption of sapropel i90 TB

Increased primary productivity likely increased oxygen-consumption throughout the water column in the Tyrrhenian Sea, and anoxic bottom water may have developed during i90. However, anti-estuarine circulation of Levantine Intermediate Water transported dissolved oxygen into the western Mediterranean and likely kept the total water column from reaching anoxia (Bethoux, 1989; Meyers and Bernasconi, 2005; Arnaboldi and Meyers, 2006). Replenishment of oxygen at

depth may have decomposed organic matter near the sediment-water interface, producing lower TOC concentrations in sapropel i90 TB than is common among eastern Mediterranean sapropels (4% versus >10%). Additionally, while the sapropel is enriched in trace metals with respect to background sediments, sapropel i90 TB contains systematically lower concentrations of the redox-sensitive trace metals Mo, Re, and U compared to other sapropels (Table 2.3; Nijenhuis et al., 1999, Warning and Brumsack, 2000; Arnaboldi and Meyers, 2003) and thus it is possible that trace metals have been mobilized from it. Evidence of oxidative diagenesis is apparent in the interruption layer sediment. The Ba concentration decreases gradually through the interruption layer (Figure 2.3), suggesting a gradual decrease in productivity. Conversely, TOC content returns to background levels immediately (Figure 2.3), likely resulting from the combined effect of lower organic carbon rain rates and minor oxidative burndown. However, fully oxic conditions probably did not return during the interruption and it is likely that in-situ sulfate reduction contributed to the observed decline in Ba concentration (e.g. Torres et al., 1996). Like Ba, the Cu concentration declines through the interruption period, but Cu/Al ratios remain elevated, likely due to precipitation of Cu sulfides (e.g. Morse and Luther, 1999). Ni, Mo, Re, and U concentrations gradually increase through the interruption layer (Figure 2.3), indicating the presence of porewater sulfides and a progressively more shallow redox boundary. Differential post-depositional preservation of trace metals affects their accumulation, and the overall enrichment of sapropel i90 TB in trace metals suggests both elevated surface productivity and a reducing water column during sapropel formation.

4.3 Comparison of Hg behavior with that of other trace metals

4.3.1 Concentration relationships among Hg, TOC, and trace metals

Concentrations of Hg and each of the other trace metals that we investigated are positively correlated with TOC through the sediment sequence. There are three distinct groupings of TOC values, corresponding to background and interruption sediments, the initial sapropel deposited before the interruption period, and the younger more fully developed sapropel (Meyers and Bernasconi, 2005). The large increase in TOC content in sapropel layers leads to decreased Hg/TOC ratios. However, the highest metal concentrations are found within the sapropel layer with the highest TOC content.

Strong positive correlations are observed within the sapropel between Hg and each of the trace metals analyzed: Ni ($r^2 = 0.96$), Cu ($r^2 = 0.80$), Zn ($r^2 = 0.80$), Mo ($r^2 = 0.79$), Ba ($r^2 = 0.70$), Re ($r^2 = 0.86$) and U ($r^2 = 0.70$). In contrast to the sapropels, correlations between Hg and most of the other trace metals are not observed in the background sediments. The pattern of positive correlations in sapropel sediments among metals sensitive to redox conditions and surface productivity affirm that trace metal enrichment in sapropels resulted from combined water column suboxia with enhanced primary productivity. It is likely that Hg accumulation in sapropels also is a response to both enhanced export productivity and oxygen depletion.

Trace metal patterns in the interruption layer suggest similar post-depositional behavior of Hg, Ni, and Re. Hg and Ni concentrations are elevated in

the lower i90 TB sapropel and decrease to background levels at the onset of the interruption. Re concentrations in the interruption layer do not decrease entirely to background levels, but they decrease significantly from the lower sapropel unit. The concentrations of Hg, Ni, and Re slightly increase through the interruption period, but do not reach concentrations equivalent to those observed in either sapropel layer (Figure 2.3). The Tyrrhenian Sea water column became oxic during the interruption layer (Meyers and Arnaboldi, 2005; Meyers and Bernasconi, 2005) and Hg and Ni concentrations likely drop to background levels during the interruption due to mineralization of organic carrier particles under oxic conditions. Re may have been liberated during minor surface sediment oxidation as well. In contrast to Hg, Ni, and Re, concentrations of the conservative redox-sensitive trace metals Mo and U increase from the lower sapropel unit through the interruption, with larger enrichment factors in the interruption sediment than in the lower sapropel (EF_{Mo} = 8.9 versus 6.7; EF_{U} = 2.6 versus 1.2). Enrichment of Mo and U is likely due to the presence of anoxic porewaters, which could have been maintained through the oxic interruption during the i90 sapropel. It is possible that a fraction of Hg, Ni, and Re liberated from organic matter mineralization and surface sediment oxidation was subsequently fixed in reducing sediments, as has been proposed for Hg by Ogrinc et al. (2007). In contrast to other metals, the Ba concentration decreases gradually through the interruption layer, likely in response to decreased export productivity and possibly persisting sediment sulfate reduction below a shallow redox gradient.

4.3.2 Trace metal enrichments in sapropel sediments

It is important to determine the mechanism by which Hg accumulates under reducing conditions in sapropel sediments to fully understand the marine Hg cycle. Trace metal concentration correlations within sapropels cannot be used to distinguish productivity-sensitive versus redox-sensitive metal behavior due to the positive reinforcement of organic matter rain rate, oxygen depletion, and organic matter preservation. In order to discriminate between enrichment mechanisms in sapropels, we determined the proportional extent to which each metal must have been removed from a column of seawater to account for the observed sediment concentrations.

It is generally believed that seawater is the primary source of trace metals fixed in sapropel sediments (e.g. Nijenhuis et al., 1999; Brumsack, 2006). As discussed in section 4.1, sapropel i90 TB and background sediments in the Tyrrhenian Basin are derived from the same atmospheric and detrital sediment sources. Thus, we subtract the average trace metal/Al ratios in background sediments from sapropel ratios and then multiply the trace metal/Al sapropel accumulation ratio by the average sapropel Al concentration (85 mg/g) to calculate the sapropel trace metal accumulation concentration. In order to calculate the flux of metals delivered to the Tyrrhenian Basin by seawater, we use published estimates of the seawater flux into the basin, the area of the Tyrrhenian Basin, and average seawater trace metal concentrations. We assume the only seawater source of dissolved trace metals to the Tyrrhenian Sea is the upper 150 m of water that enters through the Strait of Sardinia (Bethoux, 1980) and which is composed of approximately 70% North Atlantic Surface Water (NASW), 20% Gulf of Cadiz Water

(GCW), and 10% North Atlantic Central Water (NACW) (Van Geen et al., 1991). In order to calculate the flux of metals that accumulated in the i90 TB sapropel layer, we use the bulk density (Meyers and Bernasconi, 2005), sapropel layer thickness, and the concentration of trace metals. By dividing the annual accumulation of trace metals in the i90 TB sapropel by the annual delivery of seawater trace metals to the Tyrrhenian Sea, we estimate the percent of seawater trace metals that ultimately accumulated in the sediments through insolation cycle 90 (Table 2.5).

We calculate that precipitation of less than 3% of aqueous Mo, U, and Re in the basin would account for the concentrations of those metals observed in sapropel i90 TB. In contrast, concentrations of Ni and Cu in sapropel i90 TB record nearly complete (>96%) deposition and preservation of those metals in the basin. In general agreement with metals associated with organic delivery (Ni, Cu), the Hg concentration in the sapropels requires quantitative sequestration and deposition of Hg. In fact, complete removal of Hg from the surface 150 m of the water column would yield Hg accumulations only about 74% as high as those observed in sapropel i90 TB (Table 2.5), suggesting that the seawater Hg concentration that we used in our calculation (0.236 pg/g; Kotnik et al., 2007) may be a low estimate for the mid-Pleistocene Tyrrhenian Sea. The background sediment accumulation rate calculated for Hg ($4.8*10^{-6}$ g/m^2/y) is similar to that calculated from Ogrinc et al. (2007) ($7.3*10^{-6}$ g/m^2/y) and the sapropel accumulation rate is a factor of 3 higher. Sapropel accumulations do not record complete deposition and preservation of Zn (21%), possibly due to incomplete biological uptake and delivery. Sapropel accumulations of Ba account for 8% of the Ba estimated to be supplied by seawater.

Based on these seawater-sediment calculations, we surmise that it is likely that organic matter, which is the primary carrier depositing Ni and Cu to the seafloor, also delivers Hg by the same mechanism.

A growing body of evidence suggests that Hg is strongly associated with organic matter in the modern ocean. Profiles of seawater Hg exhibit minimum concentrations in the photic zone, with stable or slightly increasing concentrations with depth (Cossa et al., 1997; Ferrara et al., 2003; Cossa et al., 2004; Laurier et al., 2004; Kotnik et al., 2007). Photochemical and biological reduction of Hg(II) with subsequent evasion of Hg(0) likely contribute to the photic zone Hg concentration minima (Cossa et al., 1997; Kotnik et al., 2007). However, uptake of Hg by fresh water algae (e.g. Pickhardt et al., 2002; Karimi et al., 2007), marine plankton (e.g. Mason et al., 1996) and marine POM (Turner et al., 2004) has been documented and a positive correlation between Hg and primary productivity has been observed (Vandal et al., 1993). Hg speciation appears to be strongly influenced by particle abundance (e.g. Cossa et al., 1997; Conaway et al., 2003), and Hg cycling models suggest Hg is transported below the euphotic zone by particulate matter (Mason and Sheu, 2002). Hg has a strong affinity for dissolved organic matter (e.g. Lamborg et al., 2004; Han et al., 2006), and laboratory studies suggest that Hg-DOM bond strength is comparable to that of Hg-sulfides (Haitzer et al., 2002; Miller et al., 2007). Seawater Hg concentrations also are sufficiently low that even under oligotrophic conditions organic matter can quantitatively scavenge Hg in the surface water. Haitzer et al. (2002) observed strong binding ($K^{23\pm1}$) under aqueous Hg/DOM ratios less than 10^{-3} and suggested an excess of strong binding sites in the

1 kDa DOM for Hg/DOM less than $5*10^{-4}$. Using primary production rates in the currently oligotrophic Tyrrhenian Sea (Morel and André, 1991) and the seawater Hg concentration (Mason et al., 1998), we estimate a Hg/DOC ratio of 10^{-7}, or less than $1*10^{-5}$ Hg/DOM. Thus, Hg is likely to be quantitatively scavenged by organic matter.

Sapropel i90 TB is enriched in Hg above background sediments by a factor of 5.9. This sapropel also is enriched in Ni, Cu, and Zn with $EF_{Ni} = 4.7$, $EF_{Cu} = 3.1$, and $EF_{Zn} = 2.0$ (Table 2.3). Organic-bound metals may be either delivered to the seafloor or released to the water column during mineralization of the carrier organic matter. A suboxic water column would mineralize minor amounts of senescing organic matter, allowing significantly higher quantities of organically-associated trace metals to be transported to depth. The large concentration differences of Ni, Cu, Zn, and Hg between sapropels and background sediments can thus be attributed to organic matter conservation through the water column in addition to post-depositional preservation under oxygen-depleted bottom conditions.

4.4 Hg isotopic composition in Tyrrhenian Basin sediments

We argued above that Hg is efficiently scavenged by organic matter in the surface ocean, and therefore we expect that the i90 sapropel sediments record the isotopic composition of Hg in the Tyrrhenian Sea during the Pleistocene. Tyrrhenian Basin sapropel i90 layers, and interruption and background sediments have a narrow range of mass dependent isotopic composition with $\delta^{202}Hg = -0.91 \pm 0.15‰$ (n = 5, 1 SD) and $\delta^{202}Hg = -0.76 \pm 0.16‰$ (n = 5, 1 SD), respectively (Table 2.4). Isotopic compositions with $\delta^{202}Hg$ ranging by more than 2‰ have been

observed in other natural materials such as coals (Biswas et al., 2008) and Mesozoic volcanic and sedimentary rocks (Smith et al., 2008). The similar isotopic composition of Hg between sapropels and their accompanying background sediments is consistent with the idea that these marine sediments reflect the Hg isotopic composition of the ambient seawater. Although the isotopic compositions are nearly indistinguishable, the higher Hg concentration in sapropels compared to background sediments and the greater removal of Hg from the water column during sapropel formation, lead us to suggest that the sapropel isotopic values are probably the most accurate measure of marine Hg isotopic composition. We infer that the Hg mass dependent isotopic composition of the mid-Pleistocene Tyrrhenian Sea was close to that of the sapropel sediments with $\delta^{202}Hg = -0.91 \pm 0.15‰$.

Mass independent isotope fractionation (MIF) has been predicted (Buchachenko, 2001; Schauble, 2007) for some chemical reactions and both preferential volatilization of even Hg isotopes in laboratory experiments (Bergquist and Blum, 2007) and enrichment of odd Hg isotopes in freshwater fish tissues have been observed (Jackson et al., 2004; Bergquist and Blum, 2007). Experimental studies suggest that Hg mass independent fractionation can result from photochemical but not microbial reduction of oxidized Hg species (Bergquist and Blum, 2007; Kritee et al., 2007). If, as we have argued, the Hg isotopic composition of the sapropels studied here are representative of seawater, our measurements provide the first opportunity to explore whether marine Hg has undergone MIF. Sapropel i90 TB displays small, but significant, mass independent fractionation with $\Delta^{199}Hg = 0.11 \pm 0.03‰$ (n = 5, 1 SD) and $\Delta^{201}Hg = +0.04 \pm 0.03‰$ (n = 5, 1 SD)

(Table 2.4). The positive Δ^{199}Hg and Δ^{201}Hg values observed in sapropels suggest that the marine Hg cycle involves enough photochemical reduction and loss of Hg (with negative Δ^{199}Hg and Δ^{201}Hg) to result in marine values that are slightly positive. We infer that the Hg mass independent isotopic composition of the Pleistocene Tyrrhenian Sea was Δ^{199}Hg = +0.11 ± 0.03‰ and Δ^{201}Hg = +0.04 ± 0.03‰.

It might be anticipated that the Hg isotopic composition of the ocean should generally reflect that of Hg in the upper crust. Atmospheric deposition is the largest source of Hg to the global ocean, and pre-industrial sources of Hg to the atmosphere were primarily volcanic and hydrothermal emissions. Recent investigations into the Hg isotopic composition of volcanic and sedimentary rocks in California report an average δ^{202}Hg of -0.64 ± 0.23‰ (n=9, 1 SD) for the Clear Lake Volcanic Sequence and an average δ^{202}Hg of -0.64 ± 0.21‰ (n=16, 1 SD) for the Great Valley sedimentary sequence (Smith et al., 2008). Mass independent isotopic values are not reported for these rock sequences. The range of Hg isotopic composition of volcanic and sedimentary deposits in California is close to the isotopic composition we report for Pleistocene Mediterranean seawater (δ^{202}Hg = -0.91 ± 0.15‰).

5. Conclusions

Sapropel i90 TB sediments, which formed during a period of high primary productivity, are significantly enriched in Hg relative to background sediments (EF_{Hg} = 5.9). Sapropel sediments are also enriched in other trace metals (Ni, Cu, Zn, Mo, Ba, Re, U) with enrichment factors ranging from 2.0 (EF_{Zn}) to 75 (EF_{Mo}).

Comparison of trace metal accumulation in the i90 TB sapropel with the flux of dissolved trace metals entering the Tyrrhenian Sea suggests nearly quantitative delivery and preservation of Ni, Cu, and Hg, which indicates that organic matter delivers Hg through the suboxic water column. Sediment depth profile similarities between Hg, Ni, and Re suggest similar post-depositional response to porewater geochemistry among these metals. Elevated Hg concentrations observed in sapropel sediments are not due to changes in provenance, but instead likely result from greater conservation of organic matter through the water column and post-depositional preservation.

The Hg preserved in sapropels and background sediments have average δ^{202}Hg values of -0.91 ± 0.15‰ (1 SD) and -0.76 ± 0.16‰ (n = 5, 1 SD). The similar δ^{202}Hg values between sapropels and background sediments is consistent with a similar source and mechanism for delivery of Hg to the sediments (e.g. organic matter association) under both oxic and suboxic conditions. A small deviation from mass-dependence is observed for the sapropels (Δ^{199}Hg = +0.11 ± 0.03‰ and Δ^{201}Hg = +0.04 ± 0.03‰) and is consistent with some photochemical reduction of Hg in the marine system. Quantitative sequestration of Hg in the photic zone suggests that the Hg isotopic composition of sapropels reflects that of the seawater from which it was scavenged. We infer that the Hg isotopic composition of the mid-Pleistocene Tyrrhenian Sea was δ^{202}Hg = -0.91 ± 0.15‰, Δ^{199}Hg = +0.11 ± 0.03‰ and Δ^{201}Hg = +0.04 ± 0.03‰.

Acknowledgements. This project was funded by NSF Grant EAR 0433793 to J.D. Blum, and samples were provided by the Ocean Drilling Program. This work was partially funded by the United States Environmental Protection Agency (EPA) under the Science to Achieve Results (STAR) Graduate Fellowship Program. The EPA has not officially endorsed this publication and the views expressed herein may not reflect the views of the EPA. We thank Marcus Johnson for his expert operation and maintenance of the MC-ICP-MS for Hg isotope analyses. We thank Hans-Jürgen Brumsack and associate editor James McManus for their thorough, constructive comments and advice regarding this manuscript. This paper also benefitted from the comments of an anonymous reviewer.

References

Al-Farawati, R., and van den Berg, C. M. G., 1999. Metal-sulfide complexation in seawater. *Marine Chemistry* **63**, 331-352.

Anbar, A.D., Creaser, R.A., Papanastassiou, D.A., Wasserburg, G.J., 1992. Rhenium in seawater: Confirmation of generally conservative behavior. *Geochimica et Cosmochimica Acta* **56**, 4099-4103.

Arnaboldi, M. and Meyers, P. A., 2003. Geochemical evidence for paleoclimatic variations during deposition of two Late Pliocene sapropels from the Vrica section, Calabria. *Palaeogeography Palaeoclimatology Palaeoecology* **190**, 257-271.

Arnaboldi, M. and Meyers, P. A., 2006. Patterns of organic carbon and nitrogen isotopic compositions of latest Pliocene sapropels from six locations across the Mediterranean Sea. *Palaeogeography Palaeoclimatology Palaeoecology* **235**, 149-167.

Arnaboldi, M. and Meyers, P. A., 2007. Trace element indicators of increased primary production and decreased water-column ventilation during deposition of latest Pliocene sapropels at five locations across the Mediterranean Sea. *Palaeogeography Palaeoclimatology Palaeoecology* **249**, 425-443.

Benoit, J. M., Mason, R. P., Gilmour, C. C., and Aiken, G. R., 2001. Constants for mercury binding by dissolved organic matter isolates from the Florida Everglades. *Geochimica et Cosmochimica Acta* **65**, 4445-4451.

Bergquist, B. A. and Blum, J. D., 2007. Mass-dependent and mass-independent fractionation of Hg isotopes in aquatic systems. *Geochimica et Cosmochimica Acta* **71**, A83-A83.

Bethoux, J. P., 1980. Mean Water Fluxes across Sections in the Mediterranean-Sea, Evaluated on the Basis of Water and Salt Budgets and of Observed Salinities. *Oceanologica Acta* **3**, 79-88.

Bethoux, J. P., 1989. Oxygen-Consumption, New Production, Vertical Advection and Environmental Evolution in the Mediterranean-Sea. *Deep-Sea Research Part a-Oceanographic Research Papers* **36**, 769-781.

Bishop, J., 1988. The barite-opal-organic carbon association in oceanic particulate matter. *Nature* **332**, 341-343.

Biswas, A., Blum, J. D., Bergquist, B. A., Keeler, G. J., and Xie, Z., 2008. Natural Mercury Isotope Variation in Coal Deposits and Organic Soils. *Environmental Science and Technology* **42**, 8303-8309.

Blum, J. D. and Bergquist, B. A., 2007. Reporting of variations in the natural isotopic composition of mercury. *Analytical and Bioanalytical Chemistry* **388**, 353-359.

Böning, P., Brumsack, H.J., Bottcher, M.E., Schnetger, B., Kriete C., Kallmeyer, J., and Borchers, S.L., 2004. Geochemistry of Peruvian near-surface sediments. *Geochimica et Cosmochimica Acta* **68**, 4429-4451.

Bottcher, M. E., Rinna, J., Warning, B., Wehausen, R., Howell, M. W., Schnetger, B., Stein, R., Brumsack, H. J., and Rullkotter, J., 2003. Geochemistry of sediments from the connection between the western and the eastern Mediterranean Sea

(Strait of Sicily, ODP Site 963). *Palaeogeography Palaeoclimatology Palaeoecology* **190**, 165-194.
Bouloubassi, I., Rullkotter, J., and Meyers, P. A., 1999. Origin and transformation of organic matter in Pliocene-Pleistocene Mediterranean sapropels: organic geochemical evidence reviewed. *Marine Geology* **153**, 177-197.
Brumsack, H. J., 2006. The trace metal content of recent organic carbon-rich sediments: Implications for Cretaceous black shale formation. *Palaeogeography Palaeoclimatology Palaeoecology* **232**, 344-361.
Buchachenko, A. L., 2001. Magnetic isotope effect: Nuclear spin control of chemical reactions. *Journal of Physical Chemistry A* **105**, 9995-10011.
Calvert, S. E., Nielsen, B., and Fontugne, M. R., 1992. Evidence from Nitrogen Isotope Ratios for Enhanced Productivity During Formation of Eastern Mediterranean Sapropels. *Nature* **359**, 223-225.
Calvert, S. E. and Pedersen, T. F., 1993. Geochemistry of Recent Oxic and Anoxic Marine-Sediments - Implications for the Geological Record. *Marine Geology* **113**, 67-88.
Camargo, J. A., 2002. Contribution of Spanish-American silver mines (1570-1820) to the present high mercury concentrations in the global environment: a review. *Chemosphere* **48**, 51-57.
Canfield, D. E., Lyons, T.W., and Raiswell, R., 1996. A model for iron deposition to euxinic Black Sea sediments. *American Journal of Science* **296**, 818-834.
Collier, R.W., 1985. Molybdenum in the Northeast Pacific Ocean. *American Society of Limnology and Oceanography* **30**, 1351-1354.
Comas, M.C., Zahn, R., Klaus, A., et al., 1996. Proceedings of the Ocean Drilling Program. Initial Reports 161.
Conaway, C. H., Squire, S., Mason, R. P., and Flegal, A. R., 2003. Mercury speciation in the San Francisco Bay estuary. *Marine Chemistry* **80**, 199-225.
Cossa, D., Cotte-Krief, M. H., Mason, R. P., and Bretaudeau-Sanjuan, J., 2004. Total mercury in the water column near the shelf edge of the European continental margin. *Marine Chemistry* **90**, 21-29.
Cossa, D., Martin, J. M., Takayanagi, K., and Sanjuan, J., 1997. The distribution and cycling of mercury species in the western Mediterranean. *Deep-Sea Research Part Ii-Topical Studies in Oceanography* **44**, 721-740.
Crusius, J., Calvert, S., Pedersen, T., and Sage, D., 1996. Rhenium and molybdenum enrichments in sediments as indicators of oxic, suboxic and sulfidic conditions of deposition. *Earth and Planetary Science Letters* **145**, 65-78.
Dymond, J., Suess, E., and Lyle, M., 1992. Barium in deep-sea sediment: a geochemical proxy for paleoproductivity. *Paleoceanography* **7**, 163-181.
Dyrssen, D. and Wedborg, M., 1991. The Sulfur-Mercury(Ii) System in Natural-Waters. *Water Air and Soil Pollution* **56**, 507-519.
Ferrara, R., Ceccarini, C., Lanzillotta, E., Gardfeldt, K., Sommar, J., Horvat, M., Logar, M., Fajon, V., and Kotnik, J., 2003. Profiles of dissolved gaseous mercury concentration in the Mediterranean seawater. *Atmospheric Environment* **37**, S85-S92.

Francois, R., Honjo, S., Manganini, S.J., and Ravizza, G.E., 1995. Biogenic Barium Fluxes to the Deep-Sea – Implications for Paleoproductivity Reconstruction. *Global Biogeochemical Cycles* **9**, 289-303.

Gallego-Torres, D., Martínez-Ruiz, F., Paytan, A., Jiménez-Espejo, F.J., and Ortega-Huertas, M., 2007. Pliocene-Holocen evolution of depositional conditions in the eastern Mediterranean: Role of anoxia vs. productivity at time of sapropel deposition. *Paleogeography, Paleoclimatology, Paleoceanography* **246**, 424-439.

Haitzer, M., Aiken, G. R., and Ryan, J. N., 2002. Binding of mercury(II) to dissolved organic matter: The role of the mercury-to-DOM concentration ratio. *Environmental Science and Technology* **36**, 3564-3570.

Han, S., Gill, G. A., Lehman, R. D., and Choe, K.-Y., 2006. Complexation of mercury by dissolved organic matter in surface waters of Galveston Bay, Texas. *Marine Chemistry* **98**, 156-166.

Helz, G. R., Vorlicek, T. P., and Kahn, M. D., 2004. Molybdenum Scavenging by Iron Monosulfide. *Environmental Science and Technology* **38**, 4263-4268.

Jackson, T. A., Muir, D. C. G., and Vincent, W. F., 2004. Historical variations in the stable isotope composition of mercury in Arctic lake sediments. *Environmental Science and Technology* **38**, 2813-2821.

Jacobs, L., Emerson, S., and Skei, J., 1985. Partitioning and transport of metals across the O_2/H_2S interface in a permanently anoxic basin: Framvaren Fjord, Norway. *Geochimica et Cosmochimica Acta* **49**, 1433-1444.

Karimi, R., Chen, C. Y., Pickhardt, P. C., Fisher, N. S., and Folt, C. L., 2007. Stoichiometric controls of mercury dilution by growth. *Proceedings of the National Academy of Sciences of the United States of America* **104**, 7477-7482.

Kidd, R.B., Cita, M.B. and Ryan, W.B.F., 1978. Stratigraphy of eastern Mediterranean sapropel sequences recovered during Leg 42A and their paleoenvironmental significance. Init. Rep. DSDP, 42: 421-443.

Kotnik, J., Horvat, M., Tessier, E., Ogrinc, N., Monperrus, M., Amouroux, D., Fajon, V., Gibicar, D., Zizek, S., Sprovieri, F., and Pirrone, N., 2007. Mercury speciation in surface and deep waters of the Mediterranean Sea. *Marine Chemistry* **107**, 13-30.

Kritee, K., Blum, J. D., Johnson, M. W., Bergquist, B. A., and Barkay, T., 2007. Mercury stable isotope fractionation during reduction of Hg(II) to Hg(0) by mercury resistant microorganisms. *Environmental Science and Technology* **41**, 1889-1895.

Lamborg, C. H., Fitzgerald, W. F., Skoog, A., and Visscher, P. T., 2004. The abundance and source of mercury-binding organic ligands in Long Island Sound. *Marine Chemistry* **90**, 151-163.

Lauretta, D. S., Klaue, B., Blum, J. D., and Buseck, P. R., 2011. Mercury abundances and isotopic compositions in the Murchison (CM) and Allende (CV) carbonaceous chondrites. *Geochimica et Cosmochimica Acta* **65**, 2807-2818.

Laurier, F. J. G., Mason, R. P., Gill, G. A., and Whalin, L., 2004. Mercury distributions in the North Pacific Ocean--20 years of observations. *Marine Chemistry* **90**, 3-19.

Leonardo, R. D., Tranchida, G., Bellanca, A., Neri, R., Angelone, M., and Mazzola, S., 2006. Mercury levels in sediments of central Mediterranean Sea: A 150+ year

record from box-cores recovered in the Strait of. *Chemosphere* **65**, 2366-2376.
Lourens, L.J., Hilgen, F.J., Gudjonsson, L. and Zachariasse, W.J., 1992. Late Pliocene to Early Pleistocene Astronomically Forced Sea-Surface Productivity and Temperature-Variations in the Mediterranean. *Marine Micropaleontology* **19**, 49-78.
Mason, R. P., Reinfelder, J. R., and Morel, F. M. M., 1996. Uptake, toxicity, and trophic transfer of mercury in a coastal diatom. *Environmental Science and Technology* **30**, 1835-1845.
Mason, R. P., Rolfhus, K. R., and Fitzgerald, W. F., 1998. Mercury in the North Atlantic. *Marine Chemistry* **61**, 37-53.
Mason, R. P. and Sheu, G. R., 2002. Role of the ocean in the global mercury cycle. *Global Biogeochemical Cycles* **16**, 40-1 – 40-14.
McManus, J., Berelson, W. M., Klinkhammer, G. P., Hammond, D. E., and Holm, C., 2005. Authigenic uranium: relationship to oxygen penetration depth and organic carbon rain. *Geochimica et Cosmochimica Acta* **69**, 95-108.
Meyers, P. A. and Arnaboldi, M., 2005. Trans-Mediterranean comparison of geochemical paleoproductivity proxies in a mid-Pleistocene interrupted sapropel. *Palaeogeography Palaeoclimatology Palaeoecology* **222**, 313-328.
Meyers, P. A. and Bernasconi, S. M., 2005. Carbon and nitrogen isotope excursions in mid-Pleistocene sapropels from the Tyrrhenian Basin: Evidence for climate-induced increases in microbial primary production. *Marine Geology* **220**, 41-58.
Miller, C. L., Mason, R. P., Gilmour, C. C., and Heyes, A., 2007. Influence of dissolved organic matter on the complexation of mercury under sulfidic conditions. *Environmental Toxicology and Chemistry* **26**, 624-633.
Morel, A. and Andre, J. M., 1991. Pigment Distribution and Primary Production in the Western Mediterranean as Derived and Modeled from Coastal Zone Color Scanner Observations. *Journal of Geophysical Research-Oceans* **96**, 12685-12698.
Morley, N. H., Burton, J. D., Tankere, S. P. C., and Martin, J. M., 1997. Distribution and behaviour of some dissolved trace metals in the western Mediterranean Sea. *Deep-Sea Research Part Ii-Topical Studies in Oceanography* **44**, 675-691.
Morse, J. W., and Luther, G. W., 1999. Chemical influences on trace metal-sulfide interactions in anoxic sediments. *Geochimica et Cosmochimica Acta* **63**, 3373-3378.
Nijenhuis, I. A., Bosch, H. J., Damste, J. S. S., Brumsack, H. J., and De Lange, G. J., 1999. Organic matter and trace element rich sapropels and black shales: a geochemical comparison. *Earth and Planetary Science Letters* **169**, 277-290.
Ogrinc, N., Monperrus, M., Kotnik, J., Fajon, V., Vidimova, K., Amouroux, D., Kocman, D., Tessier, E., Zizek, S., and Horvat, M., 2007. Distribution of mercury and methylmercury in deep-sea surficial sediments of the Mediterranean Sea. *Marine Chemistry* **107**, 31-48.
Pickhardt, P. C., Folt, C. L., Chen, C. Y., Klaue, B., and Blum, J. D., 2002. Algal blooms reduce the uptake of toxic methylmercury in freshwater food webs.

Proceedings of the National Academy of Sciences of the United States of America **99**, 4419-4423.
Raiswell, R. and Berner, R.A., 1985. Pyrite Formation in Euxinic and Semi-Euxinic Sediments. *American Journal of Science* **285**, 710-724.
Rinna, J., Warning, B., Meyers, P. A., Brumsack, H. J., and Rullkotter, J., 2002. Combined organic and inorganic geochemical reconstruction of paleodepositional conditions of a Pliocene sapropel from the eastern Mediterranean Sea. *Geochimica Et Cosmochimica Acta* **66**, 1969-1986.
Rohling, E. J. and Bryden, H. L., 1994. Estimating Past Changes in the Eastern Mediterranean Fresh-Water Budget, Using Reconstructions of Sea-Level and Hydrography. *Proceedings of the Koninklijke Nederlandse Akademie Van Wetenschappen-Biological Chemical Geological Physical and Medical Sciences* **97**, 201-217.
Schauble, E. A., 2007. Role of nuclear volume in driving equilibrium stable isotope fractionation of mercury, thallium, and other very heavy elements. *Geochimica et Cosmochimica Acta* **71**, 2170-2189.
Smith, C. N., Kesler, S. E., Klaue, B., and Blum, J. D., 2005. Mercury isotope fractionation in fossil hydrothermal systems. *Geology* **33**, 825-828.
Smith, C. N., Kesler, S.E., Blum, J.D. and Rytuna, J.J. 2008. Isotope Geochemistry of Mercury in Source Rocks, Mineral Deposits and Spring Deposits of the California Coast Ranges, USA. *Earth and Planetary Science Letters* **269**, 398-406.
Stancin, A.M., Gleason, J.D., Rea, D.K., Owen, R.M., Moore, T.C., Blum, J. D., and Hovan, S.A., 2006. Radiogenic isotopic mapping of late Cenozoic eolian and hernipelagic sediment distribution in the east-central Pacific. *Earth and Planetary Science Letters* **248**, 840-850.
Torres, M. E., Brumsack, H. J., Bohrmann, G., and Emeis, K. C., 1996. Barite fronts in continental margin sediments: a new look at barium remobilization in the zone of sulfate reduction and formation of heavy barites in diagenetic fronts. *Chemical Geology* **127**, 125-139.
Tribovillard, N., Algeo, T. J., Lyons, T., and Riboulleau, A., 2006. Trace metals as paleoredox and paleoproductivity proxies: An update. *Chemical Geology* **232**, 12-32.
Turner, A., Millward, G. E., and Le Roux, S. M., 2004. Significance of oxides and particulate organic matter in controlling trace metal partitioning in a contaminated estuary. *Marine Chemistry* **88**, 179-192.
Vandal, G.M., Fitzgerald, W.F., Boutron, C.F., and Candelone, J.P., 1993. Variations in Mercury Deposition to Antarctica over the Past 34,000 Years. *Nature* **362**, 621-623.
Van Geen, A., Boyle, E. A., and Moore, W. S., 1991. Trace metal enrichments in waters of the Gulf of Cadiz, Spain. *Geochimica et Cosmochimica Acta* **55**, 2173-2191.
Warning, B. and Brumsack, H. J., 2000. Trace metal signatures of eastern Mediterranean sapropels. *Palaeogeography Palaeoclimatology Palaeoecology* **158**, 293-309.
Wedepohl, K. H., 1971. Environmental Influences on the Chemical Composition of Shales and Clays. *Physics and Chemistry of the Earth* **8**, 305-333.

Wedepohl, K. H., 1991. Chemical-Composition and Fractionation of the Continental-Crust. *Geologische Rundschau* **80**, 207-223.

Wehausen, R. and Brumsack, H.-J., 2000. Chemical cycles in Pliocene sapropel-bearing and sapropel-barren eastern Mediterranean sediments. *Palaeogeography, Palaeoclimatology, Palaeoecology* **158**, 325-352.

Whitfield, M., 2001. Interactions between phytoplankton and trace metals in the ocean, *Advances in Marine Biology,* **41**, 1-128.

Wolgemuth, K. and Broecker, W.S., 1970. Barium in Sea Water. *Earth and Planetary Science Letters* **8**, 372-378.

Yoon, Y.-Y., Martin, J.-M., and Cotte, M. H., 1999. Dissolved trace metals in the Western Mediterranean Sea: total concentration and fraction isolated by C18 Sep-Pak technique. *Marine Chemistry* **66**, 129-148.

Zheng, Y., Anderson, R.F., van Geen, A., and Fleisher, M.Q., 2002. Preservation of particulate non-lithogenic uranium in marine sediments. *Geochimica et Cosmochimica Acta* **66**, 3085-3092.

Figure 2.1:

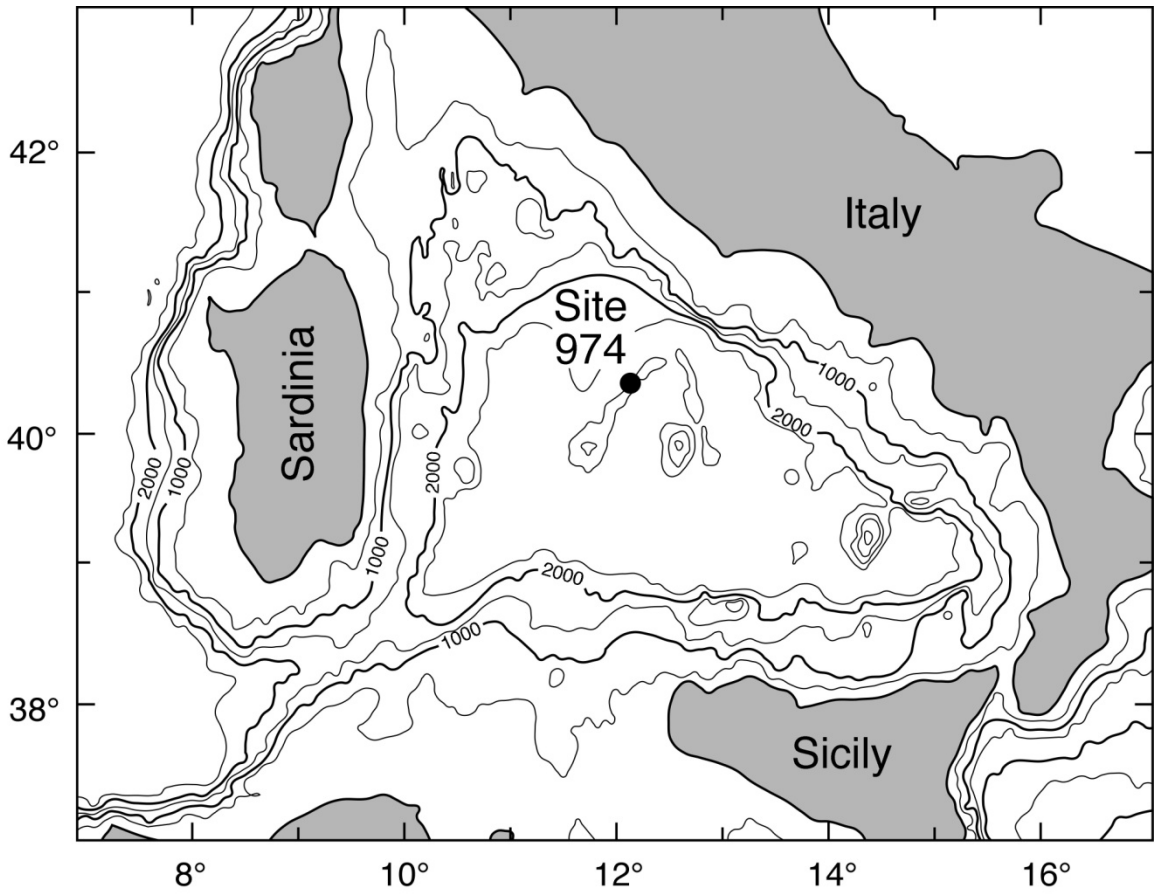

Figure 2.1: Location of ODP Site 974 in the Tyrrhenian Basin of the Mediterranean Sea with bathymetry.

Figure 2.2:

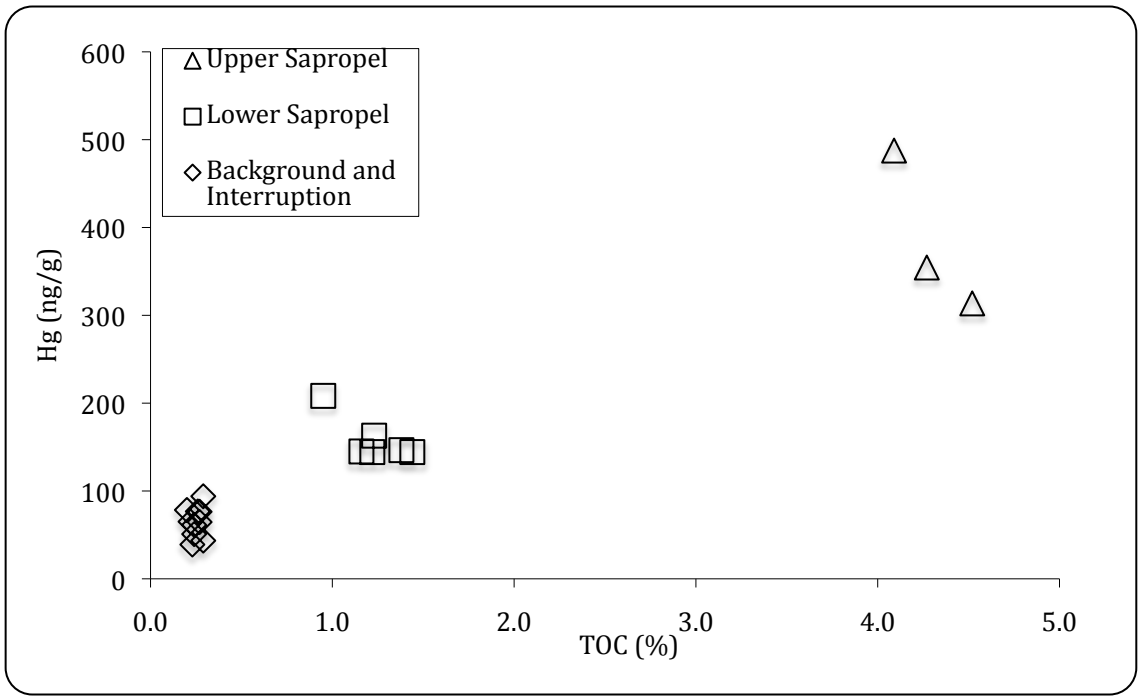

Figure 2.2: Hg concentrations plotted versus TOC. Three populations of TOC correspond to three distinct sediment units: background and interruption sediments, the upper (or initial) sapropel layer, and the lower (or strongly expressed) sapropel layer. Hg concentration has a positive correlation with TOC.

Figure 2.3:

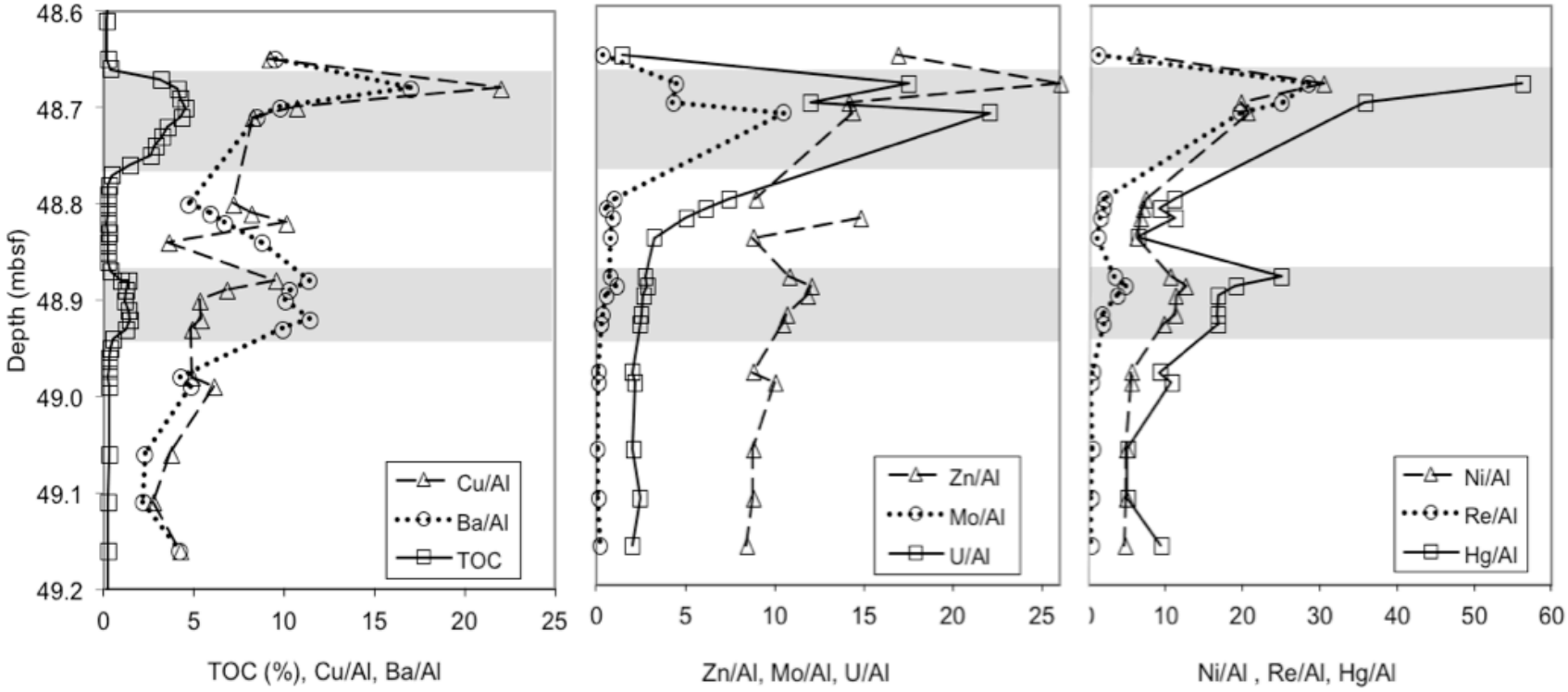

Figure 2.3: Depth profile of TOC and ratios of trace metal to Al concentrations in ODP Hole 974C-6H5. Depth is reported in meters below sea floor (mbsf). Concentrations of Ni, Cu, Zn, and Mo are reported as metal/Al weight ratios * 10^4, Ba is reported as Ba/Al weight ratio *10^3, U is reported as U/Al *10^5, and Re and Hg are reported as metal/Al weight ratios *10^7. One sample with Zn/Al = 35.8 is excluded from the figure. Sapropel sediments, defined by TOC greater than 0.5%, are shaded gray. Sapropels are enriched in all trace metals analyzed.

Table 2.1a. Trace metal concentrations in sequential digests of Core 974C 6H5 samples

Sample Depth	Digest	n	Ni	1 SD	Cu	1 SD	Zn	1 SD	Mo	1 SD	Ba	1 SD	U	1 SD	Re	1 SD
mbsf								µg/g								ng/g
48.84	$HCl-HNO_3$	2	100.4	1.2	65.7	0.5	163	15.7	15.8	0.01	1746	41	7.88	0.10	30.5	0.2
	$HF-HClO_4$	2	5.59	0.01	3.57	0.08	5.57	0.2	0.47	0.06	262	1	4.47	0.03	6.19	0.05
	$HCl-HNO_3$ Recovery (%)		95		95		97		97		87		64		83	
48.90	$HCl-HNO_3$	2	189.6	1.4	94.8	0.6	170.0	1.9	21.2	0.9	2070	7	6.80	0.03	90.2	0.5
	$HF-HClO_4$	2	9.78	0.26	4.28	0.29	5.52	0.87	1.10	0.50	257	2	4.29	0.13	7.66	0.20
	$HCl-HNO_3$ Recovery (%)		95		96		97		95		89		61		92	
49.16	$HCl-HNO_3$	1	35.1		33.4		65.6		1.31		400.1		2.33		5.75	
	$HF-HClO_4$	1	2.61		2.21		3.53		0.17		119		1.98		2.62	
	$HCl-HNO_3$ Recovery (%)		93		94		95		89		77		54		69	

Table 2.1b. Trace metal concentrations in digests of standard reference materials NIST 1646a and USGS Mag-1

Standard	Digest	Ni	1SD	Cu	1SD	Zn	1SD	Mo	1SD	Ba	1SD	U	1SD
							μg/g						
1646a	$HCl\text{-}HNO_3$	19.0		9.5		36.3		2.5		63		1.5	
NIST	$HF\text{-}HClO_4$	0.6		0.4		2.3		0.1		143		0.4	
	Sum	19.6		9.9		38.7		2.6		207		1.8	
	Certified	23*		10.01	0.34	48.9	1.6	1.8*		210*		2.0*	
	Recovery (%)	85		99		79		146		98		91	
Mag-1	$HCl\text{-}HNO_3$	45.8		24.4		118		1.9		396		2.0	
USGS	$HF\text{-}HClO_4$	1.9		1.8		3		0.2		141		1.0	
	Measured	47.7		26.3		121		2.1		537		3.1	
	Recommended	53	8	30	3	130	6	1.6*		480	41	2.7	0.3
	Recovery (%)	90		88		93		131		112		113	
Mag-1	$HCl\text{-}HNO_3$	43.4		23.3		108		1.6		370		2.0	
USGS	$HF\text{-}HClO_4$	2.0		1.8		3		0.2		142		1.0	
	Measured	45.4		25.1		111		1.8		511		3.0	
	Recommended	53	8	30	3	130	6	1.6*		480	41	2.7	0.3
	Recovery (%)	86		84		86		111		107		111	

* Not certified values.

Table 2.2a. TOC and trace metal concentrations in core 974C 6H5 samples.

Depth	TOC	Ni	Cu	Zn	Mo	Ba	U	Re	Hg
(mbsf)	(%)			μg/g				ng/g	
48.68	4.09	265	191	226	38.5	1478	15.1	247	488
48.69	4.27	184	102	128	48.8	835	10.7	180	354
48.70	4.52	173	93.5	124	37.3	856	10.5	219	314
48.71	4.28	166	66.4	116	84.0	680	17.7	157	nd
48.80	0.22	43.4	42.4	52.6	5.56	276	4.36	11.5	65.1
48.81	0.24	46.9	54.8	239	3.32	393	4.10	12.6	61.4
48.82	0.20	46.8	70.9	104	6.06	468	3.49	10.5	78.4
48.83	0.27	48.2	35.7	78.5	4.87	507	3.22	9.94	64.7
48.84	0.24	49.8	28.6	70.4	5.94	696	2.56	9.06	50.9
48.88	0.95	88.4	79.5	90.2	5.92	947	2.24	27.6	208
48.89	1.23	108	58.2	103	9.27	880	2.41	40.7	163
48.90	1.16	97.2	46.1	102	4.34	864	2.23	31.5	145
48.91	1.38	98.6	45.7	95.5	2.72	941	2.19	18.7	147
48.92	1.44	96.1	46.5	92.0	2.73	981	2.17	15.0	144
48.93	1.22	83.2	41.8	90.0	2.31	848	2.09	16.5	144
48.98	0.27	45.9	40.6	73.1	0.50	352	1.65	3.76	76.4
48.99	0.29	48.4	53.7	88.1	0.63	423	1.87	3.14	94.0
49.06	0.29	42.1	32.7	77.2	0.33	199	1.77	3.84	43.5
49.11	0.23	37.6	21.7	69.1	0.53	168	1.90	2.83	39.0
49.16	0.26	37.8	34.6	69.0	1.54	341	1.62	2.35	76.7

Sapropels are defined by TOC greater than 0.5%. "nd" indicates an undetermined concentration.

Table 2.2b. Ratios of trace metal to Al concentrations in core 974C 6H5 samples.

Depth (mbsf)	Ni/Al	Cu/Al	Zn/Al	Mo/Al	Ba/Al	Re/Al	U/Al	Hg/Al
48.68	30.5	22.0	26.0	4.43	170	28.4	1.75	56.1
48.69	*21.1*	*11.7*	*14.7*	*5.59*	*95.7*	*20.7*	*1.23*	*40.6*
48.70	19.7	10.7	14.2	4.26	97.6	25.0	1.20	35.8
48.71	20.7	8.26	14.4	10.5	84.6	19.6	2.20	nd
48.80	7.38	7.20	8.93	0.95	46.8	1.96	0.74	11.1
48.81	7.02	8.21	35.8	0.50	58.9	1.89	0.61	9.19
48.82	6.69	10.1	14.8	0.87	66.8	1.50	0.50	11.2
48.83	*6.43*	*4.76*	*10.5*	*0.65*	*67.8*	*1.33*	*0.43*	*8.63*
48.84	6.24	3.58	8.81	0.74	87.2	1.13	0.32	6.37
48.88	10.6	9.53	10.8	0.71	113	3.31	0.27	25.0
48.89	12.6	6.80	12.1	1.08	103	4.76	0.28	19.1
48.90	11.3	5.35	11.9	0.50	100.	3.65	0.26	16.8
48.91	*11.4*	*5.30*	*11.1*	*0.32*	*109*	*2.17*	*0.25*	*17.0*
48.92	11.1	5.39	10.7	0.32	114	1.73	0.25	16.7
48.93	9.67	4.86	10.5	0.27	98.6	1.92	0.24	16.9
48.98	5.53	4.89	8.81	0.06	42.5	0.45	0.20	9.21
48.99	5.50	6.11	10.0	0.07	48.1	0.36	0.21	10.7
49.06	4.80	3.72	8.80	0.04	22.6	0.44	0.20	4.95
49.11	4.79	2.77	8.80	0.07	21.4	0.36	0.24	4.97
49.16	4.62	4.22	8.42	0.19	41.6	0.29	0.20	9.36

Trace metal/Al ratios are reported as weight ratios x 10^4, except for Hg and Re which are reported as weight ratios x 10^7. Italicized weight ratios are derived from Al concentrations inferred from the average of Al concentrations of adjacent samples.

Table 2.3. Average ratios of trace metal to Al concentrations in sapropel i90 TB and background sediments.

	n	Ni/Al (±1 SD)	Cu/Al (±1 SD)	Zn/Al (±1 SD)	Mo/Al (±1 SD)	Ba/Al (±1 SD)	Re/Al (±1 SD)	U/Al (±1 SD)	Hg/Al (±1 SD)
Upper Sapropel	3	23.6 (±5.9)	13.7 (±7.4)	18.2 (±6.8)	6.4 (±3.5)	117 (±46)	24.3 (±4.5)	1.7 (±0.5)	45.9 (±14.4)
Lower Sapropel	5	11.1 (±1.1)	6.4 (±1.9)	11.2 (±0.7)	0.58 (±0.33)	106 (±7)	3.1 (±1.3)	0.26 (±0.02)	18.9 (±3.5)
Interruption Layer	4	6.8 (±0.5)	7.3 (±2.8)	17.1 (±12.8)	0.76 (±0.20)	64.9 (±17.0)	1.6 (±0.4)	0.54 (±0.18)	9.5 (±2.2)
Background Sediments	5	5.1 (±0.4)	4.3 (±1.3)	9.0 (±0.6)	0.085 (±0.059)	35.2 (±12.3)	0.38 (±0.07)	0.21 (±0.02)	7.8 (±2.7)
Pliocene Sapropel[a]		47	28	22	20	265	75.5	4.5	na
Black Sea Sapropel[b]		24.5	23.7	18	26.2	260	12.2	3.3	na
Average Shale[c]		7.7	5.1	11	0.15	66	1.1	0.42	na
Enrichment Factor		4.7	3.1	2.0	75	3.3	64	8.2	5.9

Trace metal/Al ratios are reported as weight ratios x 10^4, except for Hg and Re which are reported as weight ratio x 10^7. Enrichment factors are the trace metal concentration in the upper sapropel normalized to the concentration in background sediments (this study). "na" indicates concentrations that are not available. References: (a) Warning and Brumsack, 2000; (b) Brumsack 2006; (c) calculated from Wedepohl 1971, 1991.

Table 2.4. Hg isotopic composition of core 974C 6H5 samples.

Depth (mbsf)	Sample	δ^{202} Hg	1 SD	Δ^{201} Hg	1 SD	Δ^{199} Hg	1 SD
	Upper Sapropel Sediments						
48.68	974C 6H5 38-39	-0.79	0.04	0.05	0.04	0.08	0.04
48.68	*974C 6H5 38-39**	*-0.61*	*0.09*	*0.05*	*0.04*	*0.10*	*0.04*
48.69	974C 6H5 39-40	-0.99	0.09	0.10	0.05	0.17	0.05
48.70	974C 6H5 40-41	-1.11	0.16	0.02	0.03	0.11	0.06
	Lower Sapropel Sediments						
48.92	974C 6H5 62-63	-0.86	0.09	0.01	0.03	0.09	0.01
48.93	974C 6H5 63-64	-0.91	0.03	0.03	0.05	0.10	0.02
	Interruption Sediments						
48.80	974C 6H5 50-51	-0.74	0.03	0.01	0.06	0.07	0.06
	Background Sediments						
48.99	974C 6H5 69-70	-0.57	0.06	-0.04	0.02	0.07	0.04
49.06	974C 6H5 75-77	-0.86	0.10	-0.04	0.02	0.05	0.05
49.11	974C 6H5 80-82	-0.97	0.04	0.00	0.01	0.04	0.06
49.16	974C 6H5 85-87	-0.67	0.08	-0.02	0.01	0.04	0.01

Depth is reported in meters below sea floor (mbsf). Isotopic ratios and standard deviations are based on triplicate analyses of each sample and are reported in per mil (‰). Italicized sample 974C 6H538-39* is a replicate combustion and isotopic analysis.

Table 2.5. Results of calculations determining the proportion of dissolved trace metals delivered to the Tyrrhenian Basin by seawater that accumulate in sapropels.

	Unit	Ni	Cu	Zn	Mo	Ba	Re	U	Hg
Sapropel concentration	g/g Al $*10^4$	23.6	13.6	18.2	6.4	117	24.3*	1.7	45.9*
Background sediment concentration	g/g Al $*10^4$	5.0	4.3	9.0	0.1	35	0.4*	0.2	7.8*
Excess sapropel content	µg/g	158	79	78	54	699	203*	13	324*
Annual excess accumulation	$g/m^2/y$	1.14E-05	5.74E-06	5.67E-06	3.88E-06	5.06E-05	1.48E-05	9.28E-07	2.35E-05
Seawater concentration	g/g	1.64E-10[a]	8.01E-11[b]	3.71E-10[a]	1.01E-08[c]	8.25E-09[d]	7.30E-12[e]	3.24E-09[f]	2.36E-13[g]
Annual flux	g/y	3.11E+09	1.52E+09	7.03E+09	1.91E+11	1.56E+11	1.38E+08	6.14E+10	4.47E+06
Annual flux	$g/m^2/y$	1.20E-02	5.84E-03	2.70E-02	7.36E-01	6.01E-01	5.32E-04	2.36E-01	1.72E-05
Proportion in Sapropel	%	96	98	21	0.5	8.4	2.8	0.4	136

Seawater concentration data used in these calculations can be found in (a) Yoon Y. et al., 1999 (b) Morley N.H. et al., 1997 (c) Collier R.W., 1985 (d) Wolgemuth and Broecker, 1970 (e) Anbar A, et al., 1992 (f) Chen et al., 1986 (g) Kotnik J. et al , 2007. Seawater flux and surface area of the Tyrrhenian Basin are reported as $18.4*10^{12}$ m^2 y^{-1} and $2.6*10^{11}$ m^2 in Bethoux J-P., 1980. Excess sapropel values use Al = 85002 µg/g. *Re and Hg concentrations are reported in g/g Al $*10^7$.; excess sapropel Re and Hg values are reported in ng/g.

Table S2.1. Major element concentrations in core 974 C 6H5 samples.

Depth	Mg	Al	Si	K	Ti	Mn	Fe
(mbsf)				mg/g			
48.68	220	869	225	25.8	4.19	0.752	47.9
48.69	221	867	224	26.5	4.19	0.817	52.9
48.70	216	877	227	25.2	4.12	0.781	58.8
48.71	nd	nd	nd	nd	nd	nd	nd
48.80	154	589	158	16.9	2.76	1.72	30.5
48.81	176	668	178	20.6	3.22	1.98	31.0
48.82	181	700	188	22.2	3.32	1.99	35.2
48.83	nd	nd	nd	nd	nd	nd	nd
48.84	211	799	218	24.9	3.96	2.26	40.7
48.88	235	835	236	27.7	4.17	1.13	53.7
48.89	231	856	237	27.4	4.25	1.10	53.8
48.90	228	863	239	27.0	4.26	1.08	49.3
48.91	nd	nd	nd	nd	nd	nd	nd
48.92	231	863	239	26.5	4.29	1.06	47.7
48.93	228	860	236	27.6	4.33	1.07	46.4
48.98	225	830	228	26.2	4.34	1.36	36.9
48.99	239	880	244	28.2	4.56	1.48	39.9
49.06	234	878	255	26.6	4.36	1.74	42.1
49.11	213	785	235	22.5	4.01	1.83	37.1
49.16	223	819	221	23.9	3.87	1.40	42.0

Table S2.2. Ratios of element to Al concentrations in core 974 C 6H5 samples.

Depth	Mg/Al	Si/Al	K/Al	Ti/Al	Mn/Al	Fe/Al
(mbsf)				g/g		
48.68	0.257	2.63	0.309	0.0489	0.0090	0.558
48.69	0.260	2.62	0.319	0.0491	0.0098	0.618
48.70	0.251	2.64	0.303	0.0479	0.0094	0.681
48.71	nd	nd	nd	nd	nd	nd
48.80	0.269	2.74	0.307	0.0479	0.0300	0.530
48.81	0.271	2.72	0.330	0.0493	0.0306	0.476
48.82	0.265	2.75	0.337	0.0486	0.0292	0.514
48.83	nd	nd	nd	nd	nd	nd
48.84	0.271	2.78	0.329	0.0507	0.0290	0.520
48.88	0.287	2.88	0.349	0.0509	0.0141	0.654
48.89	0.276	2.82	0.336	0.0506	0.0134	0.639
48.90	0.269	2.81	0.328	0.0502	0.0130	0.580
48.91	nd	nd	nd	nd	nd	nd
48.92	0.273	2.82	0.324	0.0506	0.0128	0.562
48.93	0.270	2.79	0.335	0.0511	0.0129	0.548
48.98	0.278	2.81	0.333	0.0533	0.0169	0.454
48.99	0.277	2.83	0.336	0.0528	0.0174	0.462
49.06	0.272	2.95	0.319	0.0506	0.0204	0.488
49.11	0.276	3.03	0.337	0.0518	0.0238	0.479
49.16	0.278	2.75	0.309	0.0482	0.0176	0.522

Chapter 3

Mercury Concentration and Isotopic Composition in Modern and Pre-Industrial Baltic Sea Sediments

Authors: Gretchen E. Gehrke, Joel D. Blum, Caroline P. Slomp

Submitted to Chemical Geology

Abstract

Mercury (Hg) is a toxic trace metal with natural and anthropogenic sources. In this study we assess Hg concentrations and Hg isotopic compositions in Baltic Sea sediments that pre-date and post-date the Industrial Revolution to evaluate the extent to which recent anthropogenic inputs of Hg or concurrent expansion of marine hypoxia have altered the Hg content of the sediments. Surface sediments are enriched in Hg by factors of 2.8 - 3.5 compared with pre-Industrial sediments at each of four locations. There is a subtle change in the Hg isotopic composition over time: pre-Industrial sediments have δ^{202}Hg values ranging from -1.23‰ to -0.86‰ (mean= -1.04±0.17‰), while surface sediments have higher δ^{202}Hg values ranging from -0.71‰ to -0.57‰ (mean= -0.65±0.07‰), which suggests the addition of an isotopically distinct Hg source to recent sediments. Sediment δ^{202}Hg values are

correlated with 1/Hg concentrations ($r^2 = 0.62$), suggesting the mixing of background Baltic Sea marine Hg with $\delta^{202}Hg \approx -1.2‰$ and recent anthropogenic Hg emissions with $\delta^{202}Hg \approx -0.5‰$. We suggest that elevated Hg concentrations in modern Baltic Sea sediments result in part from recent changes in productivity, but are dominated by increased industrial Hg emissions, with as much as 90% of Hg in surface sediments derived from recent industrial Hg emissions.

1. Introduction

Mercury (Hg) is a globally distributed toxic metal with natural and anthropogenic sources to atmospheric, marine and terrestrial environments. The global ocean is the largest reservoir of Hg in the actively cycling environment (Mason and Sheu, 2002), and several biogeochemical factors influence the concentration and behavior of marine Hg. Such factors include the abundance and distribution of dissolved organic matter (DOM) (Han et al., 2006), salinity (Poulain et al., 2007), and ambient water-column redox conditions (Poulain et al., 2007). In most marine surface waters, Hg is nearly completely scavenged by DOM, and is transported to depth with senescing organic matter (Han et al., 2006). Thus, the deposition of Hg to, and accumulation in, marine sediments is sensitive to primary productivity and water-column redox controls on organic matter deposition and preservation. For example, a study of mid-Pleistocene Mediterranean Sea sediments observed a 6-fold increase in sediment Hg concentration due to a shift in marine primary productivity, without any apparent additional input of Hg to the Mediterranean (Gehrke et al., 2009). However, elevated marine sediment Hg

accumulations have often been observed in locations near large Hg emissions sources such as Hg mines (Bindler et al., 2009; Foucher et al., 2009) without changes in redox conditions.

Through the nineteenth and twentieth centuries Hg concentrations in Baltic Sea sediments have increased in several basins (Beldowski and Pempkowiak, 2003; Vallius, 1999). It is unclear to what extent this increase in sediment Hg concentration has been driven by accelerated marine primary productivity with enhanced organic matter deposition and preservation, or by increased terrestrial Hg emissions in the region. Northern Europe is highly industrialized and several countries surrounding the Baltic Sea refine metals as well as combust coal and oil to supply their energy needs. Through fossil fuel combustion, metals production, and other industrial activities, it is estimated that approximately 38-45 tons of Hg were emitted annually to the atmosphere from Baltic countries in 2005-2007 (Bartnicki et al., 2008). Monitoring stations also have recorded atmospheric deposition equivalent to ~3.4 tons of Hg annually deposited to the Baltic Sea surface in recent years (Bartnicki et al., 2008; Vallius, 1999). Enhanced industrial Hg emissions could have contributed to increased sediment Hg concentrations through the Industrial Age. However, anthropogenic environmental changes in the Baltic Sea unrelated to Hg emissions could also have driven the increase in sediment Hg concentration. Through intensive manufacturing and agricultural development, several contaminants such as lead and nitrogen have been discharged into the Baltic Sea (Conley et al., 2009; Conley et al., 2002; Jonsson and Carman, 1994). Stimulated by large-scale fertilizer and soil run-off, primary productivity rates have increased in

Baltic waters (Jonsson and Carman, 1994; Struck et al., 2000), and widespread hypoxia has developed in several basins (Conley et al., 2009; Zillén et al., 2008). Large areas of the Baltic Sea have undergone eutrophication (Karlson, 2002; Zillén et al., 2008) and organic matter accumulation in sediments has increased substantially (Jonsson and Carman, 1994). Since Hg is deposited to the seafloor in association with organic matter, it is plausible that Baltic Sea eutrophication has driven sediment Hg increases regardless of concurrent industrial Hg emissions.

Using Hg stable isotope analyses, it is now possible to distinguish between primary and secondary effects of anthropogenic pollution (i.e. increased Hg emissions versus water-column eutrophication) on Hg concentrations in Baltic Sea sediments. In the last five years, sediment Hg isotope composition has been used to identify isotopically distinct sources of Hg to the sediments (Feng et al., 2010; Foucher et al., 2009; Gehrke et al., 2011; Sonke et al., 2010). It is likely that recent anthropogenic Hg emissions have different Hg isotope ratios than ambient marine Hg due to contrasts in the Hg isotopic composition measured in pre-anthropogenic sediments, ores and fossil fuel emissions (Gehrke et al., 2009; Hintelmann and Lu, 2003; Stetson et al., 2009). Additionally, there are several pathways during industrial Hg production and environmental biogeochemical cycling that result in both mass-dependent fractionation (MDF) and mass-independent fractionation (MIF). As an example of MDF, Hg that is vaporized and re-condensed during the Hg ore purification process can be enriched in lighter isotopes of Hg compared to the initial Hg ore, and residual roasted ore is enriched in heavier Hg isotopes (Stetson et al., 2009). Ambient marine Hg likely has undergone several cycles of evasion and

re-deposition while in the environment and may be enriched in lighter Hg isotopes relative to recently emitted Hg. Indeed, previous studies of marine sediments have consistently observed lower δ^{202}Hg values (i.e. lighter Hg isotopic composition) than studies of Hg ore materials (Foucher et al., 2009; Gehrke et al., 2011; Gehrke et al., 2009; Stetson et al., 2009). In addition to MDF, MIF can be caused by certain reactions affected by differences in magnetic spin and nuclear volume rather than by mass. Photochemical reduction of Hg is known to produce MIF (Bergquist and Blum, 2007), and significant MIF, reported as Δ^{199}Hg and Δ^{201}Hg, has been observed in aqueous samples exposed to light, but not in Hg ore or other geologically-derived Hg (e.g. Gehrke et al., 2011; Sherman et al., 2009). Thus, we suggest that sediment Δ^{199}Hg and Δ^{201}Hg values can be used as an ancillary parameter to evaluate the history of Hg sources in sediments.

In this study, we analyzed the Hg isotopic composition of four spatially distributed sediment cores to gain insight into the primary causes of enhanced Hg accumulation in Baltic Sea sediments. Prior to the Industrial Revolution, the primary source of Hg to Baltic sediments was likely ambient marine Hg, which is reflected in the Hg isotope composition of pre-Industrial Baltic Sea sediment. Mid-Pleistocene sapropels in the Mediterranean Sea accumulated Hg from seawater and it has been argued that the Hg isotopic composition of the sapropels reflected that of contemporary marine Hg. If the main source of Hg to modern sediments was still ambient marine Hg, we would expect that the surface Baltic Sea sediments would have similar Hg isotopic composition to pre-Industrial Baltic Sea sediments, and their isotopic composition would be expected to be similar to the marine Hg source

to mid-Pleisocene Mediterranean sapropels (Gehrke et al., 2009). In this case we would expect that the Hg concentration differences between pre- and post-Industrial sediments could be explained by eutrophication. If, however, the primary source of Hg to modern sediments is recently emitted anthropogenic Hg, it is likely that surface sediments would have Hg isotope compositions that are distinct from pre-Industrial sediments and differences in Hg concentration would, therefore, not be explained solely by eutrophication.

2. Materials and Methods

2.1 Sample collection

Four study sites in the Baltic Sea were visited during a cruise of the RV Skagerak in September 2007 (Fig. 3.1). Sample locations and water depths are listed in Table S3.1. Depth profiles of water column oxygen, salinity, and temperature were determined using a CTD (Conductivity, Temperature, Depth) probe with an SBE 43 sensor. Oxygen concentrations were additionally determined using Winkler titrations and micro-electrode analyses (Unisense) of the bottom water in sediment cores (see below). At the Northern Gotland and Landsort deep sites, a major decline in dissolved oxygen was observed at the halocline (at a water depth of ca 70-72 m) and the major part of the water column below the halocline was anoxic. At the Bornholm and Arkona Basin sites, in contrast, some oxygen was still present a few meters above the sediment-water interface and only the bottom water directly above the sediment was fully anoxic.

Sediments were collected using a multi-corer equipped with eight high-density polypropylene core tubes. Each tube collected surface sediment and 18 to 50 cm of underlying sediment. Within 2 hours of collection, cores were cut into 2 cm slices using polypropylene paddles that were cleaned with nitric acid and distilled water between sediment slices. Perimeters of sediment core slices were removed and the remaining core slice centers were placed in sterile polyethylene bags and immediately frozen at -20°C. Sediment samples were later sent on dry ice to the University of Michigan where they were stored at 0°C.

Surface sample slices (0-2 cm and 2-4 cm) were deemed modern sediments and selected for Hg analyses. In each core, samples ranging from 2-6 cm above the deepest sediment collected were selected for Hg analyses of pre-Industrial sediments. Depths of the samples analyzed are listed in Table 3.1.

2.2 Sediment organic carbon

Sediments were freeze-dried and homogenized using a boron carbide mortar and pestle. Samples of 1-2 g were combusted at 500°C for 12 hours and their weight lost on ignition (LOI) was calculated (Wang et al., 2011). Sample LOI was converted to particulate organic carbon (POC) using the empirically derived conversion for Baltic Sea sediments by Leipe et al (2011) of POC = $(0.0055*(LOI^2)) + 0.2021(LOI)$. Sample POC is reported in weight percent (%).

2.3 Hg concentration and Hg isotopic compositions

Mercury concentration and isotopic analyses were performed using modifications of methods previously described (Blum and Bergquist, 2007; Gehrke et al., 2011). Hg was volatilized from the sediment matrix of freeze-dried and homogenized samples through combustion in a two-stage furnace. A combustion furnace was ramped to a maximum temperature of 750°C, Hg(0) vapor was transported in a stream of air and O_2 through a second furnace held at 1000°C and the gas stream was then bubbled into an oxidizing solution of 1% $KMnO_4$ where Hg(0) was oxidized and retained as Hg(II). Standard reference materials NIST 1944 and NIST 2711 and procedural blanks were combusted after every four samples. Following combustion, oxidizing 1% $KMnO_4$ solutions were neutralized with NH_2OH, and Hg concentrations were determined using a Nippon Instruments MA-2000 atomic absorption spectrometer using methods previously described (Gehrke et al., 2009). Replicate combustions of samples and standard reference materials yielded Hg concentrations that agreed within 10%. Procedural blanks confirmed less than 1% Hg contribution from reagents or carry-over between samples.

Hg isotopic compositions were determined on a Nu Instruments multi-collector inductively coupled plasma mass spectrometer (MC-ICP-MS) using modifications of methods previously described (Blum and Bergquist, 2007; Gehrke et al., 2011). Briefly, neutralized sample solutions were diluted to 2-6 ng/g, and NIST 3133 standards were matched to samples by matrix and Hg concentration. Hg in solution was reduced by $SnCl_2$ online and reduced Hg(0) was separated from solution using a phase separator and introduced to the MC-ICP-MS in a stream of Ar gas (Blum and Bergquist, 2007). Instrumental mass bias was corrected using an

internal Tl standard (NIST 997) added as an aerosol to the gas stream and sample-standard bracketing was performed with NIST 3133. Additionally, on-peak zero corrections were applied to all analyses.

Mass dependent Hg isotope compositions are reported in delta notation as δ^{202}Hg in permil (‰) referenced to NIST 3133, calculated as (Blum and Bergquist, 2007):

$$\delta^{202}Hg = 1000*([(^{202}Hg/^{198}Hg)_{sample}]/[(^{202}Hg/^{198}Hg)_{3133}]-1).$$

Mass independent Hg isotope fractionation is reported as Δ^{199}Hg and Δ^{201}Hg and is calculated as (Blum and Bergquist, 2007):

$$\Delta^{199}Hg = \delta^{199}Hg_{measured} - (\delta^{202}Hg_{measured}*0.252)$$

$$\Delta^{201}Hg = \delta^{201}Hg_{measured} - (\delta^{202}Hg_{measured}*0.752).$$

In this study we characterize mass-independent Hg fractionation using Δ^{199}Hg values. Analytical uncertainty was evaluated using replicate analyses of the in-house standard UM-Almadén, and was less than ±0.14‰ (2 SD) for δ^{202}Hg, and ±0.06‰ (2 SD) for Δ^{199}Hg during each isotope measurement session. Replicate analyses of sample Hg isotope composition had larger variation, likely due to sample heterogeneity, and these deviations are listed in Table 3.1.

3. Results and Discussion

3.1 Hg concentrations in surface sediments

Mercury concentrations in Baltic Sea surface sediments (0-2cm) ranged from 51 to 142 ng/g, (Table 3.1) which is consistent with sediment Hg concentrations measured in previous studies in the Baltic Sea (18-430 ng/g) (Beldowski and

Pempkowiak, 2003, 2007; Boszke, 2005), especially in sediments at similar distances from shore (~90 ng/g) (Beldowski and Pempkowiak, 2003). Each of the sites analyzed here is located in a depositional basin of the Baltic Sea (Christiansen et al., 2002; Ehlin and Aarno, 1981; Emeis et al., 2002). Of the four sites assessed in the present study, the Northern Gotland and Bornholm Basin sites are the furthest from the mainland, at approximately 87 and 85 km from shore respectively (Fig. 3.1). These sites have the lowest surface sediment Hg concentrations of 51 and 64 ng/g, respectively (Fig. 3.2, Table 3.1). The Landsort Deep and Arkona core sites are closer to shore and nearer to major industrial cities. The Landsort Deep site is closest to shore at only 25 km off the coast of Stockholm, Sweden (Fig. 3.1) and is located at 466 m depth. This is the deepest basin of the Baltic Sea and, similar to other areas in the Baltic (Emeis et al., 2002), the Landsort deep receives suspended matter that has been transported laterally from shallower areas in addition to locally produced organic matter (Boszke and Falandysz, 1999; Ehlin and Aarno, 1981; Jonsson et al., 1990). This site in Landsort Deep has a Hg concentration of 82 ng/g. The Arkona site, with the highest surface sediment Hg concentration, 142 ng/g, is located at 46 m water depth in a shallow basin 45 km from the Swedish coast and 54 km from the German coast. This site is 85 km from the large Swedish city of Malmo and ~100 km from the large Germany cities of Greifswald and Straslund (Fig. 3.1). As previously mentioned, industrial activities emit significant amounts of Hg to the environment each year in gaseous, aqueous, and particulate form (Pacyna et al., 2006). Studies that have investigated surface sediment Hg concentrations along transects near probable Hg pollution sources along the Polish

and German coasts have observed decreasing Hg concentrations with distance from the mainland shore (Beldowski and Pempkowiak, 2003; Boszke and Falandysz, 1999; Pempkowiak et al., 1998). For example, Beldowski and Pempkowiak (2003) assessed Hg concentrations in surface sediments at the mouth of the Vistual River and extending into Gdansk Bay in the Southern Baltic Sea, and reported Hg concentrations decreasing from 424 ng/g to 81 ng/g over approximately 55 km. Previous studies have ascribed decreased Hg concentrations to lower organic matter content and to sediment dilution by other fine-grained, low-Hg materials from sources other than the industrially polluted Vistual River (Beldowski and Pempkowiak, 2003). The purpose of our study was to broadly evaluate sediment Hg accumulation in the Baltic Sea rather than investigate the spatial influence of a specific Hg source, but the surface sediment Hg concentrations measured in our study are consistent with previous Hg studies in the Baltic Sea as they show generally higher Hg concentrations nearer potential on-shore Hg pollution sources.

Several studies have noted the influence of organic matter (OM) content on Hg concentrations in sediments (de Oliveira et al., 2007; Gehrke et al., 2009; Hare et al., 2010; Outridge et al., 2007). In the Baltic Sea, Boszke and Falandysz (1999) noted a high correlation ($r^2 = 0.93$) between sediment Hg concentration and LOI in surface sediments within the Bay of Puck. It is likely that the Bay of Puck sediments that were studied had a single dominant source of both Hg and OM, and the correlation observed (Boszke and Falandysz, 1999) reflects the delivery of Hg to the seafloor in association with senescing OM (see Gehrke et al., 2009; Han et al., 2006). Surface sediments across sites in our study do not demonstrate a correlation

between Hg and OM concentration, however the locations likely have differing Hg sources and OM sources with different OM composition. When assessing surface and pre-Industrial sediment Hg-OM relations together (see section 3.2), we observe that sediments with the highest POC also have the highest Hg concentration, but that POC predicts only part of the variation in Hg concentration (Fig. 3.2, $r^2 = 0.34$). The sediments from Arkona measured in our study had lower POC than sediments from Arkona measured in other studies (Beldowski and Pempkowiak, 2007; Jilbert et al., 2011; Mort et al., 2010) probably due to sediment heterogeneity in this seasonally hypoxic zone. We suggest that Hg is indeed delivered to the seafloor in association with OM at each site, and the lack of correlation between surface sediment Hg and OM across sites reflects the different initial Hg and OM sources and loads.

3.2 Comparison of surface and pre-Industrial sediments: Hg concentration and TOC

Sediments from near the base of the multi-cores at each site were selected to represent sediments deposited prior to the Industrial Revolution in the Baltic area. Mort et al (2010) analyzed sediments from the same set of multi-corer casts at each site and dated them using ^{137}Cs and ^{210}Pb; selected core depths and sediment ages are listed in Table S3.2. To demonstrate the likelihood that the sub-surface (deep) sediments we analyzed for Hg content were deposited prior to Baltic industrialization, we also provide in Table S3.1 a rough estimate of the age of the sediments assessed in our present work by assuming a constant sedimentation rate (in cm/yr) equal to that of the oldest sediments dated by Mort et al (2010) at each

site. Based on this calculation, the deeper sediments analyzed in the Northern Gotland Basin, Bornholm Basin, and Landsort Deep Basin were likely deposited between ca. 1760 and 1810, (Table S3.1). Given that sediment burial rates typically decrease with depth due to sediment compaction, these ages are most likely maximum estimates for these sediment intervals. Thus, the deeper sediments analyzed here were most likely deposited prior to industrialization in the Baltic Sea region, which commenced ca. 1900 (Conley et al., 2009). The deepest sediments analyzed in Arkona were deposited much more recently, ca. 1942 (Mort et al., 2010), in the midst of a manufacturing surge related to military production needs for World War II.

The Hg concentration of Baltic sub-surface, pre-Industrial sediments were considerably lower than in surface sediments. In the Northern Gotland, Bornholm, and Landsort Deep Basins, pre-Industrial Hg concentrations ranged from 19 to 27 ng/g (Table 3.1). This Hg concentration of ~20 to 25 ng/g likely represents a background Hg concentration for moderately organic-rich sediments (~5% TOC) in the region. The Hg concentrations measured in mid-Industrial Era sediment from Arkona Basin were higher, ~48 ng/g (Table 3.1). The pre-Industrial sediments at each site had approximately 3 times lower Hg concentration than co-located surface sediments. Interestingly, the mid-Industrial era sediments analyzed in Arkona Basin also had ~3-times lower Hg concentration than Arkona surface sediments. The surface sediment Hg enrichment factors above pre-Industrial sediments in Northern Gotland, Bornholm, and Landsort Deep Basins, and above mid-Industrial sediments in Arkona Basin were 2.8, 2.8, 3.5, and 3.0, respectively.

Studies of high-latitude peat cores and pristine lake sediment cores in many regions also have documented Hg concentration increases of approximately 3-fold (Bindler et al., 2001; Lindeberg et al., 2006; Mason and Sheu, 2002). Those peats and lacustrine sediments have been used in support of global Hg budget reconstruction models, which have proposed that the global atmospheric Hg load has tripled since the onset of the Industrial Revolution in the nineteenth century (Mason and Sheu, 2002). However, these model estimates do not account for changes in the biogeochemical factors that can strongly influence sediment Hg concentrations. In a recent study of remote Arctic lakes sediments, Outridge et al (2007) demonstrated that changes in aquatic primary productivity could account for nearly 80% of the change in sediment Hg concentration observed through the twentieth century in their study area, suggesting an overestimation of primary anthropogenic Hg contributions (Outridge et al., 2007). Furthermore, as mentioned previously, Gehrke et al (2009) observed a 6-fold increase in Hg concentration of Mediterranean marine sediments due entirely to a shift in marine productivity and water column redox conditions.

Enhanced nutrient input from agricultural development and industrial discharge, in addition to climatic forcing, has altered the marine chemistry of the Baltic Sea substantially over the last century (Conley et al., 2009; Conley et al., 2002; Jonsson and Carman, 1994; Zillén et al., 2008). Organic matter (OM) deposition increased on average ~1.7-fold between 1920 and 1980 (Jonsson and Carman, 1994), and the hypoxic zone in the Baltic Sea has increased in area 4-fold since the 1960s (Jonsson et al., 1990). Three of the four sites selected for our analyses

(Northern Gotland, Bornholm, Landsort Deep) have been below the permanent halocline throughout history (Matthaus and Schinke, 1999), but the oxygen budget below the halocline has been altered to some extent at these locales (Nehring and Matthaus, 1991). At the Northern Gotland Basin site, POC was the same in modern and pre-Industrial sediments measured in this study (2.3 and 2.2%, respectively) (Table 1), however other studies have observed substantial organic matter enrichment in modern sediments (e.g >7% POC) (Jilbert et al., 2011; Jonsson and Carman, 1994; Mort et al., 2010), and at the Landsort Deep Basin site, modern sediment POC was significantly higher than pre-Industrial sediment (8.2 versus 2.2%) (Table 3.1). Sample availability prohibited POC analyses of Bornholm Basin sediments in this study, but Mort et al (2010) observed nearly a doubling of sediment POC in modern sediments (to >11% POC) when compared to pre-Industrial sediments in a nearby core. The sampling site in Arkona Basin, at only 47m water depth, is seasonally hypoxic (Mort et al., 2010), but surface sediments did have higher POC than the mid-Industrial Era sediments sampled (4.5 and 3.5%, respectively) (Table 3.1). With these uneven changes in POC from pre-Industrial to modern sediments in our study, it is interesting that each site had a consistent increase in Hg concentration (~3-fold). Sediment TOC may not be indicative of OM preservation through the water column and deposition to sediments; however, considerable variation in relationships between bottom water oxygen and sediment TOC has been observed (Burdige, 2007). Moreover, recent studies involving the sites discussed here have demonstrated varying degrees of sediment oxidation and C, N, and P regeneration to bottom waters (Jilbert et al., 2011; Schneider et al., 2010).

The effects of differential sediment carbon oxidation are likely sufficient to partially obscure the relationship between OM and Hg in sediments, while still maintaining a general positive relationship as is seen in Fig 3.2.

Analyses of sediment Hg concentration and POC demonstrated enrichments in surface sediment Hg and an inconclusive relationship between Hg concentration and sediment POC (Fig 3.2). Thus, these analyses did not adequately discern the cause of surface sediment Hg enrichment in Baltic Sea sediments as either enhanced atmospheric Hg deposition or more efficient marine Hg deposition due to marine eutrophication.

3.3 Hg isotopic composition in Baltic Sea sediment

Sediment Hg isotope compositions were assessed in order to decipher whether or not pre-Industrial and modern Baltic Sea sediments had the same source of Hg. Pre-Industrial sediments had average δ^{202}Hg values of -1.15 ± 0.23‰, -1.23 ± 0.16‰, -0.86 ± 0.10‰, and -0.92 ± 0.06‰ in Northern Gotland, Bornholm, Landsort Deep, and Arkona Basins, respectively (Table 3.1, Fig. 3.3). With an average of -1.04 ± 0.18‰, these pre-Industrial Baltic Sea sediments have similar δ^{202}Hg values to pre-anthropogenic marine sediments from the Mediterranean Sea (-0.91 ± 0.15‰) (Gehrke et al., 2009). Baltic Sea pre-Industrial sediments also have Δ^{199}Hg values that range from 0.08 to 0.20‰ (0.13 ± 0.04‰) (Fig. 3.3, Table 3.1), which are similar to Mediterranean Sea pre-anthropogenic sapropel Δ^{199}Hg values that range from 0.09 to 0.17‰ (0.11 ± 0.03‰) (Gehrke et al., 2009). It is therefore likely that the pre-Industrial sediments have a predominantly marine source of Hg.

Baltic Sea surface sediments had significantly higher δ^{202}Hg values than their pre-Industrial counterparts. Surface sediments had δ^{202}Hg values ranging from -0.71‰ to -0.57‰, averaging -0.65 ± 0.07‰ (Table 3.1, Fig. 3.3). It is likely that the higher δ^{202}Hg values observed in surface sediments results from the influence of another Hg source in addition to the marine Hg source inferred by the Hg isotopic composition of pre-Industrial sediments. Isotopic studies of Hg in sediments near chemical manufacturing facilities, smelting, and mining operations have observed higher δ^{202}Hg values in sediments with the highest contribution of anthropogenic contaminant Hg (Estrade et al., 2011; Foucher et al., 2009; Gehrke et al., 2011; Sonke et al., 2010; Stetson et al., 2009), and it is likely that the higher δ^{202}Hg value Hg source contributing to Baltic Sea surface sediments is due to inputs of anthropogenic Hg. Additionally, Baltic Sea surface sediments have lower Δ^{199}Hg values than pre-Industrial sediments, ranging from 0.05 to 0.09‰, averaging 0.07 ± 0.02‰ (Table 3.1, Fig. 3.3). Significant Δ^{199}Hg values have not been observed in metallic Hg or Hg ore (Gehrke et al., 2011; Liu et al., 2011; Sonke et al., 2010; Stetson et al., 2009), and since positive Δ^{199}Hg values in marine sediments may be produced by photo-reduction of aqueous Hg (Bergquist and Blum, 2007), it is reasonable that recently emitted Hg would have lower Δ^{199}Hg values than ambient marine Hg. Thus we suggest that lower Δ^{199}Hg values in surface sediments are consistent with an anthropogenic Hg source to Baltic Sea surface sediments.

Plotting δ^{202}Hg values versus the inverse of the Hg concentration ($1/Hg_T$) can elucidate mixing relationships between multiple Hg sources. Pre-Industrial and surface sediment values produce a linear mixing curve on this plot consistent with two end-member sources (Fig 3.4). Extrapolation of a linear regression ($r^2 = 0.62$) indicates that the two end-member sources have δ^{202}Hg values of -1.17‰ and -0.53‰, which we suggest represent the Baltic Sea pre-Industrial marine Hg isotopic composition and a minimum estimate of anthropogenic Hg contamination δ^{202}Hg values, respectively. Interestingly, metallic Hg produced from the largest Hg deposit in the world in Almadén, Spain has a δ^{202}Hg value of ~-0.55‰ (Blum and Bergquist, 2007). While it is unlikely that Hg from Almadén directly contributes to Hg contamination in the Baltic Sea, it is possible that Hg from Almadén has been used in industrial operations in the Baltic and that Hg ore deposits in the Baltic area have similar composition to Hg ore from Almadén.

Pre-Industrial Baltic Sea sediments have a range of δ^{202}Hg values (-1.34 to -0.79‰) that encompass the linearly extrapolated end-member δ^{202}Hg value (-1.17‰) and the marine δ^{202}Hg value estimated from mid-Pleistocene sapropels (-0.91‰) (Gehrke et al., 2009). It is possible that the pre-Industrial Baltic Sea sediments reflect a range of Hg isotopic composition of Baltic Sea marine Hg under various water column conditions that preclude a homogeneous marine Hg composition. The pre-Industrial sediments of Landsort Deep Basin have the same δ^{202}Hg values as pre-anthropogenic sapropels in the Mediterranean Sea (δ^{202}Hg = -0.91 ± 0.15 ‰) (Gehrke et al., 2009), and these relatively high δ^{202}Hg values could

reflect the influence of more sulfidic bottom waters (Fonselius and Valderrama, 2003) than the other sites investigated. To account for the potential influence of water column heterogeneity on sediment δ^{202}Hg values, we suggest that the pre-Industrial Baltic Sea marine Hg δ^{202}Hg values ranged from about -1.17 to -0.91‰.

Assuming that the Hg in Baltic Sea sediments derives from mixtures of marine Hg with a δ^{202}Hg value between -1.17 and -0.91‰, and anthropogenic Hg with a δ^{202}Hg value of -0.53‰, we estimate the percent contribution of anthropogenic Hg in each Baltic Sea sediment sample. It is important to note that the estimates derived by these calculations using a marine end-member of -1.17‰ yield the maximum estimate of anthropogenic Hg because the δ^{202}Hg value calculated for natural background marine Hg (-1.17‰) is lower than several samples that likely derive Hg solely from a natural background source (e.g. pre-Industrial Baltic Sea sediments). With that caveat, surface sediments have an estimated 71-93% Hg contribution from anthropogenic sources (Table 3.1). Identifying a δ^{202}Hg value of -0.91‰ as the marine Hg end-member source (and an anthropogenic Hg source with -0.53‰) produces a more conservative estimate where surface sediments have an estimated 31-53% Hg contribution from anthropogenic sources (Table 3.1). These estimates demonstrate that recent anthropogenic emissions have had a significant influence on Hg deposition to the Baltic Sea floor.

4. Conclusions

Sediment Hg concentrations have increased by a factor of 3 since the onset of the Industrial Era in at least four depositional basins in the Baltic Sea: Northern Gotland, Bornholm, Landsort Deep, and Arkona. Pre-Industrial sediments had Hg concentrations with a narrow range from 19 to 25 ng/g and had ~2% POC. In each basin, Hg concentrations increased by factors of 2.8 to 3.5, to surface sediments with Hg concentrations of 51 to 142 ng/g. The Hg isotopic compositions of pre-Industrial and modern sediments were significantly different, averaging δ^{202}Hg values of -1.06 ± 0.18‰ and -0.65 ± 0.07‰. Assessment of the Hg concentration and Hg isotopic composition of the sediments indicates that Baltic Sea sediments obtained Hg from two dominant sources, natural background marine Hg and an anthropogenic contaminant Hg with a δ^{202}Hg value of about –0.53‰. Using a simple mixing scheme between these two end-members, we estimate that modern sediments derive 31-93‰ from recent anthropogenic Hg contamination. It is possible, and even likely, that Baltic Sea eutrophication has enhanced Hg accumulation in sediments during the Industrial Era, but Hg isotope compositions demonstrate the substantial direct influence of recent anthropogenic Hg contamination on sediment Hg.

Acknowledgments

The authors would like to thank the crew of RV Skagerak, and the September 2007 research team from Goteborg University and Utrecht University. The authors also thank Marcus Johnson for his expert operation of the MC-ICP-MS, and Sarah North and Eric Portenga for their Hg laboratory assistance. The authors would like to acknowledge the Baltic Sea 2020 Foundation and Netherlands Organisation for

Scientific Research (NWO Vidi) for funding of the research vessel and sampling campaign, and the John D MacArthur Professorship (to J.D. Blum) for funding laboratory analyses. This research was also partially funded by the United States Environmental Protection Agency (USEPA) under the Science to Achieve Results (STAR) Graduate Fellowship Program. The EPA has not officially endorsed this publication and the views expressed herein may not reflect those of the EPA.

References:

Bartnicki, J., Gusev, A., Aas, W., Fagerli, H., Valiyaveetil, S., 2008. Atmospheric Supply of Nitrogen, Lead, Cadmium, Mercury and Dioxines/Furanes to the Baltic Sea in 2006, in: *EMEP Centres Join Report for HELCOM, 3 ed*. HELCOM, Oslo, p. 171.

Beldowski, J., Pempkowiak, J., 2003. Horizontal and vertical variabilities of mercury concentration and speciation in sediments of the Gdansk Basin, Southern Baltic Sea. *Chemosphere* **52**, 645-654.

Beldowski, J., Pempkowiak, J., 2007. Mercury transformations in marine coastal sediments as derived from mercury concentration and speciation changes along source/sink transport pathway (Southern Baltic). *Estuarine Coastal and Shelf Science* **72**, 370-378.

Bergquist, B.A., Blum, J.D., 2007. Mass-dependent and -independent fractionation of Hg isotopes by photoreduction in aquatic systems. *Science* **318**, 417-420.

Bindler, R., Renberg, I., Appleby, P.G., Anderson, N.J., Rose, N.L., 2001. Mercury accumulation rates and spatial patterns in lake sediments from west Greenland: A coast to ice margin transect. *Environmental Science & Technology* **35**, 1736-1741.

Bindler, R., Renberg, I., Rydberg, J., Andren, T., 2009. Widespread waterborne pollution in central Swedish lakes and the Baltic Sea from pre-industrial mining and metallurgy. *Environmental Pollution* **157**, 2132-2141.

Blum, J.D., Bergquist, B.A., 2007. Reporting of variations in the natural isotopic composition of mercury. *Analytical and Bioanalytical Chemistry* **388**, 353-359.

Boszke, L., 2005. Fluxes and balance of mercury in the inner Bay of Puck, southern Baltic, Poland: an overview. *Oceanologia* **47**, 325-350.

Boszke, L., Falandysz, J., 1999. Mercury in the surface layer of the sediment in the Puck Bay. *Bromatologia i Chemia Toksykologiczna* **32**, 69-74.

Burdige, D.J., 2007. Preservation of organic matter in marine sediments: Controls, mechanisms, and an imbalance in sediment organic carbon budgets? *Chemical Reviews* **107**, 467-485.

Christiansen, C., Edelvang, K., Emeis, K., Graf, G., Jähmlich, S., Kozuch, J., Laima, M., Leipe, T., Löffler, A., Lund-Hansen, L.C., Miltner, A., Pazdro, K., Pempkowiak, J.,

Shimmield, G., Shimmield, T., Smith, J., Voss, M., Witt, G., 2002. Material transport from the nearshore to the basinal environment in the southern Baltic Sea: I. Processes and mass estimates. *Journal of Marine Systems* **35**, 133-150.

Conley, D.J., Bjorck, S., Bonsdorff, E., Carstensen, J., Destouni, G., Gustafsson, B.G., Hietanen, S., Kortekaas, M., Kuosa, H., Meier, H.E.M., Muller-Karulis, B., Nordberg, K., Norkko, A., Nurnberg, G., Pitkanen, H., Rabalais, N.N., Rosenberg, R., Savchuk, O.P., Slomp, C.P., Voss, M., Wulff, F., Zillen, L., 2009. Hypoxia-Related Processes in the Baltic Sea. *Environmental Science & Technology* **43**, 3412-3420.

Conley, D.J., Humborg, C., Rahm, L., Savchuk, O.P., Wulff, F., 2002. Hypoxia in the Baltic Sea and basin-scale changes in phosphorus biogeochemistry. *Environmental Science & Technology* **36**, 5315-5320.

de Oliveira, L.C., Serudo, R.L., Botero, W.G., Mendonca, A.G.R., dos Santos, A., Rocha, J.C., Neto, F.D.C., 2007. Distribution of mercury in different soils of Amazonia's mid-Negro River basin: Influence of organic matter on Mercury's biogeochemical cycle. *Quimica Nova* **30**, 274-280.

Ehlin, U., Aarno, V., 1981. Chapter 2 - Hydrology of the Baltic Sea, *Elsevier Oceanography Series*. Elsevier, pp. 123-134.

Emeis, K., Christiansen, C., Edelvang, K., Jähmlich, S., Kozuch, J., Laima, M., Leipe, T., Löffler, A., Lund-Hansen, L.C., Miltner, A., Pazdro, K., Pempkowiak, J., Pollehne, F., Shimmield, T., Voss, M., Witt, G., 2002. Material transport from the near shore to the basinal environment in the southern Baltic Sea: II: Synthesis of data on origin and properties of material. *Journal of Marine Systems* **35**, 151-168.

Estrade, N., Carignan, J., Donard, O.F.X., 2011. Tracing and Quantifying Anthropogenic Mercury Sources in Soils of Northern France Using Isotopic Signatures. *Environmental Science & Technology* **45**, 1235-1242.

Feng, X., Foucher, D., Hintelmann, H., Yan, H., He, T., Qiu, G., 2010. Tracing Mercury Contamination Sources in Sediments Using Mercury Isotope Compositions. *Environmental Science & Technology* **44**, 3363-3368.

Fonselius, S., Valderrama, J., 2003. One hundred years of hydrographic measurements in the Baltic Sea. J. Sea Res. 49, 229-241.

Foucher, D., Ogrinc, N., Hintelmann, H., 2009. Tracing Mercury Contamination from the Idrija Mining Region (Slovenia) to the Gulf of Trieste Using Hg Isotope Ratio Measurements. *Environmental Science & Technology* **43**, 33-39.

Gehrke, G.E., Blum, J.D., Marvin-DiPasquale, M., 2011. Sources of mercury to San Francisco Bay surface sediment as revealed by mercury stable isotopes. *Geochimica Et Cosmochimica Acta* **75**, 691-705.

Gehrke, G.E., Blum, J.D., Meyers, P.A., 2009. The geochemical behavior and isotopic composition of Hg in a mid-Pleistocene western Mediterranean sapropel. *Geochimica Et Cosmochimica Acta* **73**, 1651-1665.

Han, S., Gill, G.A., Lehman, R.D., Choe, K.-Y., 2006. Complexation of mercury by dissolved organic matter in surface waters of Galveston Bay, Texas. *Marine Chemistry* **98**, 156-166.

Hare, A.A., Stern, G.A., Kuzyk, Z.Z.A., Macdonald, R.W., Johannessen, S.C., Wang, F.Y., 2010. Natural and Anthropogenic Mercury Distribution in Marine Sediments from Hudson Bay, Canada. *Environmental Science & Technology* **44**, 5805-5811.

Hintelmann, H., Lu, S.Y., 2003. High precision isotope ratio measurements of mercury isotopes in cinnabar ores using multi-collector inductively coupled plasma mass spectrometry. *Analyst* **128**, 635-639.
Jilbert, T., Slomp, C.P., Gustafsson, B.G., Boer, W., 2011. Beyond the Fe-P-redox connection: preferential regeneration of phosphorus from organic matter as a key control on Baltic Sea nutrient cycles. *Biogeosciences* **8**, 1699-1720.
Jonsson, P., Carman, R., 1994. Changes in Deposition of Organic-Matter and Nutrients in the Baltic Sea During the 20th-Century. *Marine Pollution Bulletin* **28**, 417-426.
Jonsson, P., Carman, R., Wulff, F., 1990. Laminated sediments in the Baltic - A tool for evaluating nutrient mass balances. *Ambio* **19**, 152-158.
Karlson, K., 2002. Temporal and spatial large-scale effects of eutrophication and oxygen deficiency on benthic fauna in Scandinavian and Baltic waters - A review *Oceanography and marine biology* **40**, 427-489.
Leipe, T., Tauber, F., Vallius, H., Virtasalo, J., Uscinowicz, S., Kowalski, N., Hille, S., Lindgren, S., Myllyvirta, T., 2011. Particulate organic carbon (POC) in surface sediments of the Baltic Sea. *Geo-Marine Letters* **31**, 175-188.
Lindeberg, C., Bindler, R., Renberg, I., Emteryd, O., Karlsson, E., Anderson, N.J., 2006. Natural fluctuations of mercury and lead in Greenland Lake sediments. *Environmental Science & Technology* **40**, 90-95.
Liu, J., Feng, X., Yin, R., Zhu, W., Li, Z., 2011. Mercury distributions and mercury isotope signatures in sediments of Dongjiang, the Pearl River Delta, China. *Chemical Geology* **287**, 81-89.
Mason, R.P., Sheu, G.R., 2002. Role of the ocean in the global mercury cycle. *Global Biogeochemical Cycles* **16**, 1093-1106.
Matthaus, W., Schinke, H., 1999. The influence of river runoff on deep water conditions of the Baltic Sea. *Hydrobiologia* **393**, 1-10.
Mort, H.P., Slomp, C.P., Gustafsson, B.G., Andersen, T.r.J., 2010. Phosphorus recycling and burial in Baltic Sea sediments with contrasting redox conditions. *Geochimica et Cosmochimica Acta* **74**, 1350-1362.
Nehring, D., Matthaus, W., 1991. Current trends in hydrographic and chemical parameters and eutrophication in the Baltic Sea. *Internationale Revue Der Gesamten Hydrobiologie* **76**, 297-316.
Outridge, P.M., Sanei, H., Stern, G.A., Hamilton, P.B., Goodarzi, F., 2007. Evidence for control of mercury accumulation rates in Canadian High Arctic lake sediments by variations of aquatic primary productivity. *Environmental Science & Technology* **41**, 5259-5265.
Pacyna, E.G., Pacyna, J.M., Steenhuisen, F., Wilson, S., 2006. Global anthropogenic mercury emission inventory for 2000. *Atmospheric Environment* **40**, 4048-4063.
Pempkowiak, J., Cossa, D., Sikora, A., Sanjuan, J., 1998. Mercury in water and sediments of the southern Baltic Sea. *Science of the Total Environment* **213**, 185-192.
Poulain, A.J., Garcia, E., Amyot, M., Campbell, P.G.C., Raofie, F., Ariya, P.A., 2007. Biological and chemical redox transformations of mercury in fresh and salt waters of the high arctic during spring and summer. *Environmental Science & Technology* **41**, 1883-1888.

Schneider, B., Nausch, G., Pohl, C., 2010. Mineralization of organic matter and nitrogen transformations in the Gotland Sea deep water. *Marine Chemistry* **119**, 153-161.
Sherman, L.S., Blum, J.D., Nordstrom, D.K., McCleskey, R.B., Barkay, T., Vetriani, C., 2009. Mercury isotopic composition of hydrothermal systems in the Yellowstone Plateau volcanic field and Guaymas Basin sea-floor rift. *Earth and Planetary Science Letters* **279**, 86-96.
Sonke, J.E., Schaufer, J., Chmeleff, J., Audry, S., Blanc, G., DuprÈ, B., 2010. Sedimentary mercury stable isotope records of atmospheric and riverine pollution from two major European heavy metal refineries. *Chemical Geology* **279**, 90-100.
Stetson, S.J., Gray, J.E., Wanty, R.B., Macalady, D.L., 2009. Isotopic Variability of Mercury in Ore, Mine-Waste Calcine, and Leachates of Mine-Waste Calcine from Areas Mined for Mercury. *Environmental Science & Technology* **43**, 7331-7336.
Struck, U., Emeis, K.C., Voss, M., Christiansen, C., Kunzendorf, H., 2000. Records of southern and central Baltic Sea eutrophication in delta C-13 and delta N-15 of sedimentary organic matter. *Marine Geology* **164**, 157-171.
Vallius, H., 1999. Anthropogenically derived heavy metals in recent sediments of the Gulf of Finland, Baltic Sea. *Chemosphere* **38**, 945-962.
Wang, Q.R., Li, Y.C., Wang, Y., 2011. Optimizing the weight loss-on-ignition methodology to quantify organic and carbonate carbon of sediments from diverse sources. *Environmental Monitoring and Assessment* **174**, 241-257.
Zillén, L., Conley, D.J., Andrén, T., Andrén, E., Björck, S., 2008. Past occurrences of hypoxia in the Baltic Sea and the role of climate variability, environmental change and human impact. *Earth-Science Reviews* **91**, 77-92.

Figure 3.1:

Figure 3.1: Map of the Baltic Sea with sample locations marked. Italic numbers indicate the water depth at each site.

Figure 3.2:

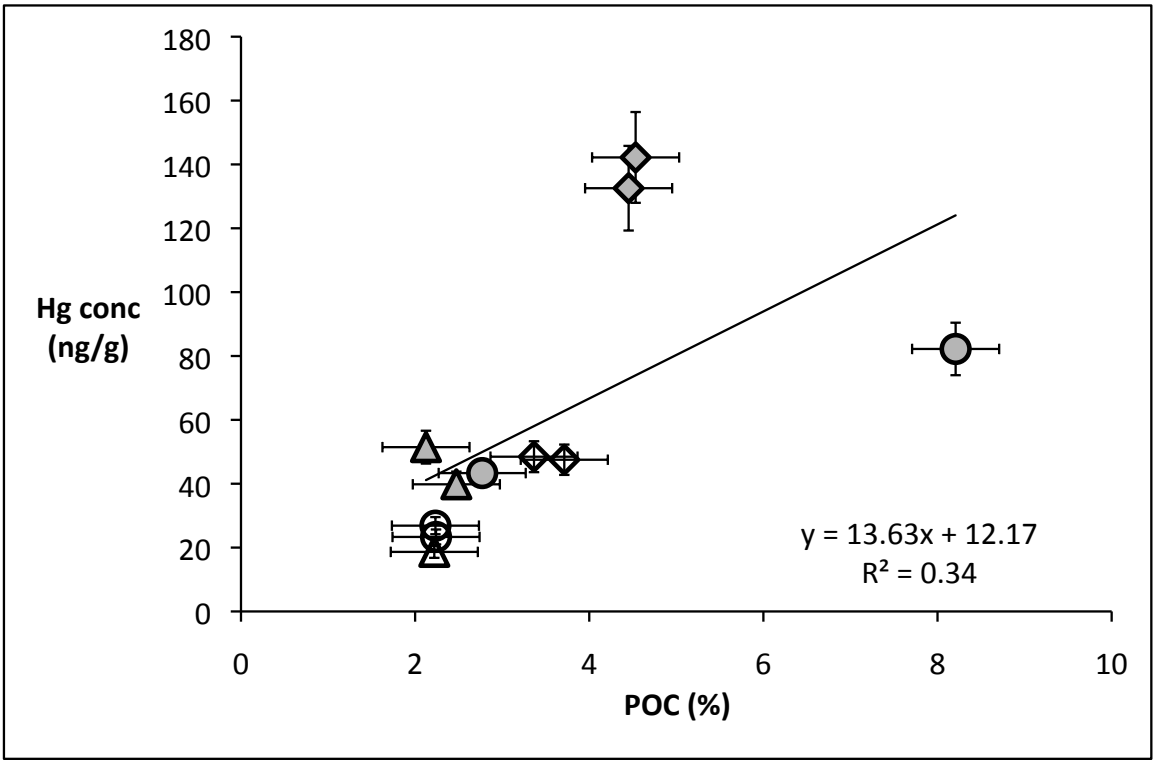

Figure 3.2: Sediment Hg concentration versus particulate organic carbon (POC). Triangles, squares, circles, and diamonds represent Northern Gotland, Bornholm, Landsort Deep, and Arkona Basins, respectively. Open symbols are pre-Industrial in age and shaded symbols are recent surface sediments.

Figure 3.3:

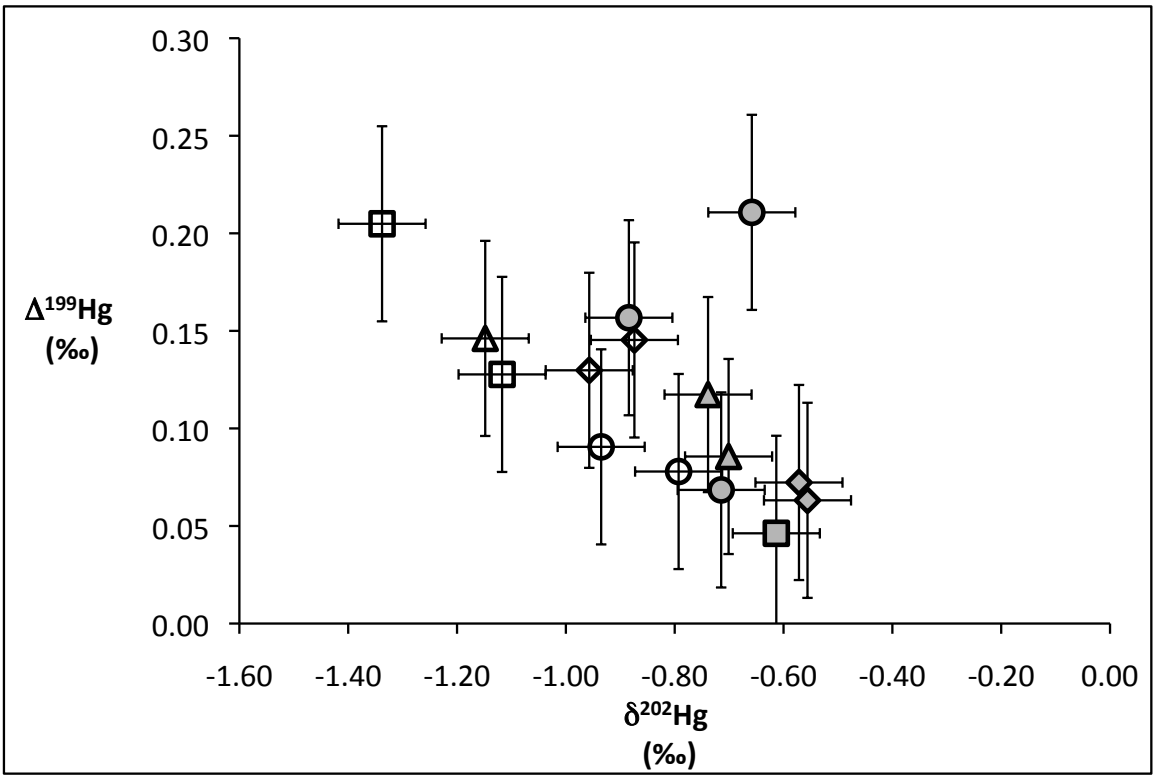

Figure 3.3: Hg isotopic composition of Baltic Sea sediments. Triangles, squares, circles, and diamonds represent Northern Gotland, Bornholm, Landsort Deep, and Arkona Basins, respectively. Open symbols are pre-Industrial in age and shaded symbols are recent surface sediments.

Figure 3.4

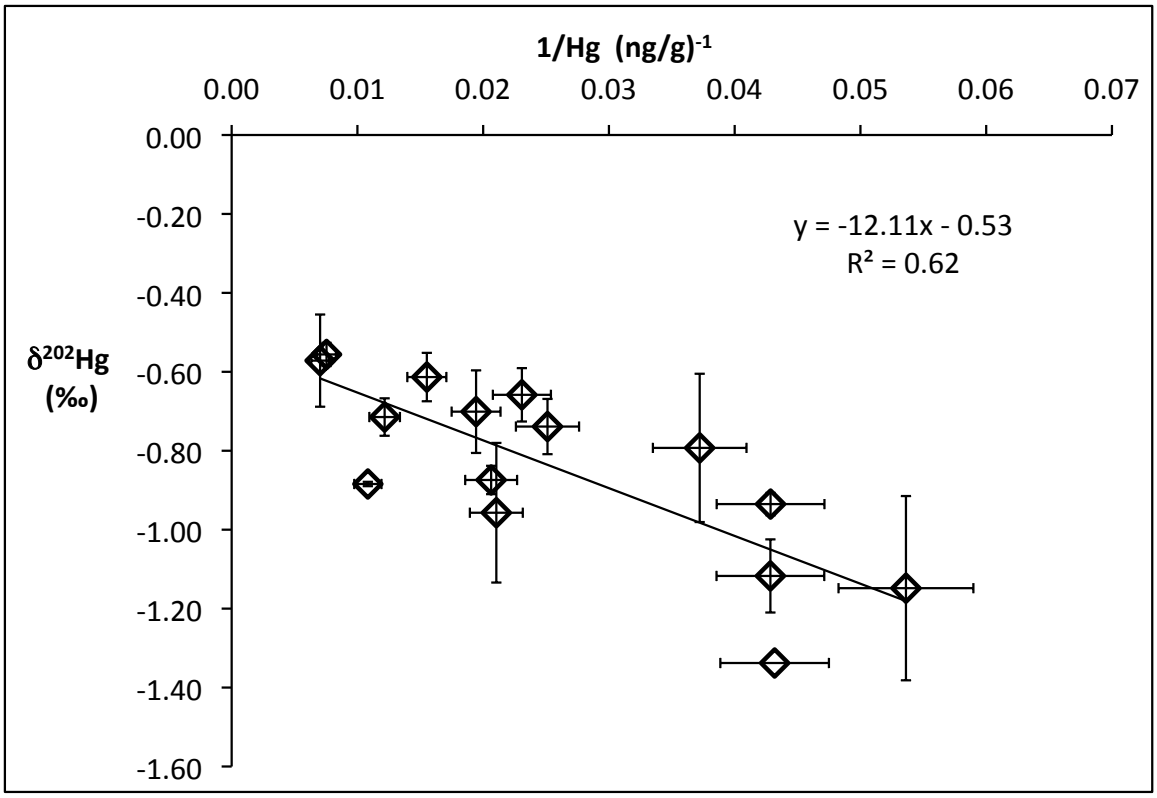

Figure 3.4: Hg isotopic composition and inverse Hg concentration. Linear regression of sediment $\delta^{202}Hg$ values and $1/Hg_T$ reflect a mixing line between two end member sources with $\delta^{202}Hg$ values of -1.17% and -0.53%, representing background marine Hg and anthropogenic Hg, respectively.

Table 3.1: Baltic Sea sediment Hg concentration and isotopic composition, particulate organic carbon, estimated date and industrial Hg pollution

Sample Site	Sediment Depth (cm)	Hg_T (ng/g)	$\delta^{202}Hg$ (‰)	1 SD (‰)	$\Delta^{199}Hg$ (‰)	1 SD (‰)	POC (%)	Age (year CE)	Anthropogenic Contribution (%)
Northern Gotland	0-2	51.5	-0.70	0.10	0.09	0.05	2.1	2005	33 - 73
Northern Gotland	2-4	39.8	-0.74	0.07	0.12	0.06	2.5	1998	27 - 67
Northern Gotland	32-34	18.7	-1.15	0.23	0.15	0.03	2.2	1765	0 - 3
Bornholm Basin	0-2	64.4	-0.61	0.07	0.05	0.03	-	2004	46 - 87
Bornholm Basin	24-26	23.2	-1.34	0.07	0.20	0.03	-	1803	0
Bornholm Basin	26-30	23.3	-1.12	0.09	0.13	0.04	-	1778	0 - 8
Landsort Deep	0-2	82.2	-0.71	0.05	0.07	0.08	8.2	1996	31 - 71
Landsort Deep	2-4	92.3	-0.88	0.07	0.16	0.03	-	1984	4 - 45
Landsort Deep	40-42	26.9	-0.79	0.19	0.08	0.04	2.2	1811	18 - 59
Landsort Deep	42-44	23.3	-0.94	0.03	0.09	0.04	2.2	1802	0 - 37
Arkona Basin	0-2	142.2	-0.57	0.12	0.07	0.05	4.5	2006	53 - 93
Arkona Basin	2-4	132.6	-0.56	0.07	0.06	0.07	4.5	2003	55 - 96
Arkona Basin	24-26	48.5	-0.87	0.07	0.15	0.11	3.4	1945	6 - 46
Arkona Basin	26-28	47.5	-0.96	0.18	0.13	0.06	3.7	1940	0 - 33

- did not measure sediment POC

Table S3.1: Sample sites and sediment core data

Site Name	Location	Water Depth (m)	Sediment Depths Processed (cm)	Sedimentation Rate[1] (cm/yr)	Avg. Deep Sample Year* (year CE)
Northern Gotland	58°52.759 N 20°18.569 W	175	0-2, 2-4, 32-34	0.13	1765
Bornholm Basin	55°15.160 N 15°59.160 W	89	0-2, 24-26, 26-30	0.12	1794
Landsort Deep Basin	58°35.341 N 18°13.963 W	466	0-2, 2-4, 40-42, 42-44	0.21	1805
Arkona Basin	54°58.504 N 14°05.937 W	47	0-2, 2-4, 24-26, 26-28	0.40	1942

(1) Mort et al., 2010

* Sediment dates estimated by applying the sedimentation rate determined by Mort et al. (2010) from the deepest sediment dated by Mort et al. (2010) to the average depth of the "deep" samples processed in the present study. For further details: see text.

Table S3.2: Baltic Sea sediment samples dated in Mort et al. (2010)

Site Name	Sample Depth (cm)	Date Deposited (year CE)
Northern Gotland	0.8	2006
	2.5	2001
	10.5	1927
Bornholm Basin	0.5	2006
	2.8	1998
	15.0	1886
Landsort Deep Basin	0.8	2002
	2.5	1985
	15.0	1935
Arkona Basin	0.5	2007
	2.5	2004
	26.0	1942

Chapter 4

Sources of mercury to San Francisco Bay surface sediment as revealed by mercury stable isotopes

Authors: Gretchen E. Gehrke, Joel D. Blum, Mark Marvin-DiPasquale

Citation: Gehrke, G. E., Blum, J. D., Marvin-DiPasquale, M., 2011. Sources of mercury to San Francisco Bay surface sediments as revealed by mercury stable isotopes. *Geochimica et Cosmochimica Acta* **75**, 691-705.

Abstract

Mercury (Hg) concentrations and isotopic compositions were examined in shallow-water surface sediment (0-2 cm) from San Francisco (SF) Bay to determine the extent to which historic Hg mining contributes to current Hg contamination in SF Bay, and to assess the use of Hg isotopes to trace sources of contamination in estuaries. Inter-tidal and wetland sediment had total Hg (Hg_T) concentrations ranging from 161 to 1529 ng/g with no simple gradients of spatial variation. In contrast, inter-tidal and wetland sediment displayed a geographic gradient of $\delta^{202}Hg$ values, ranging from -0.30‰ in the southern-most part of SF Bay (draining the New Almaden Hg District) to -0.99‰ in the northern-most part of SF Bay near the

Sacramento-San Joaquin River Delta. Similar to SF Bay inter-tidal sediment, surface sediment from the Alviso Slough channel draining into South SF Bay had a δ^{202}Hg value of -0.29‰, while surface sediment from the Cosumnes River and Sacramento-San Joaquin River Delta draining into north SF Bay had lower average δ^{202}Hg values of -0.90‰ and -0.75‰, respectively. This isotopic trend suggests that Hg-contaminated sediment from the New Almaden Hg District mixes with Hg-contaminated sediment from a low δ^{202}Hg source north of SF Bay. Tailings and thermally decomposed ore (calcine) from the New Idria Hg mine in the California Coast Range had average δ^{202}Hg values of -0.37 and +0.03‰, respectively, showing that Hg calcination fractionates Hg isotopes resulting in Hg contamination from Hg(II) mine waste products with higher δ^{202}Hg values than metallic Hg(0) produced from Hg mines. Thus, there is evidence for at least two distinct isotopic signals for Hg contamination in SF Bay: Hg associated with calcine waste materials at Hg mines in the Coast Range, such as New Almaden and New Idria; and Hg(0) produced from these mines and used in placer gold mines and/or in other industrial processes in the Sierra Nevada region and SF Bay area.

1. Introduction

San Francisco (SF) Bay is one of the largest and most anthropogenically impacted estuaries in North America (Nichols et al., 1986), and mercury (Hg) contamination in the SF Bay area has been acknowledged for more than 150 years (Conaway et al., 2007). More than 90% of Hg mined in the United States between

1850 and 1980 came from the California Coast Range (Choe, 2004), much of which is in the extensive SF Bay watershed. Hundreds of Hg mines, including the two most productive in North America (New Almaden and New Idria, which together produced 50% of the Hg mined in the United States) are located within 230 km of SF Bay (Cargill et al., 1980; Rytuba, 2000). The New Almaden Mercury District had active operations from 1847 through 1973, and is located within the watershed that contributes to the Guadalupe River, which flows into the southern end of SF Bay. The New Almaden mines and processing plants were located ~30 km south of SF Bay, with at least one off-site Hg processing plant that operated closer to the Bay. Sediment transport from Hg mining areas and leaching of Hg mine waste into waterways have been implicated as an important source of Hg contamination in the history of SF Bay (Conaway et al., 2004; Ganguli, 2000; Marvin-DiPasquale and Cox, 2007; Rytuba, 2000; Thomas et al., 2002). However, the extent to which legacy Hg mining operations continue to be a source of Hg contamination to surface sediment is debated, since significant quantities of Hg also have been introduced to SF Bay from other sources (Conaway et al., 2008). Much of the metallic Hg(0) produced at Hg mines was transported and used in placer gold (Au) mining operations in the Sierra Nevada Range, northern Coast Range, and Klamath-Trinity mountains , which are within the northern SF Bay watershed (Nriagu, 1994). Beginning in the mid-19th century, hydraulic Au mining delivered significant amounts of Hg-contaminated sediment to SF Bay, with an estimated 260 x10^6 m^3 of mining debris deposited between 1856 and 1887 (Jaffe et al., 1998; Jaffe et al., 2007). Natural and anthropogenic modifications to SF Bay and its tributaries have enhanced sediment

erosion in parts of SF Bay and exposed previously buried sediment (Fregoso et al., 2008; Jaffe and Foxgrover, 2006; Jaffe et al., 2007; Nichols et al., 1986; van Geen and Luoma, 1999), much of which has higher Hg concentrations than the sediment that is currently being transported to the bay (Hornberger et al., 1999). More recently, the development of petroleum refineries, chemical manufacturing, and chloralkali production has led to additional environmental Hg contamination in SF Bay. As a highly urbanized estuary, contaminants also enter SF Bay through wastewater effluents, urban runoff, and shipyard pollution (Flegal et al., 1990; Nichols et al., 1986). The relative contribution of these various sources has not been determined.

Total Hg concentrations (Hg_T) are generally elevated in surface sediment throughout San Francisco Bay, often 5 times higher than typical pre-Industrial SF Bay background levels of 60-80 ng/g (Conaway et al., 2007; Conaway et al., 2004; Hornberger et al., 1999). Past studies have indicated that there are a few centers of enhanced Hg contamination, namely in sediment near Alviso Slough and San Pablo Bay (Conaway et al., 2007; Hornberger et al., 1999; Thomas et al., 2002). The spatial distribution of Hg concentrations in SF Bay sediment is not necessarily indicative of the source of that Hg, however (Conaway et al., 2008), because of extensive post-depositional sediment mobility.

Recent studies demonstrate that Hg isotopes can be used to identify different sources of Hg and track them in the environment (Biswas et al., 2008; Carignan et al., 2009; Foucher and Hintelmann, 2006; Foucher et al., 2009; Stetson et al., 2009). Mercury has seven stable isotopes with masses 196, 198, 199, 200, 201, 202 and

204 amu. Multi-collector inductively coupled plasma mass spectrometry (MC-ICP-MS) techniques employed in this study (Lauretta et al., 2001; Bergquist and Blum, 2007) allow for measurement of the Hg isotopic composition with a precision of <±0.1‰ (Blum and Bergquist, 2007). Fractionation of Hg isotopes has been observed for multiple biogeochemical processes including volatilization, diffusion, photochemical reduction, microbial reduction, and microbial methylation (Bergquist and Blum, 2007; Estrade et al., 2009; Kritee et al., 2007; Rodriguez-Gonzalez et al., 2009; Zheng et al., 2007; Zheng and Hintelmann, 2009). Variations in the isotopic composition of Hg in the environment have been observed in coal, peat, soil, sediment, rock, lichen, moss, fish and snow (Bergquist and Blum, 2007; Biswas et al., 2008; Carignan et al., 2009; Foucher et al., 2009; Gehrke et al., 2009; Jackson et al., 2004; Jackson et al., 2008; Sherman et al., 2010; Sherman et al., 2009; Smith et al., 2008; Zambardi et al., 2009). In 2006 a preliminary study of variations in Hg isotopic composition in SF Bay sediment was performed, but the results were inconclusive due to a limited number of samples and high analytical uncertainty (2SD = ±0.16 to ±0.30‰) (Foucher and Hintelmann, 2006). Methods have now advanced to the point that Hg isotope ratios can be measured with high precision (2SD = ±0.08‰), sufficient to identify variations in the Hg isotopic composition of environmental samples such as SF Bay sediment.

The goal of the current study was to utilize high-precision stable Hg isotope measurements in sediments to ascertain the relative importance of legacy Hg mining sources to SF Bay at the present time. We analyzed mine tailings and thermally decomposed ore (calcine) from the non-remediated New Idria Hg Mine to

provide an estimate of the Hg isotopic composition of cinnabar (HgS) in the California Coast Range and test whether or not calcined Hg ore and unprocessed ore are isotopically distinct. We then analyzed sediment from Alviso Slough (which connects the Guadalupe R. to South SF Bay and represents the drainage channel from New Almaden Hg mining District to the Bay) to observe a potential Hg mining signal in surface sediment near SF Bay. To evaluate the influence of legacy Hg mining in New Almaden on SF Bay, we analyzed surface (0-2 cm) inter-tidal sediment from twenty coves and embayments along shores throughout SF Bay and wetland sediment from nine seasonal wetlands flanking South SF Bay (Fig. 4.1). The sampling locations selected allow for comparison of sediment with different plausible sources of Hg contamination, including legacy mining sites, as well as contemporary urban runoff, municipal waste discharge, and industrial and chemical production.

2. Methods and Materials

2.1 Sample collection and storage

Inter-tidal surface (0-2 cm) sediment was collected at twenty locations throughout SF Bay (Tables 4.1, 4.2, Fig. 4.1). Surface coastal wetland sediment was collected at nine locations in South SF Bay (Grenier et al., 2010), three locations in the Yolo Bypass Water Conservation Area near Sacramento, and two locations in marshes around the Cosumnes River (Marvin-DiPasquale et al., 2007) (Tables 4.1, 4.2). Subaqueous surface sediment was collected at two locations in the Cosumnes

River channel (Marvin-DiPasquale et al., 2007). All samples were collected using trace-metal clean methods (Marvin-DiPasquale and Cox, 2007). At each SF Bay location, four surface samples were collected at 90° intervals around the perimeter of a circle with 2 m radius using acid-cleaned polycarbonate pipe and plastic spatulas. The four samples at each site were combined into a single plastic bag, kept on dry ice in the field, and transferred to freezers (-5°C) within 6 hours of collection. Samples were logged and sub-sampled at the USGS laboratory (Menlo Park, CA) under anaerobic conditions.

Mine debris samples were collected at the New Idria Hg Mine (San Benito Co., CA) in the Diablo Range of the California Coast Ranges, approximately 230 km south of SF Bay. Two representative samples of mine tailings were collected from a tailings debris pile (3641519°N, 120.67289°W) and one sample was also collected from a calcine debris pile (36.41558°N, 120.67314°W). Polished-section optical analysis verified the occurrence of cinnabar (α-HgS) in tailings and a combination of cinnabar (α-HgS) and metacinnabar (β-HgS) in calcine samples. Samples were stored in opaque low-density polyethylene bottles at ambient temperature until analysis at the University of Michigan.

Fifteen cores were taken in the Alviso Slough, using previously described methods, for a project conducted by the USGS (Marvin-DiPasquale and Cox, 2007), and two of these cores were selected for Hg isotope analyses in this study. The cores are from the mainstream Channel (core AS-C) and from the vegetated marsh (right bank) that fringed the channel (AS-M); Hg isotopic analyses were performed

on three sediment depth intervals in each core. Cores were collected using a hand-operated piston corer, characterized, and sub-sampled at the USGS (Menlo Park, CA). Sediment was stored in a 3°C refrigerator until receipt at the University of Michigan, where samples were stored in a -20°C freezer.

Sample types and locations are distinguished by prefixes, followed by the approximate distance of each sample from the mouth of Alviso Slough (see below). **I**nter-**T**idal sediment sample names have the prefix **IT**, **W**et**L**and sediment samples have the prefix **WL**, **C**osumnes **R**iver **M**arsh and **R**iver sample names have the prefix **CR(M)** and **CR(R)**, and **Y**olo **B**ypass Wetland Conservation Area sample names have the prefix **YB**. **N**ew **I**dria **T**ailings and **C**alcine sample codes have the prefix **NI-T** and **NI-C**. **A**lviso **S**lough **C**hannel and **M**arsh sediment core samples have the prefix **AS-C** and **AS-M** and a suffix of the sample sediment depth interval in cm.

To assess the spatial distribution of Hg concentrations and isotopic compositions, the distance of each sample location from the mouth of Alviso Slough was estimated. The reference location of the mouth of Alviso Slough is marked as the solid star in Fig. 4.1. A curved line designates the center of SF Bay, with perpendicular line segments extending from the center-line to sampling locations. The approximate distance of each sample location was estimated from the mouth of Alviso Slough following the center-line to the intersection of the perpendicular line extending to each sample location.

2.2 Hg concentration and isotope analysis

Sediment samples were freeze-dried, and 0.5 to 1.5 g sub-samples were ground in an agate mortar and pestle. New Idria tailings and calcine samples were ground in an alloy tool steel mortar and pestle. Hg was thermally volatilized as Hg(0) at 750°C in a two-stage furnace. Following combustion Hg vapor was carried by a stream of air and O_2 through the second stage of the furnace at 1000°C and into an oxidizing solution of 1% $KMnO_4$ where it was retained in solution as Hg(II). Procedural blanks and the standard reference material SRM 1944 (New York-New Jersey Waterway Sediment) were analyzed for quality control assessment. Prior to isotope analysis, 1% $KMnO_4$ solutions containing the separated Hg were partially neutralized using NH_2OH. The Hg concentrations of 1% $KMnO_4$ solutions were analyzed using a Nippon Instruments MA 2000 atomic absorption spectrometer by methods previously described (Gehrke et al., 2009). Process replicates of quality control standards agreed with reference Hg concentrations within ±10%, indicating >90% recovery during combustion and trapping. All Hg concentrations are reported in ng/g dry weight. Inter-tidal and wetland sediment sample Hg concentrations were verified by independent acid-digest and atomic fluorescence spectroscopy at the USGS (Menlo Park, CA) and agreed within ±15%.

Hg isotopic compositions were determined using a Nu Instruments multi-collector inductively coupled plasma mass spectrometer (MC-ICP-MS) by methods previously described (Bergquist and Blum, 2007; Lauretta et al., 2001). Partially neutralized trapping solutions were diluted to a uniform Hg concentration of 5 ng/g for analysis. Using a continuous flow system, Hg(II) was reduced by addition of $SnCl_2$, evolved Hg(0) was separated from solution using a frosted-tip phase

separator, a Tl aerosol was produced by a desolvating nebulizer and added to the gas stream, and the sample was introduced to the MC-ICP-MS. Instrumental mass-bias was corrected using the internal Tl standard (NIST 997) and sample-standard bracketing using NIST SRM-3133 at the same concentration and in the same matrix as the samples. Additionally, on-peak zero corrections were applied. Mass-dependent Hg isotope compositions are reported as δ^{202}Hg in permil (‰), referenced to SRM-3133 (Blum and Bergquist, 2007) and are calculated as:

$$\delta^{202}Hg = 1000*([(^{202}Hg/^{198}Hg)_{sample}]/[(^{202}Hg/^{198}Hg)_{3133}]-1).$$

Mass independent Hg isotope fractionation is reported as Δ^{199}Hg and Δ^{201}Hg in permil (‰) and following (Blum and Bergquist, 2007) is calculated as:

$$\Delta^{199}Hg = \delta^{199}Hg_{measured} - (\delta^{202}Hg_{measured}*0.252)$$

$$\Delta^{201}Hg = \delta^{201}Hg_{measured} - (\delta^{202}Hg_{measured}*0.752)$$

The δ^{202}Hg and Δ^{199}Hg values of samples are discussed in the text, used in figures, and listed in tables. Sample Δ^{201}Hg values are listed in tables, and although the total variation is only twice the analytical uncertainty, they are well correlated with Δ^{199}Hg values ($\Delta^{199}Hg/\Delta^{201}Hg = 0.79\pm 0.13$; $r^2 = 0.58$). Analytical uncertainty was evaluated using replicate analyses of the in-house standard UM-Almadén, and replicate analyses of standard reference materials, with average analytical precision of at least ±0.07‰ (2 SD) for δ^{202}Hg, and ±0.04‰ (2 SD) for Δ^{199}Hg and Δ^{201}Hg. The reproducibility of sample Hg isotope compositions was evaluated by replicate combustion of samples and replicates yielded δ^{202}Hg values within analytical

uncertainty of ±0.08‰ (2 SD), and Δ^{199}Hg and Δ^{201}Hg values within the analytical uncertainty of ±0.06‰ (2 SD) (Table 4.1).

3. Results and Discussion

3.1 Hg concentration and isotopic composition in mine waste

In order to assess the Hg isotopic composition associated with Hg mine waste from the California Coast Range, we collected calcine and tailings samples from the New Idria Hg Mine in the Diablo Range, 230 km south of SF Bay. The New Almaden Hg Mine, 30 km south of SF Bay, has been extensively remediated since 1998 and surface samples of mine debris are not available for collection. The New Idria Hg Mine operated from 1854 to 1972 and, unlike the New Almaden Hg Mine, it has not been remediated since its closure in 1972 (Ganguli, 2000). Both the New Idria and New Almaden Hg deposits are associated with silica-carbonates in Franciscan sandstone and Panoche shale units of the Franciscan complex (Boctor et al., 1987; Smith et al., 2008). Therefore, we anticipate similar Hg isotopic compositions in ore mined in both Hg mining districts, and similar relationships between the isotopic composition of Hg in calcine versus tailings.

At approximately 50 Hg mines in the SF Bay watershed, including New Almaden and New Idria, cinnabar (α-HgS) and metacinnabar (β-HgS) ores were mined. Ore was roasted in rotary furnaces at 600-700°C to convert Hg(II) to gaseous Hg(0) (Boctor et al., 1987; Rytuba, 2000), producing thermally decomposed ore known as calcine. The volatilized Hg(0) was condensed and the metallic

mercury was sold for use in Au placer mines and other industries. Calcination was an incomplete process, often leaving substantial Hg (20-150 μg/g) in the roasted end-product, which can be a considerable source of Hg contamination in Hg mining areas (Kim et al., 2004; Rytuba, 2000). The incomplete processes employed in the production of metallic Hg are predicted to have significantly fractionated the Hg isotopes, with lower δ^{202}Hg values in the volatilized Hg(0) and higher δ^{202}Hg values in the residual Hg(II) (Koster van Groos et al., 2007). Additionally, evaporation of liquid Hg yields residual liquid Hg with higher δ^{202}Hg values than Hg(0) vapor (Estrade et al., 2009). A recent study investigated Hg isotopes in various materials in Hg mining districts in Texas and Nevada and observed that calcines had higher δ^{202}Hg values than cinnabar collected from the same mines, likely attributable to the volatilization of lighter isotopes of Hg, with residual HgS enriched in heavier isotopes (Stetson et al., 2009).

We found a significant difference in Hg isotopic composition between unroasted and roasted material at the New Idria mine. The two unroasted tailings samples (wall rock containing a small amount of HgS) had variable Hg concentrations of 71.3 and 46.5 μg/g, but similar δ^{202}Hg values of -0.43 and -0.33‰ and Δ^{199}Hg values of +0.05 and +0.06‰ (Table 4.2). The calcine sample (roasted ore) had a much higher Hg_T of 976 μg/g, a considerably higher δ^{202}Hg value of +0.03‰, but a similar Δ^{199}Hg value (-0.01‰), compared to the tailings (Table 4.2).

It follows that the metallic Hg(0) produced in the Coast Ranges Hg mines, and subsequently used in the Sierra Nevada placer Au mines, is expected to have lower

δ^{202}Hg values than residual HgS in the calcines left behind at the Coast Range Hg mine dumps. It is estimated that ~10% of the liquid Hg(0) sent to Au mines and other industrial plants was lost during transport and storage (Nriagu and Wong, 1997). At the placer Au mines, liquid Hg(0) was used in sluice boxes to amalgamate fine Au particles for physical separation from sediment (Alpers et al., 2005; Nriagu and Wong, 1997). On average, 10-30% of Hg was lost from the sluices (Alpers et al., 2005), and hydraulic mining debris is a large source of Hg contamination in impacted areas downstream of Au mines (Alpers et al., 2005; Hunerlach et al., 2005; Jasinski, 1995). Additionally, there has been extensive use of Hg(0) in chemical and material production plants and refineries in the area. Based on available evidence we suggest that metallic Hg produced and used at Au mines and other industries should have lower δ^{202}Hg values than the Hg emanating from tailings or calcine at legacy Hg mines. To test this idea, we analyzed Hg isotopes in sediments from Alviso Slough, which drains the New Almaden Hg mining district and from the Cosumnes River, which flows through former Au mining districts in the Sierra foothills (Fig. 4.1).

3.2 Hg concentration and isotopic composition in Alviso Slough sediment core

The New Almaden Mining District has been implicated as a major source of Hg contamination to South SF Bay, particularly in sediment deposited during the period of active Hg mining and processing (Marvin-DiPasquale and Cox, 2007; Thomas et al., 2002). The two sediment cores that we analyzed from Alviso Slough,

which connects the Guadalupe River to South SF Bay, exhibited elevated Hg_T (409-4011 ng/g) concentrations (Table 4.2) consistent with the previous analyses of these cores and thirteen other cores from the slough (Marvin-DiPasquale and Cox, 2007). Of the three depth intervals analyzed, the lowest concentrations were found in the near surface sediments in both the main channel core (AS-C[0-7.5]) (508 ng/g) and in the vegetated marsh core (AS-M[0-17]) (409 ng/g) (Table 4.2). The highest concentrations were found in the intermediate depth cores in both the main channel core (AS-C[109-123]) (4011 ng/g) and in the vegetated marsh core (AS-M[174-199]) (2346 ng/g) (Table 4.2). Sediment chronology was determined on a core in Triangle Marsh approximately 3 km northeast of the Alviso Slough cores that indicated sediment at 35 cm depth was deposited circa 1983 (Conaway et al., 2004). The New Almaden Hg mine was operational through the mid 1970s, and it is likely that the deeper sediment depth intervals of the Alviso Slough cores analyzed in this study were deposited prior to mine closure. Analyses of sediment loss on ignition (LOI) and grain size found lower LOI percentage and larger average grain size in most subsurface sediment (Marvin-DiPasquale and Cox, 2007), which is consistent with a higher proportion of mining debris (James, 2005; Osleger et al., 2008). Thus it is likely that these deeper sediment layers were deposited while mining operations were active at multiple ore processing facilities in the New Almaden mining District. Previous studies of the Guadalupe River and Lower South SF Bay have suggested that surface sediments have lower Hg concentrations due to restoration efforts and gradual environmental recovery after closure of the New Almaden Hg mine in 1973 (Conaway et al., 2004; Thomas et al., 2002).

The Hg isotopic composition variation with depth in the Alviso Slough sediment cores suggests a lower contribution of Hg from calcine associated with New Almaden Hg mine waste in recently deposited sediment. The lowest δ^{202}Hg values measured in the two cores were in the near surface sediments (-0.29 and -0.32‰) and higher δ^{202}Hg values were measured deeper in the cores (Table 4.2, Fig. 4.2). The highest δ^{202}Hg value measured in the channel core (+0.29‰) was in the deepest sample (AS-C[183-196]), whereas the highest δ^{202}Hg value measured in the marsh core (+0.20‰) was in the intermediate depth sample (AS-M[100-131]) (Table 4.2, Fig. 4.2). As discussed above, calcines have been observed to have higher δ^{202}Hg values than unroasted ore (Stetson et al., 2009; this study). It is likely that Hg in the intermediate and deepest sediment samples from Alviso Slough results, at least in part, from calcine waste emanating from New Almaden Hg mine. Several of these deeper sediment δ^{202}Hg values, however, are even higher than the single calcine δ^{202}Hg value (+0.03‰) that we measured. The calcine analysis that we carried out was from the New Idria Mine and clearly did not sample the range of δ^{202}Hg values for calcine that might exist in the New Almaden Mining District. We speculate that some calcines have δ^{202}Hg values as high or higher than the highest sediment value (+0.29‰). Stetson et al (2009) measured calcines from mines in Texas and Nevada with δ^{202}Hg >1‰ higher than accompanying ores. Lower δ^{202}Hg values in more recent sediments are consistent with a lower contribution of Hg from mine calcines to the total Hg in the Alviso Slough surface sediment. Smith et al. (2008) measured the Hg isotopic composition of sedimentary and volcanic rocks in the San Francisco Bay area, which contribute to the background sediment of San

Francisco Bay, and reported an average δ^{202}Hg value of -0.63 ± 0.20‰. A mixture of Hg from calcine with high δ^{202}Hg values mixing with ambient Hg from sediments or with unroasted mine tailings could produce the isotopic depth profiles observed (Fig. 4.2).

3.3 Hg concentration and isotopic composition in Cosumnes River and Yolo Bypass

Suspended sediment from hydraulic Au mining has been proposed to have been a dominant source of sediment to the Sacramento-San Joaquin delta and San Francisco Bay during the active mining period (Dunlap et al., 2008; Jaffe et al., 2007). Studies of Hg concentrations in water and sediment of the Sacramento river system have implicated this historic Au mining as a major source of Hg contamination (Domagalski, 1998; Domagalski, 2001; Hornberger et al., 1999). Depth profiles of sediment cores analyzed in other studies show that Hg_T peaked in sediment deposited during the height of Au mining operations and has decreased in recent decades to surface sediment concentrations averaging 200-300 ng/g in the Sacramento - San Joaquin Delta (Conaway et al., 2003; Hornberger et al., 1999) and lower Hg concentrations (100-180 ng/g) in riverbed sediment within the Sacramento River system (Domagalski, 2001; Heim et al., 2007). The Cosumnes River, a tributary to the Sacramento - San Joaquin Delta, flows undammed through former Au mining regions in the western Sierra-Nevada foothills. We analyzed surface sediment from the Cosumnes River main channel and fringing emergent

marshes in order to evaluate the Hg isotopic composition of Hg associated with Au mining in this area.

The Hg_T measured in this study was similar to previous studies (Conaway et al., 2003; Hornberger et al., 1999), with Hg_T concentrations of 65-114 ng/g in the Cosumnes River main channel (CR(Ra), CR(Rb)) and 303-419 ng/g in the fringing marsh (CR(Ma), CR(Mb)) (Table 4.2). Surface sediments from the river channel (CR(Ra), CR(Rb)) have δ^{202}Hg values of -0.91 and -0.88‰ and the marsh samples (CR(Ma) and CR(Mb)) both have δ^{202}Hg values of -0.75‰. These values in the Cosumnes River are significantly lower than those measured in surface sediments from the Alviso Slough (-0.29‰ and -0.32‰). As discussed in section 3.1, it is likely that Hg(0) used in Au mining operations had lower δ^{202}Hg values than HgS ore and calcine. Therefore, lower δ^{202}Hg values in sediment from the Cosumnes River are consistent with a Hg source emanating from Hg used in placer Au mines, and it is likely that the δ^{202}Hg value of the metallic Hg used is approximately -0.9‰.

Northwest of the Cosumnes River, the Yolo Bypass Water Conservation Area (YBWCA) is within the Sacramento River watershed, downstream of both Sierra Nevada and Coast Range Au and Hg mine sources. Surface sediment (0-2 cm) from wetlands in YBWCA (YB(a), YB(b), YB(c)) had a mean Hg_T of 135 ± 14 ng/g. The δ^{202}Hg values of YBWCA rice fields are similar but slightly higher than those measured in the Cosumnes River marshes (-0.70 ± 0.04‰, n=3). It is likely that the higher δ^{202}Hg values in YBWCA result from a mixture of metallic Hg with low δ^{202}Hg

values used in industry and placer Au mines, and HgS ore and calcine waste with higher δ^{202}Hg values from nearby Hg mines.

3.4 Hg concentrations in San Francisco Bay inter-tidal and wetland surface sediments

All intertidal surface sediment samples analyzed in this study had Hg_T elevated above pre-Industrial San Francisco Bay sediment concentrations (60-80 ng/g) (Conaway et al., 2004; Hornberger et al., 1999), and ranged from 161 to 846 ng/g (Fig. 4.3, Table 4.2). Previous studies have suggested that legacy Hg mining in the New Almaden mining District is the dominant source of Hg contamination to South SF Bay, as evidenced by elevated Hg_T in sediment and wildlife (Ackerman et al., 2008; Conaway et al., 2004; Greenfield et al., 2005; Greenfield and Jahn, 2010). However, there are several other locations in SF Bay with equally elevated Hg_T (Marvin-DiPasquale et al, 2003a). Atmospheric deposition of Hg is believed to be relatively uniform throughout SF Bay (Tsai and Hoenicke, 2001) and does not adequately explain spatial variation in sediment Hg_T concentrations. Moreover, mass-balance calculations suggest that atmospheric deposition is most likely a minor source of Hg to sediments (Macleod et al., 2005), with annual atmospheric Hg deposition to SF Bay an order of magnitude less than the Hg load entering SF Bay in suspended sediment alone (Abu-Saba and Tang, 2000; David et al., 2009; Tsai and Hoenicke, 2001). Our analyses do not show a simple spatial pattern in surface inter-

tidal sediment Hg_T in SF Bay and the causes of the spatial Hg_T concentration variations observed are not readily identifiable.

Inter-tidal and wetland sediment at the southern extent of SF Bay in Guadalupe Slough (IT(-5b)) and Alviso Slough (IT(-7), IT(-5a), IT(-2), IT(-1)) downstream of the Guadalupe River had elevated Hg_T ranging from 320 to 538 ng/g. Similar sediment Hg_T in Alviso Slough and neighboring areas have been measured in previous studies of subaqueous surface sediment (Conaway et al., 2004; Marvin-DiPasquale and Cox, 2007; Thomas et al., 2002; Topping et al., 2004). Some researchers have suggested that current industrial activity is the most dominant source of Hg to surface sediment in the South Bay because the volume of freshwater input from urban runoff, municipal waste discharge, and industrial waste discharge are all higher than discharge from the Guadalupe River (Flegal et al., 1990). Runoff and discharge from Moffett Federal Airfield and the City of Sunnyvale waste-water treatment ponds in Sunnyvale Baylands Park are also potential sources of Hg contamination in Guadalupe and Alviso sloughs. Other researchers have asserted that upstream legacy Hg mining continues to be the primary source of Hg to sediment (Marvin-DiPasquale and Cox, 2007; Thomas et al., 2002). Studies of Hg_T concentration alone are inadequate to settle this debate regarding Hg sources to South Bay sediment.

Interestingly, the highest Hg_T values (679 to 1529 ng/g) were measured in sediment from the Central Bay at sites along the Martin Luther King (MLK) Regional Shoreline (Oakland, CA) (IT(42a), IT(42b)) and along Point Isabel (Richmond, CA)

(IT(62a), IT(62b)). Studies of benthic surface sediments in SF Bay had relatively lower Hg_T concentrations in the Central Bay and relatively higher Hg_T in sediments of the South Bay and San Pablo Bay (Conaway et al., 2007). It is possible that Hg has been transported south from the Sacramento-San Joaquin Delta and north from the Guadalupe Delta into the Central Bay (Jaffe et al., 2007), but there are also many additional local sources that could have contributed Hg to these sediments. Oakland and Richmond are both highly urbanized centers. The Oakland International Airport is less than 1 km from the two Oakland sites, and a municipal waste incinerator and a chloraklali plant operated in Oakland in previous decades (Conaway et al., 2008). Richmond is the site of several oil refineries and Pt. Isabel was previously used as a battery disposal area (Levine-Fricke, 1992). Sediment at the MLK Regional Shoreline is derived from a combination of Oakland watersheds and sediment transported from both the Central and the South Bay during freshwater pulses and flood/ebb tides (Ruhl et al., 2001). Sediment at Point Isabel is transported primarily from a combination of the urban watersheds of El Cerrito and Richmond and from San Pablo Bay (Ruhl et al., 2001). The Oakland and Richmond sampling site areas are highly influenced by tidal currents, and there is significant sediment re-suspension (Ruhl et al., 2001), and post-depositional vertical mixing (Fuller et al., 1999). These and other physical processes may resurface deeper sediment containing more elevated Hg_T concentrations (Fuller et al., 1999).

More than 85 km north from the Guadalupe delta and to the north, San Pablo Bay tidal sediment had Hg_T concentrations ranging from 286 to 314 ng/g near the Petaluma River and San Pedro Peninsula (IT(85), IT(87), IT(90), IT(91)). Other

studies have measured similar Hg_T in subaqueous sediment in this area (Conaway et al., 2004; Heim et al., 2007; Hornberger et al., 1999; Marvin-DiPasquale et al., 2003a; Marvin-DiPasquale et al., 2003b). Several small historical Au and Hg mines operated in watersheds that contribute to the Petaluma and Napa rivers, which flow into San Pablo Bay, although the majority of sediment load to this region is delivered from the Sacramento and San Joaquin Rivers, which drain the Sierra Nevada (Conaway et al., 2007; Hornberger et al., 1999; Jaffe et al., 2007; Marvin-DiPasquale et al., 2003a). San Pablo Bay experienced substantial sediment accumulation during the late 19th century due to hydraulic Au-mining discharge (Jaffe et al., 2007) and there is currently a significant input of older sediment eroded from upstream drainage basins (Fuller et al., 1999).

To the east of San Pablo Bay, sediment in Suisun Bay near the Carquinez Strait (IT(110), IT(115), IT(119)) had Hg_T ranging from 161 to 253 ng/g, and sediment at Kirker Creek near the confluence of the San Joaquin and Sacramento River (IT(143)) had 327 ng/g Hg_T (Fig. 4.3). Au mining was prevalent in watersheds contributing to the San Joaquin and Sacramento Rivers, and has been implicated as a source of Hg and other contaminants to both deep and surface sediment (Bouse et al., 2010; Dunlap et al., 2008; Hornberger et al., 1999; Jaffe et al., 2007). However, there is also extensive industrial activity in this region, including a large chemical production plant near the site at Kirker Creek, several petroleum refineries, and a waste-water treatment plant near the Carquinez Strait. With this multitude of potential Hg sources, it is interesting that sediment in the Carquinez Strait had the lowest Hg_T measured in this study. It is possible that the relatively lower Hg

concentrations in Carquinez Strait derive from differences in sediment deposition dynamics in the narrow passage, but it is also possible that much of the Hg emitted in the area is not locally deposited to sediments. Significant spatial variation in sediment Hg_T has been observed in previous studies and attributed to geochemical and physical sediment characteristics (Conaway et al., 2003; Heim et al., 2007). Complex regions like Suisun Bay and the Carquinez Straight highlight the need for greater understanding of the Hg sources and sediment transport dynamics that contribute to sediment Hg contamination.

Seasonally-flooded wetland surface sediment in the South Bay had slightly lower Hg_T than most inter-tidal sediment, ranging from 188 to 292 ng/g. The one sample collected from the fringing vegetated marsh along Alviso Slough (WL(-3)) had higher Hg_T (292 ng/g) than the other wetland sediments (215 ± 20 ng/g), all of which were collected 7-25 km north of the mouth of Alviso Slough. There is no other apparent pattern of Hg_T, regardless of geographic location or assumed point-sources including urban runoff from Newark, Union City, Redwood City, and several wetlands reconstruction projects. SF Bay wetlands have been suggested as important areas of Hg bioaccumulation in local aquatic food webs (Ackerman et al., 2010 ; Eagles-Smith and Ackerman, 2009; Heim et al., 2007; Marvin-DiPasquale et al., 2003b), and effective ecological protection requires the reliable identification of Hg sources.

In summary, dominant sources of Hg to sediment in San Francisco Bay could not be identified solely by variations in Hg_T. Specifically, the extent to which historic

Hg mining in the New Almaden mining District currently influences sediment Hg contamination throughout San Francisco Bay is difficult to determine by the use of Hg_T values alone. Highly elevated Hg_T was measured in South SF Bay, but the highest Hg_T were found in the Oakland and Richmond urban watersheds. The variety of potential sources and lack of spatial patterns of sediment Hg_T demonstrates the need for additional tracers to determine the Hg source(s) in this study area.

3.5 Mass Dependent Hg isotopic composition of San Francisco Bay inter-tidal and wetland sediment

There is a systematic spatial gradient in Hg isotopic composition throughout San Francisco Bay. This is reflected by a strong correlation of δ^{202}Hg values with distance from the Alviso Slough ($r^2 = 0.83$), with sediment from the Lower South and South Bay ranging from -0.30 to -0.53‰ and sediment from San Pablo Bay and Suisun Bay ranging from -0.59 to -0.99‰ (Table 4.2; Fig. 4.4). Three sites in the Central Bay (IT(42a), IT(42b), IT(52)) had intermediate δ^{202}Hg values (-0.65, -0.66, -0.65‰). Sediment δ^{202}Hg values did not show a significant correlation with Hg_T ($r^2 = 0.06$; Table 4.2).

This geographic pattern in δ^{202}Hg values suggests that the sources of Hg to the sediment are regionally rather than locally controlled. Hg delivered from the Guadalupe River system is a likely dominant southern source and Hg delivered from the Sacramento-San Joaquin River system is a likely northern source. The Hg

isotopic composition of sediment does not reflect significant contributions from isotopically distinct local point-sources of Hg. While this study did not specifically analyze the Hg isotopic composition of potential Hg point sources, it is likely that Hg pollution from chlor-alkali plants, battery waste, medicinal waste, and shipyard anti-fouling paint have isotopic compositions reflecting the Hg(0) produced from Hg mines and used in industrial applications. If these individual point-sources dominated SF Bay surface sediment Hg contamination, we would expect that the sediments near each source would have Hg isotopic compositions of the metallic Hg endmember within a limited geographic area. Our results do not show significant localized variation. Rather, the gradually changing spatial pattern in sediment Hg isotopes is consistent with sediment Hg contamination derived from the mixture of Hg emanating from the Guadalupe and Hg emanating from the northern portion of SF Bay.

Inter-tidal sediments south of SF Bay in Alviso Slough (IT(-7), IT(-5a), IT(-2)) had similar Hg isotopic composition, with δ^{202}Hg values ranging from -0.36 to -0.30‰, identical to subaqueous surface sediment in the Alviso Slough channel (AS-C[0-7.5]) with a δ^{202}Hg value of -0.29‰ (Table 4.2, Figs. 4.2, 4.4). Sediment from neighboring Guadalupe Slough (IT(-5b)) and the confluence of Coyote Creek with the Alviso Slough (IT(-1)) had slightly lower δ^{202}Hg values, ranging from -0.46 to -0.43‰, and wetland sediment flanking Coyote Creek has a δ^{202}Hg value of -0.44‰. It is likely that sediment in these sloughs that neighbor Alviso Slough primarily contain Hg-contaminated sediment transported down the Guadalupe River, but they also contain some Hg from surrounding watersheds. The Great Valley sedimentary

rock sequence and Clear Lake volcanic rock sequence from the northern and central California coastline have a mean δ^{202}Hg value of -0.63 ±20‰ (Smith et al., 2008), which is likely to be a good estimate of the value for uncontaminated sediment in the San Francisco Bay area. The slightly lower δ^{202}Hg values observed in Guadalupe Slough and Coyote Creek could result from a mixture of Hg transported down the Guadalupe River and Hg from background sediment or industrial operations. Moving north, sediment in South Bay (IT(14) to IT(42b)) have lower δ^{202}Hg values ranging from -0.53 to -0.59‰ (Table 4.2, Fig. 4.4). Wetland sediments from South Bay have similar Hg isotopic composition to neighboring inter-tidal sediment, with δ^{202}Hg values ranging from -0.50 to -0.68‰, and display the same geographic gradient in Hg isotopic composition (Fig. 4.4).

Sediments in the northern parts of San Francisco Bay have lower δ^{202}Hg values than those in the South Bay. Surface sediments in the Central Bay (IT(52), IT(62a), IT(62b)) and San Pablo Bay (IT(85) to IT(91)) have δ^{202}Hg values ranging from -0.59 to -0.73‰ (Table 4.2, Fig. 4.4). To the northeast, surface sediments in the Carquinez Strait (IT(110), IT(115), IT(119)) and Suisun Bay (IT(143)) have the lowest δ^{202}Hg values, ranging from -0.74 to -0.99‰. In general, sediments further north and nearer the Sacramento-San Joaquin Delta have lower δ^{202}Hg values (Fig. 4.4), and their δ^{202}Hg values are lower than are expected for uncontaminated sediment, assumed to be ~-0.6‰ (Smith et al., 2008). The δ^{202}Hg values in Sacramento Delta sediments are similar to those measured in the Cosumnes River channel (CR(Ra,Rb) δ^{202}Hg = -0.91‰, -0.88‰; CR(Ma,Mb) δ^{202}Hg = -0.75‰) and suggest that the source of Hg in the Cosumnes River is also the source of Hg in the

Delta. Therefore, it is likely that metallic Hg is the low δ^{202}Hg (-0.9‰) source of Hg entering SF Bay via the Sacramento Delta.

The geographic pattern of Hg isotopic composition in surface sediment is moderated by sediment transport and mixing in San Francisco Bay. The Sacramento River is the primary source of sediment to Suisun and San Pablo Bay, and may supply up to 90% of the sediment entering the greater San Francisco Bay (Jaffe et al., 2007). Fifty-year reconstructions of bathymetry in South San Francisco Bay suggest a net transport of sediment from the Central Bay southward (Jaffe and Foxgrover, 2006). We suggest that contaminated sediment transported southward from the Sacramento River system, with δ^{202}Hg values of ~-0.9‰, gradually mixes with sediment from the Guadalupe River system, with δ^{202}Hg values of ~-0.3‰, producing the observed spatial δ^{202}Hg gradient through San Francisco Bay. We cannot rule out the possibility that a third source of Hg with intermediate δ^{202}Hg value (between -0.3‰ and-0.9‰) emanates from the Central Bay and mixes with the northern and southern Hg sources. Thus, our results are consistent with the mixing of two, or possibly three, dominant regional Hg sources to SF Bay.

The spatial gradient of sediment δ^{202}Hg values suggests that locations with highly elevated Hg_T (e.g. IT(42a,b), IT(42a,b), IT(-7)) are not due to the influence of contemporary local point sources. Rather, elevated Hg_T in San Francisco Bay sediment likely arises from re-suspension or exposure of buried sediments that were deposited with higher Hg_T. Numerous studies have shown that Hg_T in sediments were generally higher in past decades (Conaway et al., 2007) and natural

erosion and dredging operations in the Bay routinely expose older sediments, including those initially deposited during the peak Hg mining and hydraulic Au mining era (Fregoso et al., 2008; van Geen and Luoma, 1999). Studies have suggested that exposure of this older sediment is a significant source of Hg to the surface environment (Conaway et al., 2007; van Geen and Luoma, 1999), and the Hg isotopic data are consistent with this hypothesis.

Within sediment, it may be possible for Hg isotopes to be fractionated by biotic or abiotic reduction of Hg(II) to volatile Hg(0). If Hg volatilization were due to photoreduction, laboratory studies indicate that the observed 0.6‰ range of δ^{202}Hg values would be expected to be accompanied by a concurrent mass independent fractionation of ~0.7‰ in Δ^{199}Hg (Bergquist and Blum, 2007). There is only a 0.09‰ total range in Δ^{199}Hg values (Table 4.2) in SF Bay sediments, therefore differing degrees of Hg photoreduction cannot explain the observed Hg isotope variation in SF Bay sediments.

To assess the potential magnitude of in-situ biotic Hg isotope fractionation, which does not have accompanying shifts in Δ^{199}Hg, on the observed sediment isotope composition, we calculated the fraction of Hg(0) production and subsequent volatilization that would be required to produce a 0.1‰ shift in sediment δ^{202}Hg values. We used the Raleigh distillation equation:

$$\ln(R_{sed\text{-}R}/R_{sed\text{-}0}) = [(1/\alpha) - 1]*\ln(f)$$

where $R_{sed\text{-}R}$ is the ratio of ^{202}Hg/^{198}Hg in the remaining sediment, $R_{sed\text{-}0}$ is the ratio of ^{202}Hg/^{198}Hg in the sediment prior to any in-situ reduction and volatilization, α is

the fractionation factor between volatilized Hg and initial Hg, and f is the fraction of Hg remaining in the sediment. Using the range of published fractionation factors for Hg(II) reduction (α = 1.0004 -1.0020) (Bergquist and Blum, 2007; Kritee et al., 2008; Kritee et al., 2007), we estimate between 5 and 22% of the total Hg in sediment would need to be removed via volatilization to produce a 0.1‰ shift in the residual sediment δ^{202}Hg value. Overall, San Francisco Bay sediment had a 0.6‰ range of δ^{202}Hg values. We calculate that removal of 26-74% of sediment Hg would be required to produce the total observed range of δ^{202}Hg values. It is extremely unlikely that in-situ reduction and volatilization processes could liberate such a large proportion of Hg(0), and this process does not provide an explanation for the observed spatial trend in sediment δ^{202}Hg values. Furthermore, mass-balance estimates suggest that there is a net flux of Hg into the sediment from the water column (Macleod et al., 2005). Therefore, we suggest that the range of SF Bay sediment δ^{202}Hg values reflect the δ^{202}Hg values of Hg inputs to the Bay.

3.6 Mass-Independent Fractionation of Hg in San Francisco Bay Area Sediment

In addition to mass-dependent fractionation (MDF) of Hg isotopes, Hg isotopes undergo mass-independent fractionation (MIF), reported here as Δ^{199}Hg values. While many processes are known to cause MDF of Hg isotopes, only a few processes are known to cause MIF (Bergquist and Blum, 2007; Estrade et al., 2009). MIF is thought to result from either differences in reaction probabilities due to different magnetic spins in even and odd isotopes (magnetic isotope effect)

(Buchachenko et al., 2008) or differences in the relationship between nuclear volume and nuclear charge radii between isotopes (nuclear field shift effect) (Schauble, 2007). In the environment, MIF is believed to principally result from photochemical reduction of Hg(II) and MeHg species (Bergquist and Blum, 2007; Zheng and Hintelmann, 2009). In San Francisco Bay sediment, it is likely that the Δ^{199}Hg values reflect a combination of the Δ^{199}Hg value of the source Hg, modified somewhat by photo-reduction of dissolved Hg(II) prior to initial incorporation into sediment. The inter-tidal surface sediment had a narrow range of Δ^{199}Hg values from +0.04 to +0.14‰ (Table 4.2, Fig. 4.5; mean = 0.08±0.03‰), with no geographic pattern or correlation to point sources. The small range of Δ^{199}Hg values in the sediment sampled suggests that a only a small degree (< 10%) (Bergquist and Blum, 2007) of photochemical Hg-reduction has occurred in each location.

Wetland sediment had slightly elevated Δ^{199}Hg values compared to intertidal sediment, ranging from +0.08 to +0.16‰ (Table 4.2, Fig. 4.5; mean = 0.13±0.03‰), which suggests that a slightly greater proportion (< 15%) of the Hg(II) pool had been photochemically reduced and evaded from wetland sediment, compared to inter-tidal sediment. MIF signatures can be preserved through multiple photo-reduction cycles, producing a summed effect on the MIF measured. The wetlands seasonally flood and dry, which could promote seasonal exposure to direct sunlight. Additionally, wetlands are higher on the landscape than inter-tidal sediment and receive more prolonged daily exposure to sunlight. Enhanced seasonal and daily exposure of wetlands to sunlight could result in higher Δ^{199}Hg values. Interestingly, deep marine sediment from the mid-Pleistocene Mediterranean Sea have an average

Δ^{199}Hg value of 0.09±0.5‰ (Gehrke et al., 2009), which is similar to both wetland and inter-tidal sediment in San Francisco Bay.

4. Conclusions

Mercury concentrations (Hg_T) of surface inter-tidal and wetland sediments in San Francisco Bay were elevated above background levels, ranging from 161 to 1529 ng/g. Although sediment Hg_T concentrations were elevated, there was no consistent spatial pattern of Hg_T. The New Almaden Hg mining District historically contributed Hg contamination to SF Bay via the Guadalupe River and we measured significantly elevated Hg_T in Guadalupe Delta sediments. The highest Hg_T measured were in Oakland and Richmond in the Central Bay and the lowest Hg_T measured were in sediments along the Carquinez Strait. The spatial distribution of Hg concentration does not distinguish the primary sources of Hg to current surface sediments. To improve our ability to infer contributing Hg sources, Hg stable isotopes were employed as a method for Hg source identification and to determine the relative influence of Hg from legacy mining in the New Almaden mining District versus other Hg sources on Hg contamination in SF Bay.

The Hg isotopic composition of tailings and calcine waste from New Idria Hg Mine suggests that Hg contamination emanating from Hg mine waste is isotopically distinct from the metallic Hg produced and used in industrial and Au mining practices. Tailings had an average δ^{202}Hg value of -0.38 ± 0.07‰, and calcine had a δ^{202}Hg value of +0.03 ± 0.03‰, indicating that Hg mine waste should have higher

δ^{202}Hg values than Hg(0) products. Sediment cores from Alviso Slough have δ^{202}Hg values ranging from --0.32 to +0.29, increasing from surface sediment to deeper samples. This suggests that the Hg isotopic composition of Hg contamination entering Alviso Slough from the New Almaden Hg mining District has changed over time, but currently has a δ^{202}Hg value of ~-0.3‰. In northern watersheds of SF Bay, wetland and riverbed surface sediment from the Cosumnes River and Yolo Bypass have δ^{202}Hg values ranging from -0.91 to -0.72‰, and it is likely that a δ^{202}Hg of ~-0.9‰ is representative of Hg contamination emanating from Au mining and industrial districts in the Sierra-Nevada foothills.

There is a clear spatial pattern in the Hg isotopic composition of surface sediment in SF Bay that suggests the gradual mixing of two dominant regional Hg sources that are isotopically distinct from each other. Inter-tidal sediment has δ^{202}Hg values ranging from -0.30 to -0.99‰ with a systematic transition from higher δ^{202}Hg values in the Alviso Slough and South Bay to lower δ^{202}Hg values in San Pablo Bay and Suisun Bay in northern SF Bay. Wetland surface sediments in the South Bay have a narrow range of δ^{202}Hg values (-0.67 to -0.50‰) that are consistent with inter-tidal surface sediment from the same geographic area. The observed Hg isotopic pattern leads us to the interpretation that Hg mine waste with δ^{202}Hg ~-0.3‰ emanates from the New Almaden Hg mining District and enters the southern portions of SF Bay, and that a second Hg source, such as Hg(0) used in Au mining and industrial activities with δ^{202}Hg ~-0.9‰, emanates from the Sacramento and San Joaquin watersheds and extends into the northern SF Bay. These two sources gradually mix throughout the SF Bay system, driven by the

significant currents and tidal action. The spatial pattern of Hg isotopic composition also suggests that these two major sources, rather than multiple localized sources, dominate Hg contamination in SF Bay. This study demonstrates that Hg isotope ratios in environmental samples can be used effectively to distinguish and trace different sources of Hg contamination in coastal areas.

Acknowledgments. The authors would like to acknowledge funding provided by the Regional Monitoring Program (RMP) for Water Quality in the San Francisco Bay. The RMP is administered by the San Francisco Estuary Institute under a memorandum of understanding with the Regional Water Quality Control Board. The research described in this paper also was partially funded by the United States Environmental Protection Agency (USEPA) under the Science to Achieve Results (STAR) Graduate Fellowship Program. EPA has not officially endorsed this publication and the views expressed herein may not reflect the views of the EPA. The authors thank Darell Slotton, Shaun Ayers, Ben Greenfield, Katie Harrold, and other staff at the San Francisco Estuary Institute for study design and sample collection. We also thank Marcus Johnson for skillful maintenance and operation of the MC-ICP-MS. The manuscript benefited from helpful reviews by Dave Krabbenhoft, Ben Greenfield and two anonymous reviewers.

References

Abu-Saba, K. E. and Tang, L. W., 2000. Watershed management of mercury in the San Francisco Bay estuary: Total maximum daily load report to the US EPA. In: Board, C. R. W. Q. C. (Ed.). California Regional Water Quality Control Board

Ackerman, J. T., Eagles-Smith, C. A., Takekawa, J. Y., Bluso, J. D., and Adelsbach, T. L., 2008. Mercury concentrations in blood and feathers of prebreeding Forster's terns in relation to space use of San Francisco Bay, California, USA, habitats. *Environmental Toxicology and Chemistry* **27**, 897-908.

Ackerman, J. T., Miles, A. K., and Eagles-Smith, C. A., 2010. Invertebrate mercury bioaccumulation in permanent, seasonal, and flooded rice wetlands within California's Central Valley. *Science of the Total Environment* **408**, 666-671.

Alpers, C. N., Hunerlach, M. P., May, J. T., and Hothem, R. L., 2005. Mercury contamination from historical gold mining in California. *U.S. Geological Survey Fact Sheet* **2005-3014**, 6p.

Bergquist, B. A. and Blum, J. D., 2007. Mass-dependent and -independent fractionation of Hg isotopes by photoreduction in aquatic systems. *Science* **318**, 417-420.

Biswas, A., Blum, J. D., Bergquist, B. A., Keeler, G. J., and Xie, Z. Q., 2008. Natural Mercury Isotope Variation in Coal Deposits and Organic Soils. *Environmental Science & Technology* **42**, 8303-8309.

Blum, J. D. and Bergquist, B. A., 2007. Reporting of variations in the natural isotopic composition of mercury. *Analytical and Bioanalytical Chemistry* **388**, 353-359.

Boctor, N. Z., Shieh, Y. N., and Kullerud, G., 1987. Mercury Ores from the New Idria Mining District, California - Geochemical and Stable Isotope Studies. *Geochimica Et Cosmochimica Acta* **51**, 1705-1715.

Bouse, R., Fuller, C., Luoma, S. N., Hornberger, M. I., Jaffe, B. E., and Smith, R. E., 2010. Mercury-contaminated hydraulic mining debris in San Francisco Bay. *San Francisco Estuary and Watershed Science*.

Buchachenko, A. L., Ivanov, V. L., Roznyatovskii, V. A., Vorob'ev, A. K., and Ustynyuk, Y. A., 2008. Inversion of the sign of the magnetic isotope effect of mercury in photolysis of substituted dibenzylmercury. *Doklady Physical Chemistry* **420**, 85-87.

Cargill, S. M., Root, D. H., and Bailey, E. H., 1980. Resource estimation from historical data: Mercury, a test case. *Mathematical Geology* **12**, 489-522.

Carignan, J., Estrade, N., Sonke, J. E., and Donard, O. F. X., 2009. Odd Isotope Deficits in Atmospheric Hg Measured in Lichens. *Environmental Science & Technology* **43**, 5660-5664.

Choe, K., 2004. Sediment-water exchange of total mercury and monomethyl mercury in the San Francisco Bay-Delta. *Limnology and oceanography* **49**, 1512-1527.

Conaway, C. H., Black, F. J., Grieb, T. M., Roy, S., and Flegal, A. R., 2008. Mercury in the San Francisco estuary. *Reviews of Environmental Contamination and Toxicology,* **194**, 29-54.

Conaway, C. H., Ross, J. R. M., Looker, R., Mason, R. P., and Flegal, A. R., 2007. Decadal mercury trends in San Francisco Estuary sediments. *Environmental Research* **105**, 53-66.

Conaway, C. H., Squire, S., Mason, R. P., and Flegal, A. R., 2003. Mercury speciation in the San Francisco Bay estuary. *Marine Chemistry* **80**, 199-225.

Conaway, C. H., Watson, E. B., Flanders, J. R., and Flegal, A. R., 2004. Mercury deposition in a tidal marsh of south San Francisco Bay downstream of the historic New Almaden mining district, California. *Marine Chemistry* **90**, 175-184.

David, N., McKee, L. J., Black, F. J., Flegal, A. R., Conaway, C. H., Schoellhamer, D. H., and Ganju, N. K., 2009. Mercury Concentrations and Loads in a Large River System Tributary to San Francisco Bay, California, USA. *Environmental Toxicology and Chemistry* **28**, 2091-2100.

Domagalski, J., 1998. Occurrence and transport of total mercury and methyl mercury in the Sacramento River Basin, California. *Journal of Geochemical Exploration* **64**, 277-291.

Domagalski, J., 2001. Mercury and methylmercury in water and sediment of the Sacramento River Basin, California. *Applied Geochemistry* **16**, 1677-1691.

Dunlap, C. E., Alpers, C. N., Bouse, R., Taylor, H. E., Unruh, D. M., and Flegal, A. R., 2008. The persistence of lead from past gasoline emissions and mining drainage in a large riparian system: Evidence from lead isotopes in the Sacramento River, California. *Geochimica Et Cosmochimica Acta* **72**, 5935-5948.

Eagles-Smith, C. A. and Ackerman, J. T., 2009. Rapid Changes in Small Fish Mercury Concentrations in Estuarine Wetlands: Implications for Wildlife Risk and Monitoring Programs. *Environmental Science & Technology* **43**, 8658-8664.

Estrade, N., Carignan, J., Sonke, J. E., and Donard, O. F. X., 2009. Mercury isotope fractionation during liquid-vapor evaporation experiments. *Geochimica et Cosmochimica Acta* **73**, 2693-2711.

Flegal, A. R., Smith, G. J., Gill, G. A., Sanudowilhelmy, S., and Anderson, L. C. D., 1990. Dissolved Trace-Element Cycles in the San-Francisco Bay Estuary*11th International Symp on Chemistry of the Mediterranean : Reactivity of Chemical Species in Aquatic Environments*, Primosten, Yugoslavia.

Foucher, D. and Hintelmann, H., 2006. High-precision measurement of mercury isotope ratios in sediments using cold-vapor generation multi-collector inductively coupled plasma mass spectrometry. *Analytical and Bioanalytical Chemistry* **384**, 1470-1478.

Foucher, D., Ogrinc, N., and Hintelmann, H., 2009. Tracing Mercury Contamination from the Idrija Mining Region (Slovenia) to the Gulf of Trieste Using Hg Isotope Ratio Measurements. *Environmental Science & Technology* **43**, 33-39.

Fregoso, T. A., Foxgrover, A. C., and Jaffe, B. E., 2008. Sediment deposition, erosion, and batymetric change in central San Francisco Bay: 1855-1979. U. S. Geological Survey.

Fuller, C. C., van Geen, A., Baskaran, M., and Anima, R., 1999. Sediment chronology in San Francisco Bay, California, defined by Pb-210, Th-234, Cs-137, and Pu-239,Pu-240. *Marine Chemistry* **64**, 7-27.

Ganguli, P., 2000. Mercury speciation in drainage from the New Idria mercury mine, California. *Environmental science & technology* **34**, 4773-4779.
Gehrke, G. E., Blum, J. D., and Meyers, P. A., 2009. The geochemical behavior and isotopic composition of Hg in a mid-Pleistocene western Mediterranean sapropel. *Geochimica Et Cosmochimica Acta* **73**, 1651-1665.
Greenfield, B. K., Davis, J. A., Fairey, R., Roberts, C., Crane, D., and Ichikawa, G., 2005. Seasonal, interannual, and long-term variation in sport fish contamination, San Francisco Bay. *Science of the Total Environment* **336**, 25-43.
Greenfield, B. K. and Jahn, A., 2010. Mercury in San Francisco Bay forage fish. *Environmental Pollution* **158**, 2716-2724.
Grenier, L., Robinson, A., Bezalel, S., Melwani, A., Hunt, J., Harrold, K., Gilbreath, A., Collins, J., Marvin-DiPasquale, M., Windham-Myers, L., and Drury, D., 2010. South Baylands Mercury Project: Final Report to the California State Coastal Conservancy. *Prepared by: San Francisco Estuary Institute, U.S. Geological Survey, and Santa Clara Valley Water District*, 92.
Heim, W. A., Coale, K. H., Stephenson, M., Choe, K. Y., Gill, G. A., and Foe, C., 2007. Spatial and habitat-based variations in total and methyl mercury concentrations in surficial sediments in the san francisco bay-delta. *Environmental Science & Technology* **41**, 3501-3507.
Hornberger, M. I., Luoma, S. N., van Geen, A., Fuller, C., and Anima, R., 1999. Historical trends of metals in the sediments of San Francisco Bay, California. *Marine Chemistry* **64**, 39-55.
Hunerlach, M. P., Alpers, C. N., and Marvin-DiPasquale, M., 2005. Mercury and methylmercury distribution in sediments affected by historical gold mining, Sierra Nevada, California. *Geochimica Et Cosmochimica Acta* **69**, A705-A705.
Jackson, T. A., Muir, D. C. G., and Vincent, W. F., 2004. Historical variations in the stable isotope composition of mercury in Arctic lake sediments. *Environmental Science & Technology* **38**, 2813-2821.
Jackson, T. A., Whittle, D. M., Evans, M. S., and Muir, D. C. G., 2008. Evidence for mass-independent and mass-dependent fractionation of the stable isotopes of mercury by natural processes in aquatic ecosystems. *Applied Geochemistry* **23**, 547-571.
Jaffe, B., Smith, R. E., and Torresan, L. Z., 1998. Sedimentation and bathymetric change in San Pablo Bay, 1856-1983*Open-File Report*. United States Geological Survey.
Jaffe, B. E. and Foxgrover, A. C., 2006. Sediment Deposition and Erosion in South San Francisco Bay, California from 1956 to 2005. U. S. Geological Survey.
Jaffe, B. E., Smith, R. E., and Foxgrover, A. C., 2007. Anthropogenic influence on sedimentation and intertidal mudflat change in San Pablo Bay, California: 1856-1983. *Estuarine, Coastal and Shelf Science* **73**, 175-187.
James, L. A., 2005. Sediment from hydraulic mining detained by Englebright and small dams in the Yuba basin. *Geomorphology* **71**, 202-226.
Jasinski, S. M., 1995. The materials flow of mercury in the United States. *Resources, Conservation and Recycling* **15**, 145-179.

Kim, C. S., Rytuba, J. J., and Brown, G. E., 2004. Geological and anthropogenic factors influencing mercury speciation in mine wastes: an EXAFS spectroscopy study. *Applied Geochemistry* **19**, 379-393.

Koster van Groos, P. G., Esser, B. K., Williams, R., and Hunt, J. R., 2007. Identifying environmental sources of mercury using stable mercury isotopes, *Geochimica Et Cosmochimica Acta* **71**, A516-A516.

Kritee, K., Blum, J. D., and Barkay, T., 2008. Mercury Stable Isotope Fractionation during Reduction of Hg(II) by Different Microbial Pathways. *Environmental Science & Technology* **42**, 9171-9177.

Kritee, K., Blum, J. D., Johnson, M. W., Bergquist, B. A., and Barkay, T., 2007. Mercury stable isotope fractionation during reduction of Hg(II) to Hg(0) by mercury resistant microorganisms. *Environmental Science & Technology* **41**, 1889-1895.

Lauretta, D. S., Klaue, B., Blum, J. D., and Buseck, P. R., 2001. Mercury abundances and isotopic compositions in the Murchison (CM) and Allende (CV) carbonaceous chondrites. *Geochimica Et Cosmochimica Acta* **65**, 2807-2818.

Levine-Fricke, I., 1992. Five-Year Review of Operations and Maintenance: Point Isabel Site, Richmond, California. Catellus Development Corporation, San Francisco, CA.

Macleod, M., McKone, T. E., and Mackay, D., 2005. Mass balance for mercury in the San Francisco Bay Area. *Environmental Science & Technology* **39**, 6721-6729.

Marvin-DiPasquale, M., Agee, J., Bouse, R., and Jaffe, B., 2003a. Microbial cycling of mercury in contaminated pelagic and wetland sediments of San Pablo Bay, California. *Environmental geology* **43**, 260-267.

Marvin-DiPasquale, M., Cox, M.H. , 2007. Legacy Mercury in Alviso Slough, South San Francisco Bay, California: Concentration, Speciation and Mobility. U.S. Geological Survey Open File Report 2007-1240, Menlo Park, CA, 98 p.

Marvin-DiPasquale, M., Stewart, A. R., Fisher, N. S., Pickhardt, P. C., Mason, R. P., Heyes, A., and Windham-Myers, L., 2007. Evaluation Of Mercury Transformations and Trophic Transfer in the San Franciscoc Bay/Delta: Identifying Critical Processes for the Ecosystem Restoration Program: Final Report for Project #ERP-02-P40. *California Bay Delta Authority (CBDA)*, 40.

Marvin-DiPasquale, M. C., Agee, J. L., Bouse, R. M., and Jaffe, B. E., 2003b. Microbial cycling of mercury in contaminated pelagic and wetland sediments of San Pablo Bay, California. *Environmental Geology* **43**, 260-267.

Nichols, F. H., Cloern, J. E., Luoma, S. N., and Peterson, D. H., 1986. The Modification of an Estuary. *Science* **231**, 567-573.

Nriagu, J. O., 1994. Mercury Pollution from the Past Mining of Gold and Silver in the America. *Science of the Total Environment* **149**, 167-181.

Nriagu, J. O. and Wong, H. K. T., 1997. Gold rushes and mercury pollution, *Metal Ions in Biological Systems,* **34**.

Osleger, D. A., Zierenberg, R. A., Suchanek, T. H., Stoner, J. S., Morgan, S., and Adam, D. P., 2008. Clear Lake Sediments: Anthropogenic Changes in Physical Sedimentology and Magnetic Response. *Ecological Applications* **18**, A239-A256.

Rodriguez-Gonzalez, P., Epov, V. N., Bridou, R., Tessier, E., Guyoneaud, R., Monperrus, M., and Amouroux, D., 2009. Species-Specific Stable Isotope Fractionation of Mercury during Hg(II) Methylation by an Anaerobic Bacteria (Desulfobulbus propionicus) under Dark Conditions. *Environmental Science & Technology* **43**, 9183-9188.

Ruhl, C. A., Schoellhamer, D. H., Stumpf, R. P., and Lindsay, C. L., 2001. Combined use of remote sensing and continuous monitoring to analyse the variability of suspended-sediment concentrations in San Francisco Bay, California. *Estuarine Coastal and Shelf Science* **53**, 801-812.

Rytuba, J. J., 2000. Mercury mine drainage and processes that control its environmental impact. *Science of the Total Environment* **260**, 57-71.

Schauble, E. A., 2007. Role of nuclear volume in driving equilibrium stable isotope fractionation of mercury, thallium, and other very heavy elements. *Geochimica Et Cosmochimica Acta* **71**, 2170-2189.

Sherman, L. S., Blum, J. D., Johnson, K. P., Keeler, G. J., Barres, J. A., and Douglas, T. A., 2010. Mass-independent fractionation of mercury isotopes in Arctic snow driven by sunlight. *Nature Geoscience* **3**, 173-177.

Sherman, L. S., Blum, J. D., Nordstrom, D. K., McCleskey, R. B., Barkay, T., and Vetriani, C., 2009. Mercury isotopic composition of hydrothermal systems in the Yellowstone Plateau volcanic field and Guaymas Basin sea-floor rift. *Earth Planet. Sci. Lett.* **279**, 86-96.

Smith, C. N., Kesler, S. E., Blum, J. D., and Rytuba, J. J., 2008. Isotope geochemistry of mercury in source rocks, mineral deposits and spring deposits of the California Coast Ranges, USA. *Earth Planet. Sci. Lett.* **269**, 398-406.

Stetson, S. J., Gray, J. E., Wanty, R. B., and Macalady, D. L., 2009. Isotopic Variability of Mercury in Ore, Mine-Waste Calcine, and Leachates of Mine-Waste Calcine from Areas Mined for Mercury. *Environmental Science & Technology* **43**, 7331-7336.

Thomas, M. A., Conaway, C. H., Steding, D. J., Marvin-DiPasquale, M., Abu-Saba, K. E., and Flegal, A. R., 2002. Mercury contamination from historic mining in water and sediment, Guadalupe River and San Francisco Bay, California.

Topping, B. R., Kuwbaram, J. S., Marvin-DiPasquale, M., Agee, J. L., Kieu, L. H., Flanders, J. R., Parchaso, F., Hager, S. W., Lopez, C. B., and Krabbenhoft, D. P., 2004. Sediment remobilization of Mercury in South San Francisco Bay, California*Scientific Investigations Report*. USGS, Menlo Park, CA.

Tsai, P. and Hoenicke, R., 2001. San Francisco Bay Atmospheric Deposistion Pilot Study art 1: Mercury*San Francisco Esturay Regional Monitoring Program for Trace Substances*. San Francisco Estuary Institute, Oakland, CA.

van Geen, A. and Luoma, S. N., 1999. The impact of human activities on sediments of San Francisco Bay, California: an overview. *Marine Chemistry* **64**, 1-6.

Zambardi, T., Sonke, J. E., Toutain, J. P., Sortino, F., and Shinohara, H., 2009. Mercury emissions and stable isotopic compositions at Vulcano Island (Italy). *Earth Planet. Sci. Lett.* **277**, 236-243.

Zheng, W., Foucher, D., and Hintelmann, H., 2007. Mercury isotope fractionation during volatilization of Hg(0) from solution into the gas phase. *Journal of Analytical Atomic Spectrometry* **22**, 1097-1104.

Zheng, W. and Hintelmann, H., 2009. Mercury isotope fractionation during photoreduction in natural water is controlled by its Hg/DOC ratio. *Geochimica et Cosmochimica Acta* **73**, 6704-6715.

Figure 4.1: Locations for all samples analyzed in this study. The large map shows inter-tidal and wetland surface sediment sample locations. The detailed map inset in the middle-right shows the Lower South Bay sample locations. The regional map inset in the lower-left shows the New Idria Hg Mine, Cosumnes River, and Yolo Bypass sample locations as well as the general location of the New Almaden Hg Mine. The star marks the mouth of the Alviso Slough; a curved line depicts the approximate center-line of San Francisco Bay. Perpendicular lines are drawn between sample locations and the SF Bay center-line to approximate the distance of each sampling location from the mouth of Alviso Slough. Open triangles indicate inter-tidal sediment sampling locations, open squares indicate wetland locations, and the open circles indicate the location of Alviso Slough cores. Sediment sample names have the following prefixes: **I**nter-**T**idal (**IT**), **W**et**L**and (**WL**), **C**osumnes **R**iver **M**arsh and **R**iver [**CR(M)** and **CR(R)**], **Y**olo **B**ypass (**YB**), **N**ew **I**dria **T**ailings and **C**alcine (**NI-T and NI-C**) and **A**lviso **S**lough **C**hannel and **M**arsh (**AS-C** and **AS-M)**.

Figure 4.1

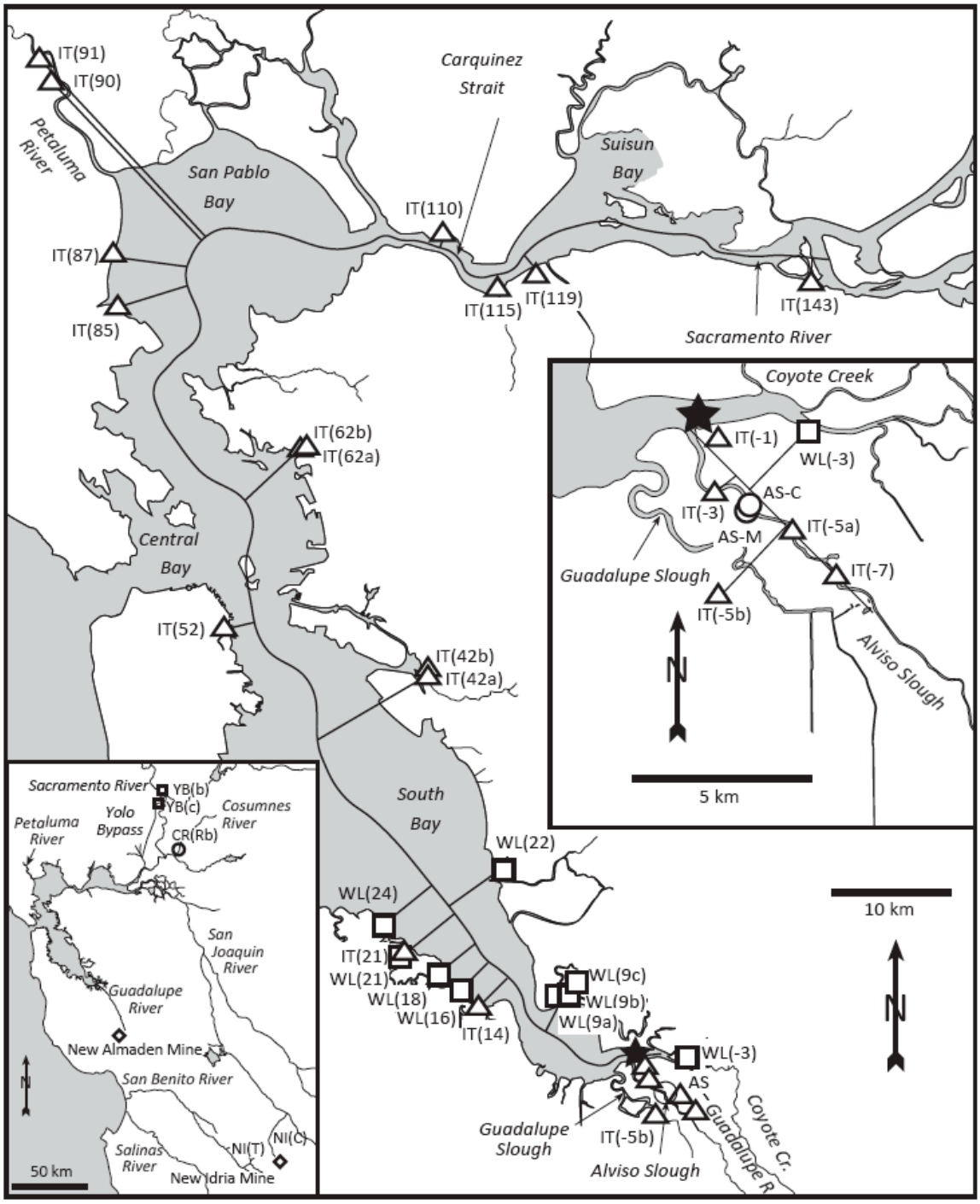
IT(91)
IT(90)
Petaluma River
San Pablo Bay
Carquinez Strait
Suisun Bay
IT(110)
IT(87)
IT(85)
IT(115)
IT(119)
IT(143)
Sacramento River
IT(62b)
IT(62a)
Central Bay
IT(52)
IT(42b)
IT(42a)
South Bay
WL(22)
WL(24)
IT(21)
WL(21)
WL(18)
WL(16)
IT(14)
WL(9c)
WL(9b)
WL(9a)
WL(-3)
AS
IT(-5b)
Guadalupe Slough
Alviso Slough
Coyote Cr.
Guadalupe R.
10 km
Coyote Creek
IT(-1)
WL(-3)
AS-C
IT(-3)
AS-M
IT(-5a)
IT(-7)
Guadalupe Slough
IT(-5b)
Alviso Slough
5 km
Sacramento River
YB(b)
YB(c)
Yolo Bypass
Cosumnes River
Petaluma River
CR(Rb)
San Joaquin River
Guadalupe River
New Almaden Mine
San Benito River
Salinas River
NI(T)
NI(C)
New Idria Mine
50 km

Figure 4.2

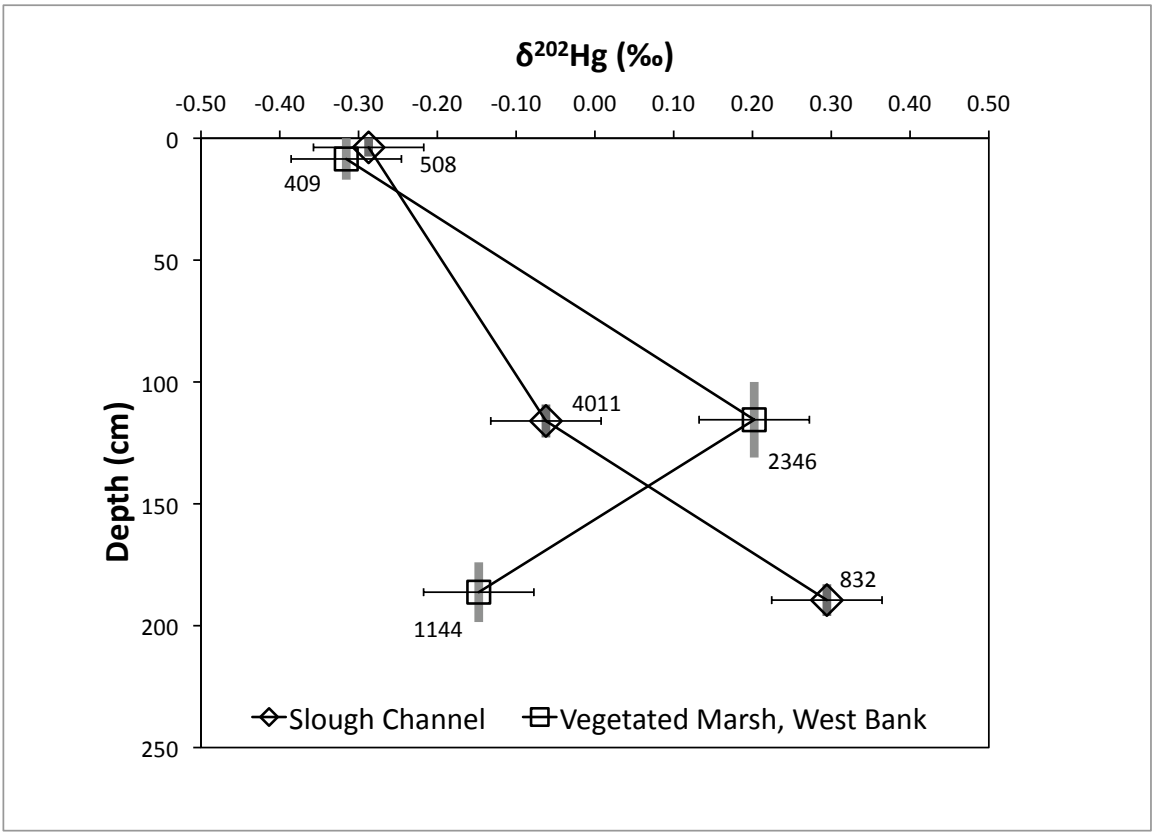

Figure 4.2: Depth profile of $\delta^{202}Hg$ in sediment cores from the Alviso Slough channel center and vegetated marsh along the west bank. The New Almaden Hg Mine is 30 km upstream of the sampling location (Fig. 4.1). The depth plotted for each symbol is the average depth of each sediment sample analyzed and grey vertical bars indicate the sample depth interval that is integrated by each core sample. Sample Hg_T concentrations (ng/g) are labeled next to each symbol. The $\delta^{202}Hg$ in each core is higher at depth compared to the near surface sample, indicating a higher $\delta^{202}Hg$ in older sediment, likely associated with greater influence from mining activity.

Figure 4.3

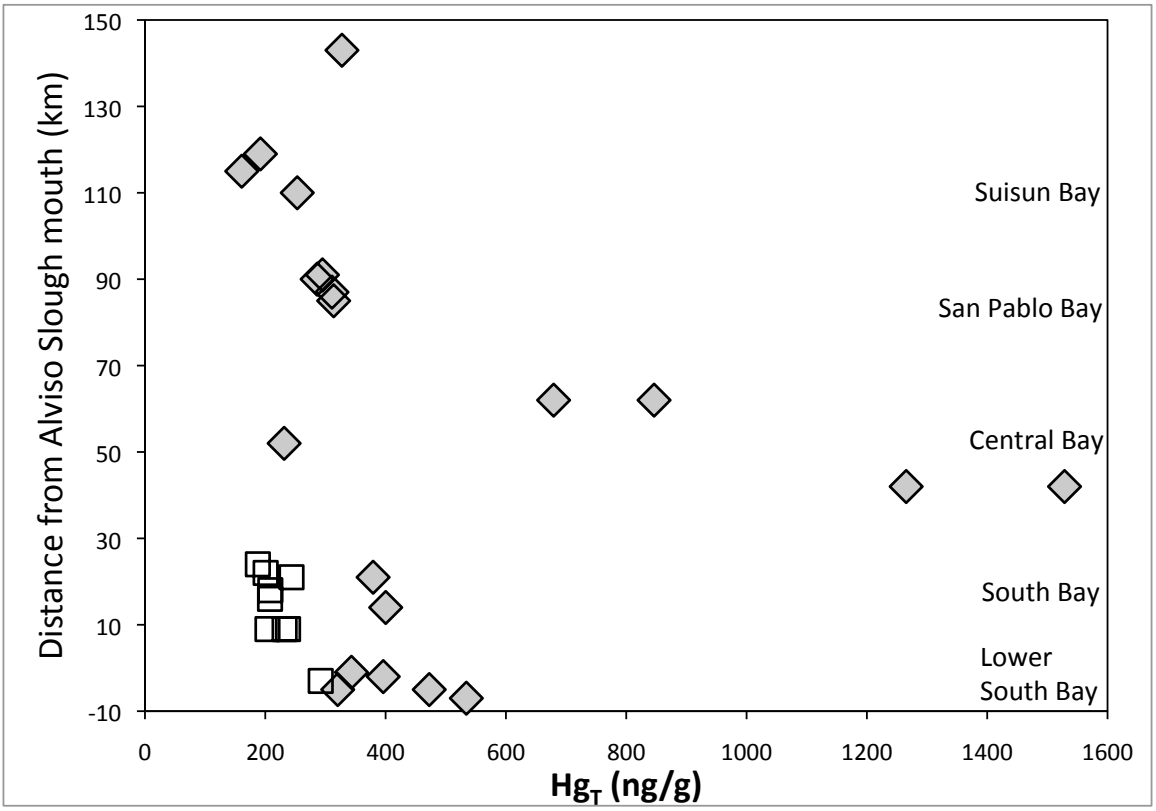

Figure 4.3: The Hg_T concentration versus the approximate distance of each sample site from the mouth of Alviso Slough. Distances were estimated using the procedure described in Fig. 1. Smaller bays within San Francisco Bay are listed to the right at the corresponding distances from the mouth of Alviso Slough. Grey diamonds represent tidal surface (0-2 cm) sediments and white squares represent wetland surface (0-2 cm) sediments. Error bars are smaller than the symbol sizes.

Figure 4.4

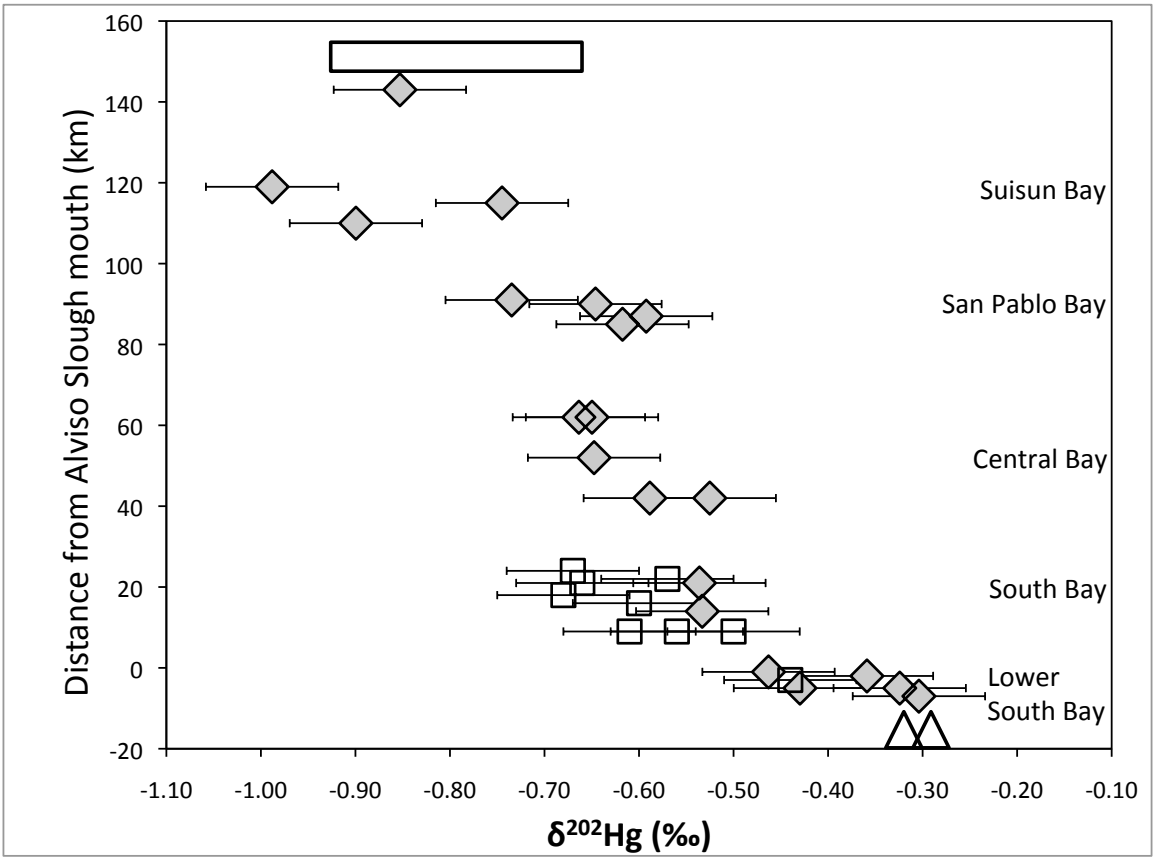

Figure 4.4: The δ^{202}Hg of sediments versus the approximate distance of each sample site from the mouth of Alviso Slough. Distances were estimated using the procedure described in Fig. 1. Smaller bays within San Francisco Bay are listed to the right at the corresponding distances from the mouth of Alviso Slough. Grey diamonds represent inter-tidal surface (0-2 cm) sediments; white squares represent wetland surface (0-2 cm) sediments; the triangles represent near-surface sediments from the Alviso Slough channel and marsh cores. The rectangle near the top of the diagram represents the range of δ^{202}Hg values of surface sediments from the Cosumnes River channel (n=2) and Cosumnes River wetlands (n=5). Cosumnes River samples are located further northeast of SF Bay than is represented on the figure (see Fig. 4.1).

Figure 4.5

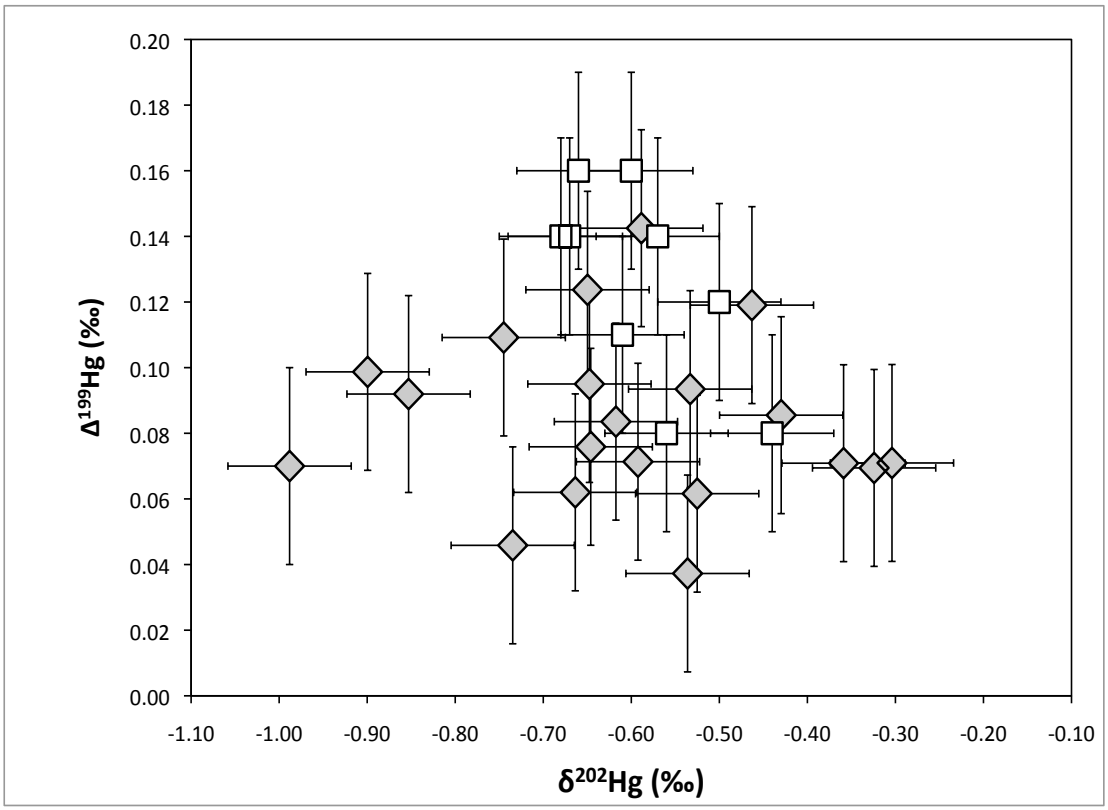

Figure 4.5: The Hg isotopic composition of inter-tidal and wetland sediments. Grey diamonds represent inter-tidal surface (0-2 cm) sediments and white squares represent wetland surface (0-2 cm) sediments. Wetland sediments had a narrow range of Δ^{199}Hg values from +0.08 to +0.16‰ (mean = 0.13 ±0.03‰, 1SD), slightly higher than the average inter-tidal sediment Δ^{199}Hg values, which range from +0.03 to +0.12‰ (mean Δ^{199}Hg = 0.08 ±0.03‰, 1SD).

Table 4.1: Hg concentrations and isotopic compositions of sample replicate analyses demonstrating reproducibility of measurements.

Sample Code	Latitude (N)	Longitude (W)	Hg_T (ng/g)	$\delta^{202}Hg$ (‰)	$\Delta^{201}Hg$ (‰)	$\Delta^{199}Hg$ (‰)
NI(C)	36.41558	120.67314	1,013,400	0.05	0.01	0.00
NI(C)	36.41558	120.67314	939,060	0.00	-0.02	-0.02
NI(C) average	36.41558	120.67314	976,230	0.03	0.00	-0.01
1 SD			52,560	0.03	0.02	0.02
CR(Ma)	38.25867	121.42783	297	-0.78	0.00	0.08
CR(Ma)	38.25867	121.42783	310	-0.73	-0.04	0.07
CR(Ma) average	38.25867	121.42783	303	-0.75	-0.02	0.07
1 SD			9	0.03	0.01	0.01
IT(90)	38.18214	122.56315	248	-0.71	0.06	0.09
IT(90)	38.18214	122.56315	324	-0.59	0.06	0.06
IT(90) average	38.18214	122.56315	286	-0.65	0.06	0.08
1 SD			53	0.08	0.00	0.02
IT(-2)	37.44747	121.01978	431	-0.45	0.01	0.04
IT(-2)	37.44747	121.01978	361	-0.35	0.03	0.05
IT(-2) average	37.44747	121.01978	396	-0.36	0.03	0.07
1 SD			49	0.07	0.02	0.01
IT(-5b)	37.42397	122.01451	335	-0.42	0.05	0.12
IT(-5b)	37.42397	122.01451	306	-0.44	0.03	0.05
IT(-5b) average	37.42397	122.01451	320	-0.43	0.04	0.09
1 SD			20	0.02	0.01	0.04
IT(-7)	37.42284	121.97562	538	-0.31	0.06	0.11
IT(-7)	37.42284	121.97562	531	-0.30	0.05	0.03
IT(-7) average	37.42284	121.97562	534	-0.30	0.05	0.07
1 SD			5	0.01	0.01	0.05

Table 4.2: Hg concentrations and isotopic compositions of all mine materials and sediments.

Site Code	Latitude (N)	Longitude (W)	Hg_T (ng/g)	$\delta^{202}Hg$ (‰)	$\Delta^{201}Hg$ (‰)	$\Delta^{199}Hg$ (‰)
New Idria Hg Mine Materials						
NI(Ta)	36.41519	120.67289	46,470	-0.33	0.03	0.06
NI(Tb)	36.41506	120.67244	71,260	-0.43	0.04	0.05
NI(C)	36.41558	120.67314	976,230	0.03	0.00	-0.01
Alviso Slough Sediment Core						
AS-C[0-7.5]	37.44381	122.00564	508	-0.29	0.08	0.07
AS-C[109-123]	37.44381	122.00564	4011	-0.06	0.03	0.03
AS-C[183-196]	37.44381	122.00564	832	0.29	0.01	0.03
AS-M[0-17]	37.44347	122.00639	409	-0.32	0.01	0.01
AS-M[100-131]	37.44347	122.00639	2346	0.20	-0.03	0.00
AS-M[174-199]	37.44347	122.00639	1144	-0.15	0.02	0.03
Cosumnes River and Yolo Bypass Sediment						
CR(Ra)	38.25447	121.42277	65	-0.88	-0.01	0.06
CR(Rb)	38.25750	121.43338	114	-0.91	0.00	0.09
CR(Ma)	38.25867	121.42783	303	-0.75	-0.02	0.07
CR(Mb)	38.25815	121.43704	419	-0.75	0.02	0.04
YB(a)	38.55204	121.59633	147	-0.72	0.03	0.12
YB(c)	38.52253	121.60132	119	-0.65	0.02	0.08
YB(b)	38.54918	121.59082	139	-0.73	0.10	0.16
Inter-tidal Sediment						
IT(-7)	37.42284	121.97562	534	-0.30	0.05	0.07
IT(-5b)	37.42397	122.01451	320	-0.43	0.04	0.09
IT(-5a)	37.43853	121.99225	473	-0.32	0.02	0.07
IT(-2)	37.44747	121.01978	396	-0.36	0.03	0.07
IT(-1)	37.45940	122.02139	343	-0.46	0.08	0.12
IT(14)	37.50275	122.16677	400	-0.53	0.08	0.09
IT(21)	37.53339	122.23190	379	-0.54	0.04	0.06
IT(42b)	37.74245	122.20955	1265	-0.59	0.10	0.14
IT(42a)	37.74244	122.20967	1529	-0.53	0.04	0.06
IT(52)	37.77322	122.39388	231	-0.65	0.07	0.10
IT(62a)	37.90430	122.31963	679	-0.65	0.11	0.12
IT(62b)	37.90330	122.32509	846	-0.66	0.05	0.06
IT(91)	38.20895	122.57868	295	-0.73	0.02	0.05

IT(90)	38.18214	122.56315	286	-0.65	0.06	0.08
IT(85)	38.01280	122.49023	314	-0.62	0.04	0.08
IT(87)	38.04815	122.49757	311	-0.59	0.05	0.07
IT(110)	38.06389	122.19289	253	-0.90	0.03	0.10
IT(115)	38.02093	122.14083	161	-0.74	0.06	0.11
IT(119)	38.01966	122.09418	192	-0.99	-0.01	0.07
IT(143)	38.02472	121.84380	327	-0.85	0.02	0.09
		Wetland Sediment				
WL(-3)	37.46171	121.98881	292	-0.44	0.06	0.08
WL(9c)	37.51592	122.08149	238	-0.50	0.07	0.12
WL(9a)	37.50623	122.09018	204	-0.61	0.06	0.11
WL(9b)	37.50835	122.09745	232	-0.56	0.03	0.08
WL(16)	37.51171	122.18037	208	-0.60	0.12	0.16
WL(18)	37.52216	122.19995	208	-0.68	0.10	0.14
WL(21)	37.53107	122.23251	244	-0.66	0.11	0.16
WL(22)	37.59131	122.14605	201	-0.57	0.04	0.14
WL(24)	37.55169	122.24841	188	-0.67	0.11	0.14

Chapter 5

Mercury isotopes link mercury in San Francisco Bay forage fish to surface sediments

Authors: Gretchen E. Gehrke, Joel D. Blum, Darell G. Slotton, Ben K. Greenfield

Citation: Gehrke, G. E., Blum, J. D., Slotton, D. G., and Greenfield, B. K., 2011. Mercury isotopes link mercury in San Francisco Bay forage fish to surface sediments. *Environmental Science & Technology* **45**, 1264-1270.

Abstract

Identification of sources of biologically accessible Hg is necessary to fully evaluate Hg exposure in aquatic ecosystems. This study assesses the relationship between Hg in forage fish and Hg in surface sediments throughout San Francisco Bay (SF Bay) and evaluates processes influencing the incorporation of Hg into the aquatic food web. We measured the Hg stable isotope compositions of two nearshore fish species and compared them with previously reported analyses of co-located inter-tidal surface sediments. Fish δ^{202}Hg values (mass dependent fractionation) demonstrated a distinct spatial gradient within SF Bay that ranged from 0.60‰ in the south to -0.25‰ in the north. Fish δ^{202}Hg values were

consistently higher than sediment δ^{202}Hg values by 0.73‰ (±0.16‰, 1SD). Fish and sediment δ^{202}Hg values in SF Bay proper were well correlated (r^2= 0.83), suggesting that sediment is a primary source of Hg to the nearshore aquatic food web. Fish Δ^{199}Hg values (mass independent fractionation) ranged from 0.46 to 1.55‰, did not correlate with sediment values, and yielded a Δ^{199}Hg/Δ^{201}Hg ratio of 1.26 (±0.01, 1SD; r^2=0.99). This mass independent fractionation is consistent with photodegradation of MeHg to varying degrees at each site prior to incorporation into the food web.

1. Introduction

San Francisco Bay (SF Bay) is a large estuary that has been significantly impacted by human activities (Nichols et al., 1986). Historic mercury (Hg) and gold mining, industrialization, and urbanization of the greater San Francisco Area have resulted in the release of large quantities of Hg to the environment, and elevated Hg concentrations in sediments have been observed throughout SF Bay (Conaway et al., 2008; Gehrke et al., 2011). The form of Hg of greatest environmental concern is monomethyl mercury (MeHg), which is the dominant Hg species in fish (Harris et al., 2003), and bioaccumulates in the aquatic food web (Morel et al., 1998). Consumption of contaminated fish is a primary vector of human MeHg exposure (Sunderland, 2006). Several species of sport fish within SF Bay and its fluvial tributaries exceed Hg concentration guidelines for human consumption (Davis et al., 2008; Greenfield et al., 2005). Additionally, highly elevated Hg concentrations in SF

Bay wetland forage fish have been observed during peak nesting and hatching periods for Hg-sensitive waterbirds (Eagles-Smith et al., 2009). To reduce wildlife and human exposure to Hg it is important to first identify Hg sources to aquatic biota in SF Bay.

Previous studies have demonstrated that young-of-year (~4 month old) Mississippi silverside (*Menidia audens*) and topsmelt (*Atherinops affinis*) are appropriate biosentinel fish species for identifying small scale spatial and temporal patterns in food web Hg uptake (Greenfield and Jahn, 2010; Slotton et al., 2007). Silverside and topsmelt inhabit shallow waters, and in SF Bay both species feed predominantly on epibenthic invertebrates (Jahn, 2008; Visintainer et al., 2006). Although often found at the same locations, silverside are more polyhaline than topsmelt, and they often inhabiting brackish margins of SF Bay while topsmelt primarily inhabit more saline and shallower waters closer to the open bay. Both silverside and topsmelt are important prey fish for larger sport fish and other estuarine piscivores and thus are vectors of MeHg contamination between primary Hg sources and higher trophic level organisms (Greenfield and Jahn, 2010).

Microbial methylation of Hg often occurs at the anoxic boundary in sediments, and several studies have compared the relationship between the concentrations of total Hg (Hg_T) and MeHg in surface waters, shallow sediments, and biota. Results in estuaries and coastal areas have varied; some studies have reported positive correlations between sediment and biota Hg_T and suggested sediments as the primary source of Hg to the aquatic food web (Gantner et al., 2009;

Hammerschmidt and Fitzgerald, 2004), whereas other studies have reported no significant relationship between sediment and biota Hg_T (Lawrence and Mason, 2001; Sunderland et al., 2010). It has been suggested that other Hg sources, such as atmospherically deposited Hg, might be more bioavailable than Hg in sediments, and may therefore constitute the primary source of Hg to some aquatic food webs. Some studies have indicated a positive, proportional relationship between atmospheric Hg loading and biotic Hg uptake, particularly in remote and pristine areas (Hammerschmidt and Fitzgerald, 2006a; Orihel et al., 2008). However, these studies have mostly been conducted at locations with conditions markedly different from SF Bay, which is a shallow estuary with multiple Hg sources including elevated Hg concentrations in sediments (Conaway et al., 2008; Gehrke et al., 2011).

Mercury stable isotope ratios can be used to trace Hg sources in the environment (Foucher et al., 2009; Gantner et al., 2009; Laffont et al., 2009; Senn et al., 2010) and provide insight to processes influencing Hg cycling (Bergquist and Blum, 2007; Das et al., 2009; Gehrke et al., 2009; Gratz et al., 2010; Jackson et al., 2008). Hg has seven stable isotopes (196-204 amu) and multi-collector inductively coupled plasma mass spectrometry (MC-ICP-MS) allows for precise measurement ($\sim \pm 0.1‰$ 2SD) of Hg isotope ratios (Blum and Bergquist, 2007). Laboratory experiments have demonstrated Hg isotope fractionation during environmentally relevant processes including microbial methylation, demethylation, and photochemical redox reactions (Bergquist and Blum, 2007; Kritee et al., 2008; Kritee et al., 2007; Rodriguez-Gonzalez et al., 2009; Zheng and Hintelmann, 2009). Studies of environmental samples have reported variations in Hg isotope ratios in fish,

sediment, soil, snow, moss, lichen, peat, coal, and Hg ore (Bergquist and Blum, 2007; Biswas et al., 2008; Carignan et al., 2009; Gantner et al., 2009; Jackson et al., 2004; Jackson et al., 2008; Laffont et al., 2009; Sherman et al., 2010; Smith et al., 2008; Zheng and Hintelmann, 2009). Hg isotopes can be fractionated by reaction selectivity based on nuclear mass (mass-dependent fractionation, MDF) and by radical-pair spin-selectivity and nuclear volume differences, which can produce both MDF and mass-independent fractionation (MIF) (Buchachenko et al., 2008; Schauble, 2007). Different reactions can produce distinct Hg isotope ratios and recent studies have used these Hg isotope signatures to identify and trace Hg sources (Carignan et al., 2009; Foucher et al., 2009; Gantner et al., 2009). Some studies have used MIF signatures specifically to discern photo-mediated reactions that have transformed Hg in aquatic reservoirs (Gantner et al., 2009; Laffont et al., 2009). Studies of Hg isotopes have demonstrated the ability to identify Hg sources and transformations that were not identifiable using Hg concentrations alone, highlighting the importance of further advancing Hg isotope methodologies.

This study investigates the relationship between Hg in small fish and in co-located surface sediments in SF Bay and assesses the biogeochemical processes that influence the Hg isotopic composition of SF Bay fish. We analyzed Hg_T and the Hg isotopic composition of Mississippi silverside and/or topsmelt from 26 sites throughout SF Bay and compare these data to analyses of surface sediments collected concurrently at 16 of the sites and reported previously (Gehrke et al., 2011). This study uses Hg isotopes to evaluate the potential for sediments to be a primary source of Hg to SF Bay fish. It also provides insight into the various Hg

isotope fractionations that may occur during the transfer of Hg from sediments to fish in a natural estuarine environment.

2. Experimental Section

2.1 Sample collection.

Fish were collected by beach seine at 26 nearshore sites throughout SF Bay (Fig. S5.1) in October 2008 following a sampling strategy that has been described previously (Greenfield and Jahn, 2010). The distribution of sampling sites provided broad spatial coverage of SF Bay and spanned a range of shallow water habitats (<2 m water depth), including wetlands, tidal mudflats, semi-enclosed and open embayments, and brackish fluvial zones. Sampling sites also encompassed a range of possible localized Hg sources including areas influenced by wastewater effluent, urban runoff, industrial and chemical manufacturing, and sediment discharge from historical Hg and gold mining regions. Samples of the top 2 cm of sediment were collected at the same time and in the same locations as the fish. Details of the sampling and analysis of Hg_T and Hg isotopic compositions of the sediments are given in Gehrke et al (2011).

At each location, 4 composite samples of ~4 month old silversides and topsmelt were collected, measured, rinsed, placed in freezer bags with ambient water, and frozen using dry ice. Each composite sample included 5 closely matching individuals within a 10 mm length range. Composite samples were size-distributed

in 10 mm intervals across a length range of 40-80 mm for silverside and 60-100 mm for topsmelt, and most were in the higher half of the length ranges. Sample names are abbreviations of the smaller bays (within SF Bay) in which they were collected: Lower South Bay (LSB), South Bay (SoB), Central Bay (CB), San Pablo Bay (SPB), and Suisun Bay (SuiB). Numbers following the prefix distinguish between sample sites and increase from more southern to more northern sites in LSB, SoB, CB, and SPB, and from western to eastern sites in SuiB. Spatial variation of Hg concentration and isotopic composition was assessed using the approximate distance of each sampling location from the mouth of Alviso Slough (Fig S5.1). Perpendicular lines were drawn from each sample site to the approximate center line of SF Bay, and the distance was measured between the Alviso Slough mouth and the intersect of the sample site and center-line.

2.2 Hg concentration and isotope analysis of fish

Samples were thawed, weighed, dried at 55°C and re-weighed. Dried whole fish composite samples were powdered using a stainless steel grinder (Slotton et al., 2007). Subsamples were thermally decomposed in a stream of air at 750°C in the first stage of a two-stage furnace. Volatilized Hg(0) and combustion products were carried by a stream of air mixed with O_2 through a 1000°C furnace for further decomposition and bubbled into a 1% $KMnO_4$ oxidizing solution. $KMnO_4$ solutions were partially neutralized with NH_2OH and then analyzed for Hg_T by $SnCl_2$ reduction using a Nippon Instruments MA-2000 atomic absorption spectrometer. All Hg

concentrations given in this paper are reported as ng/g *dry weight* unless otherwise noted. Procedural blanks and standard reference materials (DOLT-2, DORM-2, Tuna ERMCE 464) were analyzed for quality control and demonstrated a blank contribution of <0.03 ng/g and a Hg recovery from standards of >90% (Table S5.2). Hg isotope ratios were measured using a Nu Instruments multi-collector inductively coupled plasma mass spectrometer (MC-ICP-MS) following methods previously described (Blum and Bergquist, 2007). Briefly, $KMnO_4$ solutions were partially reduced with NH_2OH and diluted to uniform Hg concentrations of 5.0 ± 0.2 ng/g. Hg(II) in solution was reduced using $SnCl_2$, and evolved Hg(0) was separated from solution on a frosted glass phase separator and introduced to the MC-ICP-MS. On-peak zero corrections were applied and instrumental mass bias was corrected using an internal Tl standard (NIST SRM-997) and sample-standard bracketing at uniform Hg_T and matrix concentration. Mass-dependent Hg isotope composition is reported as $\delta^{202}Hg$ in permil (‰) referenced to NIST SRM-3133 (Blum and Bergquist, 2007). Mass-independent Hg isotope composition is the difference between the measured $\delta^{XXX}Hg$ value and that which would be predicted based on mass dependence (Blum and Bergquist, 2007). Mass-independent Hg isotope composition is reported as $\Delta^{199}Hg$ and $\Delta^{201}Hg$ in permil (‰). Isotope compositions are calculated as:

$$\delta^{xxx}Hg = 1000*((((^{xxx}Hg/^{198}Hg)_{sample})/(^{xxx}Hg/^{198}Hg)_{SRM3133})-1)$$

$$\Delta^{199}Hg = \delta^{199}Hg_{measured} - (\delta^{202}Hg_{measured} * 0.252)$$

$$\Delta^{201}Hg = \delta^{201}Hg_{measured} - (\delta^{202}Hg_{measured} * 0.752)$$

Analytical uncertainty was monitored by replicate analyses of the UM-Almadén standard and replicate combustions and analysis of samples and of the standard reference materials DOLT-2 and ERMCE 464 Tuna (Table S5.2). Reproducibility of δ^{202}Hg and Δ^{199}Hg measurements are estimated to be ±0.10‰ (2SD, n = 26) and ±0.06‰ (2SD, n = 26), respectively, based on analysis of the secondary standard UM-Almadén (Blum and Bergquist, 2007). Replicate combustion and analysis of standard reference materials were within error of previously published δ^{202}Hg and Δ^{199}Hg values (Bergquist and Blum, 2007) and demonstrated reproducibility within ±0.14‰ (2SD) and ±0.02‰ (2SD), respectively. Replicate analyses of samples were consistent with these estimated uncertainties (Table S5.2).

3. Results and Discussion

3.1 Hg concentrations in fish

Mercury concentrations (Hg_T) in young-of-year Mississippi silverside and topsmelt in SF Bay ranged from 50 to 1308 ng/g and 112 to 908 ng/g, respectively (Table S5.1, Fig. S5.2). At sites where both species were collected silverside Hg_T ranged from 1.4 to 2.9 times higher than topsmelt Hg_T. Previous studies have measured similar Hg_T in silverside and topsmelt of similar length and weight from SF Bay (Greenfield and Jahn, 2010; Greenfield et al., 2006; Slotton et al., 2007). Differences in Hg_T between the two species may result from habitat or metabolic differences. As noted above, topsmelt exhibit more offshore movement, and silverside movement is more restricted to wetlands, creek mouths, and other

nearshore areas (Slotton et al., 2007), which could influence the bioavailability of Hg to food sources for each species (Benoit et al., 2003; Greenfield and Jahn, 2010).

Silverside and topsmelt are vectors for Hg bioaccumulation in higher trophic levels of piscivorous fish and birds, and most silverside (24 out of 27) and topsmelt (12 out of 17) composites sampled in our study exceeded the San Francisco Bay Regional Water Quality Control Board 2006 proposed target maximum Hg_T for prey fish of 30 ng/g wet weight (~150 ng/g dry weight) (SFBRWQCB, 2006). Silverside from Alviso Slough in the Guadalupe River Delta in southern SF Bay (LSB 1-6) had the highest Hg_T (631 to 1308 ng/g) and silverside from the Petaluma River in northern SF Bay (SPB 4,5) also had elevated Hg_T (411 to 510 ng/g). Silverside and topsmelt collected at one site in Alviso Slough (LSB 4) had Hg_T close to a proposed threshold (~1000 ng/g) for sub-lethal health effects in juvenile fish (1308 and 908 ng/g) (Beckvar et al., 2005). The lowest Hg_T measured in silverside were in sloughs tributary to Suisun Bay in the northeast part of SF Bay (SuiB 1-6) (50 to 320 ng/g). The lowest Hg_T for a single composite sample was measured in silverside collected near a wastewater treatment plant effluent stream in the Carquinez Strait (SuiB 3) (50 ng/g).

Previous studies of Hg in prey fish and avian species in SF Bay suggested that biota in wetlands and marshes had elevated Hg_T relative to less vegetated embayments (Greenfield et al., 2006), but that was not observed in this study. Rather, fish from the Guadalupe River Delta and from the Petaluma River had elevated Hg_T relative to fish from other marshy and open-bay sampling sites.

Previous studies have also indicated that there is significant seasonal and annual variation in Hg_T (Eagles-Smith et al., 2009; Slotton et al., 2007), but we are unable to test this with our study design, which included only one sampling period.

Analyses of surface (0-2 cm) sediments collected concurrently with the fish from this study have been reported previously (Gehrke et al., 2011). They had Hg_T elevated above background levels, with notably high Hg_T in sediments from the Guadalupe River Delta and the Petaluma River, and extremely high Hg_T measured in sediments from a single Central Bay site (CB5, Fig. S5.1) (Gehrke et al., 2011). Excluding this single outlier site in the Central Bay (CB5), we found that concentrations in fish and sediment were correlated (silverside, $r^2 = 0.40$, $p = 0.016$; topsmelt, $r^2 = 0.56$, $p = 0.020$) (Fig S5.2). Rates of microbial methylation and demethylation in surface sediments and water column Hg species concentrations were not measured in this study, precluding evaluation of the relationship between water column MeHg and fish Hg_T. Studies of atmospheric Hg deposition in SF Bay have shown that there is little spatial variation in atmospheric Hg loading rates within the greater SF Bay area (Tsai and Hoenicke, 2001). Therefore, differences in direct atmospheric Hg deposition and consequent food web uptake are not likely to explain the significant spatial variations in fish Hg_T in this study. In the context of the variable relationships between sediment and fish Hg_T observed in coastal environments, the positive relationship we observed between Hg_T in sediments and fish suggests that sediments may be a predominant source of Hg to the food web. However, Hg_T correlations alone do not unambiguously indicate that sediment Hg is the primary source of MeHg to the aquatic food web in SF Bay.

3.2 Fish Hg isotope composition

The fish analyzed in this study displayed both mass-dependent and mass-independent Hg isotope fractionation (Table S5.1, Fig 5.1). The δ^{202}Hg values for silverside and topsmelt ranged from -0.25 to 0.60‰ and the Δ^{199}Hg values ranged from 0.46 to 1.55‰. Fish δ^{202}Hg and Δ^{199}Hg values were not correlated in either silverside or topsmelt (Fig 5.1, r^2=0.023, p = 0.498 and r^2=0.044, p=0.806), which is consistent with other studies (Bergquist and Blum, 2009; Gantner et al., 2009; Laffont et al., 2009; Senn et al., 2010). δ^{202}Hg values were correlated with Hg_T in both silverside and topsmelt (Fig S5.3a, r^2=0.30, p<0.001 and r^2=0.46, p<0.001) and Δ^{199}Hg values were not correlated with Hg_T in either silverside or topsmelt (Fig S5.3b, r^2=0.07, p=0.23 and r^2=0.08, p=0.27). At the nine sites where both species were sampled, silverside and topsmelt had indistinguishable Hg isotopic composition (except for one site with contrasting Δ^{199}Hg values) (Fig S5.4). For the purposes of this study, we conclude that silverside and topsmelt can generally be used interchangeably in Hg isotope comparisons between fish from different sampling sites and between fish and sediment at a given site. Fish length was not correlated with δ^{202}Hg or Δ^{199}Hg values in either species. A more detailed species comparison is provided in the Supporting Information.

3.3 Spatial variation of Hg isotopes in fish

Silverside and topsmelt demonstrated a south to north spatial gradient of δ^{202}Hg values in SF Bay decreasing from 0.60‰ in Alviso Slough (LSB1) to -0.25‰

in San Pablo Bay (SPB2). Fish δ^{202}Hg values in Suisun Bay increased from -0.11‰ (SuiB2) in Carquinez Strait to 0.30‰ (SuiB5) near the Sacramento-San Joaquin confluence (Fig. S5.1 and Fig. 5.2). The dominant spatial pattern of SF Bay δ^{202}Hg values decreasing from the Lower South Bay to San Pablo Bay has also been observed in surface sediments (Gehrke et al., 2011). The similar spatial pattern of δ^{202}Hg values in SF Bay surface sediments and small fish suggests that sediments are a significant source of Hg to fish, as discussed further below. The spatial gradient of δ^{202}Hg values in small fish is consistent with fish acquiring Hg from three dominant Hg sources that enter the estuary in Lower South Bay, San Pablo Bay, and Suisun Bay. Conversely, the δ^{202}Hg value gradient observed is not consistent with small fish acquiring Hg from a variety of localized point-sources or from atmospheric deposition. If local point sources were the dominant source of Hg to small fish, we would not expect a discernable spatial pattern in δ^{202}Hg values. Instead we would expect significant variation in δ^{202}Hg values within small geographic areas, reflecting the variety of δ^{202}Hg values emitted by local point sources, and this is not observed. If atmospheric deposition of Hg provided the dominant source of Hg to fish, we would not expect to see the observed south-to-north spatial variation in δ^{202}Hg values, nor would we expect them to be correlated with the δ^{202}Hg values of bulk sediments.

3.4 Hg isotope values in fish and sediments

All fish had δ^{202}Hg values and Δ^{199}Hg values higher than those in SF Bay surface sediments (Fig. 5.1). Recent studies of Hg isotopes in other aquatic ecosystems also have observed isotopic differences between sediments and fish (Gantner et al., 2009; Jackson et al., 2008). Laboratory experiments demonstrate that microbial Hg methylation and MeHg degradation fractionate Hg isotopes following a mass dependent pattern (Kritee et al., 2009; Kritee et al., 2008; Kritee et al., 2007; Rodriguez-Gonzalez et al., 2009), equilibrium sorption of aqueous Hg produces significant mass-dependent and minor mass-independent fractionation (Wiederhold et al., 2010), and photoreduction of Hg(II) and MeHg produces significant mass-independent and lesser mass-dependent fractionation (Bergquist and Blum, 2007; Zheng and Hintelmann, 2009). Additionally, abiotic redox reactions and Hg species partitioning are likely to occur in estuarine sediments and these processes may also result in mass dependent fractionation. Thus, differences in isotopic composition between fish and bulk sediments are expected. There was not a consistent relationship between sediment and fish Δ^{199}Hg values across sites. However, there was a significant relationship ($r^2 = 0.68$, $p<0.001$) between sediment and fish δ^{202}Hg values (Fig 5.3). Prior studies have used δ^{202}Hg values to identify and track specific Hg sources (Foucher et al., 2009; Laffont et al., 2009) and Δ^{199}Hg values have been used to discern specific processes, such as photochemical degradation of MeHg (Bergquist and Blum, 2009). In this study we use δ^{202}Hg values to make inferences about Hg sources and Δ^{199}Hg values to discuss biogeochemical transformations of the bioavailable pool of Hg.

3.5 Hg mass dependent fractionation in fish and sediments.

The δ^{202}Hg values of silverside and topsmelt were significantly correlated with the δ^{202}Hg values of sediments co-located throughout SF Bay ($r^2 = 0.68$, $p<0.001$), and especially in SF Bay south of Carquinez Strait ($r^2 = 0.83$, $p<0.001$) (Fig. 5.3). There was a greater variability in the offset of δ^{202}Hg values between fish and co-located sediments at sites north of Carquinez Strait in Suisun Bay than in the rest of SF Bay. Suisun Bay is somewhat separated hydrographically from the rest of SF Bay by the Carquinez Strait (McKee et al., 2006; Ruhl et al., 2001; Warner et al., 2002), with lower average salinity as the result of freshwater discharge from the Sacramento-San Joaquin Delta, and episodic flooding and sediment transport during high river flows (David et al., 2009; McKee et al., 2006; Warner et al., 2002). SF Bay west of the Carquinez Strait has higher average salinity and has more significant tidal fluxes and sediment mixing. The highly significant correlation ($r^2 = 0.83$, $p<0.001$) of δ^{202}Hg values of SF Bay fish and sediments south of the Carquinez Strait suggests that surface sediments are an important source of Hg to silverside and topsmelt in SF Bay. Since the primary food source of the silverside and topsmelt analyzed is epibenthic invertebrates (Greenfield and Jahn, 2010) and active Hg methylation and demethylation has been shown to occur in SF Bay surface sediments (Choe, 2004; Heim et al., 2007; Marvin-DiPasquale and Agee, 2003), it is plausible that fish are acquiring MeHg predominantly from sediments. However, we cannot rule out a contribution from atmospheric Hg deposition, nor can we quantify this possible contribution at the present time.

Fish δ^{202}Hg values were consistently higher than in-situ sediments by a difference of 0.73 ± 0.16‰ (1SD). Studies have demonstrated that microbial methylation of Hg(II) and microbial degradation of MeHg fractionate Hg isotopes, producing observable δ^{202}Hg differences between Hg species (Kritee et al., 2009; Kritee et al., 2008; Kritee et al., 2007; Rodriguez-Gonzalez et al., 2009). Additionally, a study of Hg isotopes in fish and human hair reported significant MDF between fish and humans living on a largely fish diet, with human hair δ^{202}Hg values 2.0 ± 0.2‰ (1SD) higher than fish (Laffont et al., 2009). Perrot et al (2010) examined sediments, plankton, and two fish species in Baikal Lake and reported a consistent pattern of progressively higher δ^{202}Hg values in higher trophic levels. Gantner et al (2009) also observed MDF within an aquatic foodweb, with significant differences in δ^{202}Hg values between sediments, chironomids, zooplankton, and char within individual arctic lakes, however, the direction of fractionation (i.e. higher versus lower δ^{202}Hg values in higher trophic levels) was not consistent. These studies indicate that microbial methylation of Hg(II) and demethylation of MeHg, as well as trophic transfer of MeHg, can fractionate Hg isotopes according to mass-dependence. The offset observed in δ^{202}Hg values of fish and sediments in SF Bay could have resulted from the net effect of microbial methylation and demethylation in the sediments and the subsequent trophic transfer of MeHg to silverside and topsmelt. Abiotic demethylation of aqueous MeHg, reduction of Hg(II), and species partitioning also could have contributed to the offset in δ^{202}Hg values between fish and sediments.

Fish and sediment δ^{202}Hg values in Suisun Bay (SuiB1-6) did not show as consistent a correlation as in the SF Bay proper, with δ^{202}Hg value offsets ranging from 0.63 to 0.98‰. It is possible that this variability results from isotopic heterogeneity in Suisun Bay sediments at the spatial scale of the small fish foraging areas (~1 km). As discussed above, Suisun Bay is somewhat separated hydrographically from the rest of SF Bay by the Carquinez Strait and sediments may not be as well mixed as they are further south in SF Bay (Ruhl et al., 2001). Though silverside and topsmelt have a small habitat range, it is possible that there is significant heterogeneity of surface sediments within a 1 km range such that the sediment Hg isotopic composition sampled at each site is not representative of the entire habitat of the sampled fish. Heterogeneity of Hg_T and MeHg concentration in surface sediments on this spatial scale in Suisun Bay has been observed (Heim et al., 2007), which could result from different Hg sources. Sediment heterogeneity could produce the observed decoupling between the Hg isotopic composition of sediments and fish in Suisun Bay. It is also likely that heterogeneity of sediment δ^{202}Hg values within the silverside home range at SPB2 causes the substantially different δ^{202}Hg value offset observed at SPB2 (0.34‰) compared to other (well-mixed) sites, since low tides can dry this site completely, forcing fish to migrate and extend their foraging range. The variability of fish-sediment δ^{202}Hg value offsets in Suisun Bay also could result from the fish in Suisun Bay acquiring MeHg produced in the surrounding wetland areas, which are extensive near some sites in this part of the study area. Studies have indicated that considerable MeHg is produced in, and

exported from, the wetland areas around Suisun Bay, and have suggested that exported MeHg is acquired by biota within Suisun Bay (Heim et al., 2007).

3.6 Hg mass independent fractionation in fish

In order to utilize Hg MIF in biota to gain information about pathways of Hg cycling, it is necessary to assess which processes produce the MIF observed in fish. Photochemical reactions involving radical pairs can produce MIF due to the magnetic isotope effect (Buchachenko et al., 2008) and are likely responsible for MIF observed in many aqueous systems (Bergquist and Blum, 2009). Laboratory experiments have demonstrated that photochemical reduction of aqueous Hg(II) and photodegradation of MeHg in the presence of natural DOC can produce Δ^{199}Hg/ Δ^{201}Hg ratios averaging 1.0 and 1.3, respectively (Bergquist and Blum, 2007), which contrasts with higher (~1.7) ratios predicted for MIF resulting from nuclear volume effects (NVE) (Schauble, 2007; Wiederhold et al., 2010).

The Δ^{199}Hg and Δ^{201}Hg values are well correlated in silverside and topsmelt from SF Bay ($r^2 = 0.99$, $p < 0.001$) with a Δ^{199}Hg/ Δ^{201}Hg ratio of 1.26 ± <0.01 (1SD) (Fig. S5.5). This is consistent with other studies of fish from a variety of ecosystems, all of which report a narrow range of Δ^{199}Hg/ Δ^{201}Hg ratios that average between 1.2 and 1.3 (Bergquist and Blum, 2007; Gantner et al., 2009; Laffont et al., 2009; Senn et al., 2010). Δ^{199}Hg/ Δ^{201}Hg ratios in fish are similar to laboratory photochemical MeHg degradation experiments. Thus, it has been argued that Δ^{199}Hg and Δ^{201}Hg values in fish are the result of photodegradation of MeHg in the

water column prior to incorporation into the food web, implying that subsequent biological transformations of MeHg do not produce MIF (Bergquist and Blum, 2007). However, one recent study from a freshwater lake observed a correlation between Δ^{199}Hg values and δ^{15}N values in fish in trophic levels 1 and 2 and suggested that fish MIF is produced during bioaccumulation and biomagnification (Das et al., 2009). Other studies of Hg isotopes in aquatic ecosystems have not found any significant relationships between Δ^{199}Hg values and fish trophic position. Senn et al (2010) did not observe a correlation between Δ^{199}Hg values and δ^{15}N values in higher level fish from the Gulf of Mexico, and Laffont et al (2009) did not observe differences in Δ^{199}Hg values between fish and hair of piscivorous humans. The majority of published data and theoretical arguments suggest that only photochemical reactions involving Hg(II) and MeHg impart significant MIF (Bergquist and Blum, 2007; Kritee et al., 2009). Thus, we interpret the MIF observed in SF Bay silverside and topsmelt to be the result of photochemical degradation of MeHg in the water column, but acknowledge that additional research is needed in this area.

Silverside and topsmelt in SF Bay have Δ^{199}Hg values that range from 0.46 to 1.55‰ (Table S5.1, Fig 5.1). The MIF of Hg isotopes in silverside and topsmelt indicates that photochemical degradation of MeHg varies spatially in SF Bay and thus likely impacts MeHg accumulation in the aquatic food web. By comparing SF Bay fish Δ^{199}Hg values to the results of the Bergquist and Blum (2007) laboratory aqueous MeHg photodegradation experiments (using water with 10 mgC/L and natural sunlight) we estimate that ~10-30% of MeHg is lost from the water column

due to photodegradation of aqueous MeHg. These estimates are in keeping with other estimates of MeHg loss in freshwater and estuarine environments (Hammerschmidt and Fitzgerald, 2006b; Sellers et al., 1996).

3.7 Possible Causes of MDF

If we assume that MIF in fish results from only photochemical reactions, we can then distinguish between the MDF that results from photochemistry versus the MDF resulting from biological and abiotic reactions that are not photo-mediated. Experiments by Bergquist and Blum (2007) demonstrated that photochemical degradation of MeHg fractionates Hg isotopes such that δ^{202}Hg and Δ^{199}Hg values of a 10 mg C/L DOC aqueous solution (a reasonable estimate for DOC in SFB waters) increases with a Δ^{199}Hg/ δ^{202}Hg slope of 4.8 ± 1.5 as the reaction proceeds. We applied this experimental slope to fish Δ^{199}Hg values to "correct" fish δ^{202}Hg values for the effects of photochemical degradation of MeHg. This estimated shift in δ^{202}Hg values from MeHg degradation was relatively small, ranging from 0.08 to 0.27‰. When the estimated photochemical effect on δ^{202}Hg values in fish is removed, the offset between sediment and fish δ^{202}Hg values in the entire SF Bay decreases from 0.73 ± 0.16‰ (r^2 = 0.68, p <0.001) to 0.60 ± 0.16‰ (r^2 = 0.69, p <0.001) (Fig. 5.3).

We hypothesize that the offset between fish and sediment δ^{202}Hg values that is not associated with photochemistry is the net result of multiple processes related to the mobilization of Hg from bulk sediments to overlying water and the various biotic and abiotic transformations of Hg in sediment and water. Hg isotope

fractionation associated with some, but not all, of these processes has been studied experimentally. Wiederhold et al (2010) observed MDF produced upon the equilibrium binding of aqueous Hg(II) species onto a thiol resin such that unbound aqueous Hg(II) had higher δ^{202}Hg values. It is plausible that thiol groups in sediment organic matter and DOC sequester aqueous Hg mobilized from sediments prior to methylation, producing a remaining bioavailable pool of Hg with higher δ^{202}Hg values. Experiments have also shown that microbial reduction of Hg(II) and degradation of MeHg shifts these reservoirs toward higher δ^{202}Hg values as Hg(0) is lost by evasion (Kritee et al., 2008; Kritee et al., 2007). It is possible that this leads to higher δ^{202}Hg values of the MeHg that is taken up by plankton and that bioaccumulates in the aquatic foodweb. It is also possible that trophic transfer in the aquatic foodweb contributes to fractionation resulting in fish δ^{202}Hg values that are higher than sediment values (Gantner et al., 2009; Laffont et al., 2009; Perrot et al., 2010). Methylation of Hg(II), however, appears to produce MeHg with a lower δ^{202}Hg value (Rodriguez-Gonzalez et al., 2009), and this fractionation is apparently overcome by the other processes mentioned above, which lead to higher δ^{202}Hg values in fish compared to sediment. Although we do not know the relative importance of these processes to the MDF of Hg isotopes, we observe a remarkably consistent offset of δ^{202}Hg values of ~0.6‰ between bulk sediment and fish due to the net effect of Hg mobilization from sediments, Hg methylation, MeHg demethylation, and MeHg trophic transfer to young-of-year silverside and topsmelt.

The correlation and consistent offset between co-located sediment and fish δ^{202}Hg values leads us to suggest that in-situ methylation of Hg in sediments is a

dominant source of Hg to the aquatic food web throughout SF Bay. Additional research will be required to determine the relative importance of the various biotic and abiotic transformations that lead to this mass dependent fractionation and whether or not a similar offset would be expected in other ecosystems. We caution that fish do not directly preserve the Hg isotopic signal of bulk sediments, and that isotopic tracing of the source of MeHg in SF Bay was made possible only by studying a broad spatial area with varying Hg sources and δ^{202}Hg values in sediments. This highlights the utility of Hg isotopes to track Hg sources and also underscores the necessity to gain broad environmental context in order to use Hg isotopes to interpret Hg source-receptor relationships.

Acknowledgements

Funding for this study was provided by the Regional Monitoring Program for Water Quality in the San Francisco Bay, administered by the San Francisco Estuary Institute (SFEI) in collaboration with the Regional Water Quality Control Board. The research described in this paper also was partially funded by the United States Environmental Protection Agency (USEPA) under the Science to Achieve Results (STAR) Graduate Fellowship Program. EPA has not officially endorsed this publication and the views expressed herein may not reflect the views of the EPA. The authors would like to thank Shaun Ayers of UC Davis for sample collection and initial processing, Katie Harrold and other staff at SFEI for sample collection, Marcus Johnson for expert maintenance and operation of the MC-ICP-MS, Jay Davis for

comments on an earlier version of the manuscript, and three anonymous referees for helpful reviews.

References

Beckvar, N., Dillon, T.M., Read, L.B., 2005. Approaches for linking whole-body fish tissue residues of mercury or DDT to biological effects thresholds. *Environmental Toxicology and Chemistry* **24**, 2094-2105.

Benoit, J.M., Gilmour, C.C., Heyes, A., Mason, R.P., Miller, C.L., 2003. Geochemical and biological controls over methylmercury production and degradation in aquatic ecosystems, in: Cai, Y., Braids, O.C. (Eds.), *Biogeochemistry of Environmentally Important Trace Elements*, pp. 262-297.

Bergquist, B.A., Blum, J.D., 2007. Mass-dependent and -independent fractionation of Hg isotopes by photoreduction in aquatic systems. *Science* **318**, 417-420.

Bergquist, B.A., Blum, J.D., 2009. The Odds and Evens of Mercury Isotopes: Applications of Mass-Dependent and Mass-Independent Isotope Fractionation, *Elements* **5**, 353-357.

Biswas, A., Blum, J.D., Bergquist, B.A., Keeler, G.J., Xie, Z.Q., 2008. Natural Mercury Isotope Variation in Coal Deposits and Organic Soils. *Environmental Science & Technology* **42**, 8303-8309.

Blum, J.D., Bergquist, B.A., 2007. Reporting of variations in the natural isotopic composition of mercury. *Analytical and Bioanalytical Chemistry* **388**, 353-359.

Buchachenko, A.L., Ivanov, V.L., Roznyatovskii, V.A., Vorob'ev, A.K., Ustynyuk, Y.A., 2008. Inversion of the sign of the magnetic isotope effect of mercury in photolysis of substituted dibenzylmercury. *Doklady Physical Chemistry* **420**, 85-87.

Carignan, J., Estrade, N., Sonke, J.E., Donard, O.F.X., 2009. Odd Isotope Deficits in Atmospheric Hg Measured in Lichens. *Environmental Science & Technology* **43**, 5660-5664.

Choe, K., 2004. Sediment-water exchange of total mercury and monomethyl mercury in the San Francisco Bay-Delta. *Limnology and oceanography* **49**, 1512-1527.

Conaway, C.H., Black, F.J., Grieb, T.M., Roy, S., Flegal, A.R., 2008. Mercury in the San Francisco estuary. *Reviews of Environmental Contamination and Toxicology* **194**, 29-54.

Das, R., Salters, V.J.M., Odom, A.L., 2009. A case for in vivo mass-independent fractionation of mercury isotopes in fish. *Geochemistry Geophysics Geosystems* **10** pp.12.

David, N., McKee, L.J., Black, F.J., Flegal, A.R., Conaway, C.H., Schoellhamer, D.H., Ganju, N.K., 2009. Mercury Concentrations and Loads in a Large River System Tributary to San Francisco Bay, California, USA. *Environmental Toxicology and Chemistry* **28**, 2091-2100.

Davis, J.A., Greenfield, B.K., Ichikawa, G., Stephenson, M., 2008. Mercury in sport fish from the Sacramento-San Joaquin Delta region, California, USA. *Science of the Total Environment* **391**, 66-75.

Eagles-Smith, C.A., Ackerman, J.T., De La Cruz, S.E.W., Takekawa, J.Y., 2009. Mercury bioaccumulation and risk to three waterbird foraging guilds is influenced by foraging ecology and breeding stage. *Environmental Pollution* **157**, 1993-2002.

Foucher, D., Ogrinc, N., Hintelmann, H., 2009. Tracing Mercury Contamination from the Idrija Mining Region (Slovenia) to the Gulf of Trieste Using Hg Isotope Ratio Measurements. *Environmental Science & Technology* **43**, 33-39.

Gantner, N., Hintelmann, H., Zheng, W., Muir, D.C., 2009. Variations in Stable Isotope Fractionation of Hg in Food Webs of Arctic Lakes. *Environmental Science & Technology* **43**, 9148-9154.

Gehrke, G.E., Blum, J.D., Marvin-DiPasquale, M., 2011. Sources of mercury to San Francisco Bay surface sediment as revealed by mercury stable isotopes. *Geochimica et Cosmochimica Acta* **75**, 691-705.

Gehrke, G.E., Blum, J.D., Meyers, P.A., 2009. The geochemical behavior and isotopic composition of Hg in a mid-Pleistocene western Mediterranean sapropel. *Geochimica Et Cosmochimica Acta* **73**, 1651-1665.

Gratz, L.E., Keeler, G.J., Blum, J.D., Sherman, L.S., 2010. Isotopic Composition and Fractionation of Mercury in Great Lakes Precipitation and Ambient Air. *Environmental Science & Technology* **44**, 7764-7770.

Greenfield, B.K., Davis, J.A., Fairey, R., Roberts, C., Crane, D., Ichikawa, G., 2005. Seasonal, interannual, and long-term variation in sport fish contamination, San Francisco Bay. *Science of the Total Environment* **336**, 25-43.

Greenfield, B.K., Jahn, A., 2010. Mercury in San Francisco Bay forage fish. *Environmental Pollution* **158**, 2716-2724.

Greenfield, B.K., Jahn, A., Grenier, J.L., Shonkoff, S., Sandheinrich, M., 2006. Mercury in biosentinel fish in San Francisco Bay: First-year project report, *Regional Monitoring Program Exposure and Effects Pilot Study*. Oakland, CA, pp. 1-36.

Hammerschmidt, C.R., Fitzgerald, W.F., 2004. Geochemical controls on the production and distribution of methylmercury in near-shore marine sediments. *Environmental Science & Technology* **38**, 1487-1495.

Hammerschmidt, C.R., Fitzgerald, W.F., 2006a. Methylmercury in freshwater fish linked to atmospheric mercury deposition. *Environmental Science & Technology* **40**, 7764-7770.

Hammerschmidt, C.R., Fitzgerald, W.F., 2006b. Photodecomposition of methylmercury in an arctic Alaskan lake. *Environmental Science & Technology* **40**, 1212-1216.

Harris, H.H., Pickering, I.J., George, G.N., 2003. The chemical form of mercury in fish. *Science* **301**, 1203-1203.

Heim, W.A., Coale, K.H., Stephenson, M., Choe, K.Y., Gill, G.A., Foe, C., 2007. Spatial and habitat-based variations in total and methyl mercury concentrations in surficial sediments in the san francisco bay-delta. *Environmental Science & Technology* **41**, 3501-3507.

Jackson, T.A., Muir, D.C.G., Vincent, W.F., 2004. Historical variations in the stable isotope composition of mercury in Arctic lake sediments. *Environmental Science & Technology* **38**, 2813-2821.

Jackson, T.A., Whittle, D.M., Evans, M.S., Muir, D.C.G., 2008. Evidence for mass-independent and mass-dependent fractionation of the stable isotopes of mercury by natural processes in aquatic ecosystems. *Applied Geochemistry* **23**, 547-571.

Jahn, A., 2008. RMP Food Web Analysis; Data Report on Gut Contents of Four Fish Species, *SFEI*, Oakland, p. 34.

Kritee, K., Barkay, T., Blum, J.D., 2009. Mass dependent stable isotope fractionation of mercury during mer mediated microbial degradation of monomethylmercury. *Geochimica Et Cosmochimica Acta* **73**, 1285-1296.

Kritee, K., Blum, J.D., Barkay, T., 2008. Mercury Stable Isotope Fractionation during Reduction of Hg(II) by Different Microbial Pathways. *Environmental Science & Technology* **42**, 9171-9177.

Kritee, K., Blum, J.D., Johnson, M.W., Bergquist, B.A., Barkay, T., 2007. Mercury stable isotope fractionation during reduction of Hg(II) to Hg(0) by mercury resistant microorganisms. *Environmental Science & Technology* **41**, 1889-1895.

Laffont, L., Sonke, J.E., Maurice, L., Hintelmann, H., Pouilly, M., Bacarreza, Y.S., Perez, T., Behra, P., 2009. Anomalous Mercury Isotopic Compositions of Fish and Human Hair in the Bolivian Amazon. *Environmental Science & Technology* **43**, 8985-8990.

Lawrence, A.L., Mason, R.P., 2001. Factors controlling the bioaccumulation of mercury and methylmercury by the estuarine amphipod Leptocheirus plumulosus. *Environmental Pollution* **111**, 217-231.

Marvin-DiPasquale, M., Agee, J.L., 2003. Microbial mercury cycling in sediments of the San Francisco Bay-Delta. *Estuaries* **26**, 1517-1528.

McKee, L.J., Ganju, N.K., Schoellhamer, D.H., 2006. Estimates of suspended sediment entering San Francisco Bay from the Sacramento and San Joaquin Delta, San Francisco Bay, California. *Journal of Hydrology* **323**, 335-352.

Morel, F.M.M., Kraepiel, A.M.L., Amyot, M., 1998. The chemical cycle and bioaccumulation of mercury. *Annual Review of Ecology and Systematics* **29**, 543-566.

Nichols, F.H., Cloern, J.E., Luoma, S.N., Peterson, D.H., 1986. The Modification of an Estuary. *Science* **231**, 567-573.

Orihel, D.M., Paterson, M.J., Blanchfield, P.J., Bodaly, R.A., Gilmour, C.C., Hintelmann, H., 2008. Temporal changes in the distribution, methylation, and bioaccumulation of newly deposited mercury in an aquatic ecosystem. *Environmental Pollution* **154**, 77-88.

Perrot, V., Epov, V.N., Pastukhov, M.V., Grebenshchikova, V.I., Zouiten, C., Sonke, J.E., Husted, S.r., Donard, O.F.X., Amouroux, D., 2010. Tracing Sources and Bioaccumulation of Mercury in Fish of Lake Baikal,àí Angara River Using Hg Isotopic Composition. *Environmental Science & Technology* **44**, 8030-8037.

Rodriguez-Gonzalez, P., Epov, V.N., Bridou, R., Tessier, E., Guyoneaud, R., Monperrus, M., Amouroux, D., 2009. Species-Specific Stable Isotope Fractionation of Mercury during Hg(II) Methylation by an Anaerobic Bacteria (Desulfobulbus

propionicus) under Dark Conditions. *Environmental Science & Technology* **43**, 9183-9188.
Ruhl, C.A., Schoellhamer, D.H., Stumpf, R.P., Lindsay, C.L., 2001. Combined use of remote sensing and continuous monitoring to analyse the variability of suspended-sediment concentrations in San Francisco Bay, California. *Estuarine Coastal and Shelf Science* **53**, 801-812.
Schauble, E.A., 2007. Role of nuclear volume in driving equilibrium stable isotope fractionation of mercury, thallium, and other very heavy elements. *Geochimica Et Cosmochimica Acta* **71**, 2170-2189.
Sellers, P., Kelly, C.A., Rudd, J.W.M., MacHutchon, A.R., 1996. Photodegradation of methylmercury in lakes. *Nature* **380**, 694-697.
Senn, D.B., Chesney, E.J., Blum, J.D., Bank, M.S., Maage, A., Shine, J.P., 2010. Stable Isotope (N, C, Hg) Study of Methylmercury Sources and Trophic Transfer in the Northern Gulf of Mexico. *Environmental Science & Technology* **44**, 1630-1637.
SFBRWQCB, 2006. Mercury in San Francisco Bay Total Maximum Daily Load (TMDL) Proposed Basin Plan Amenment and Staff Report for Revised Total Maximum Daily Load (TMDL) and Proposed Mercury Water Quality Objectives. *California Regional Water Quality Control Board San Francisco Region*, Oakland, CA.
Sherman, L.S., Blum, J.D., Johnson, K.P., Keeler, G.J., Barres, J.A., Douglas, T.A., 2010. Mass-independent fractionation of mercury isotopes in Arctic snow driven by sunlight. *Nature Geoscience* **3**, 173-177.
Slotton, D.G., Ayers, S.M., Weyland, R.D., 2007. CBDA biosentinel monitoring program: 2nd year report, covering sampling conducted through December 2006. *Report for CALFED Bay-Delta Agency*, p. 92.
Smith, C.N., Kesler, S.E., Blum, J.D., Rytuba, J.J., 2008. Isotope geochemistry of mercury in source rocks, mineral deposits and spring deposits of the California Coast Ranges, USA. *Earth and Planetary Science Letters* **269**, 398-406.
Sunderland, E.M., 2006. Mercury Exposure from Domestic and Imported Estuarine and Marine Fish in the U.S. Seafood Market. *Environmental Health Perspectives* **115**, 2.
Sunderland, E.M., Dalziel, J., Heyes, A., Branfireun, B.A., Krabbenhoft, D.P., Gobas, F.A.P.C., 2010. Response of a Macrotidal Estuary to Changes in Anthropogenic Mercury Loading between 1850 and 2000. *Environmental Science & Technology* **44**, 1698-1704.
Tsai, P., Hoenicke, R., 2001. San Francisco Bay Atmospheric Deposistion Pilot Study Part 1: Mercury, *San Francisco Esturay Regional Monitoring Program for Trace Substances*. San Francisco Estuary Institute, Oakland, CA, p. 46.
Visintainer, T.A., Bollens, S.M., Simenstad, C., 2006. Community composition and diet of fishes as a function of tidal channel geomorphology. *Marine Ecology-Progress Series* **321**, 227-243.
Warner, J., Schoellhamer, D., Burau, J., Schladow, G., 2002. Effects of tidal current phase at the junction of two straits. *Continental Shelf Resources* **22**, 1629-1642.
Wiederhold, J.G., Cramer, C.J., Daniel, K., Infante, I., Bourdon, B., Kretzschmar, R., 2010. Equilibrium Mercury Isotope Fractionation between Dissolved Hg(II) Species and Thiol-Bound Hg. *Environmental Science & Technology* **44**, 4191-4197.

Zheng, W., Hintelmann, H., 2009. Mercury isotope fractionation during photoreduction in natural water is controlled by its Hg/DOC ratio. *Geochimica et Cosmochimica Acta* **73**, 6704-6715.

Figure 5.1

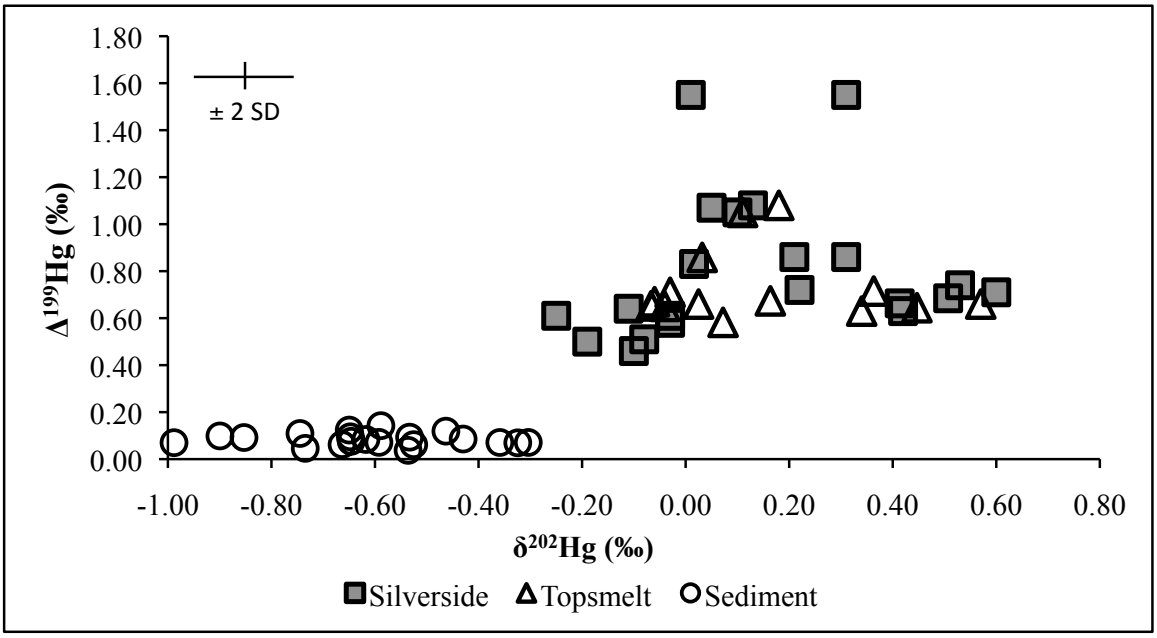

Figure 5.1. Hg isotopic composition of fish *(this study)* and sediments (Gehrke et al., 2011) in SF Bay. Silverside and topsmelt have similar Hg isotopic composition, with higher δ^{202}Hg and Δ^{199}Hg values than SF Bay surface sediments.

Figure 5.2

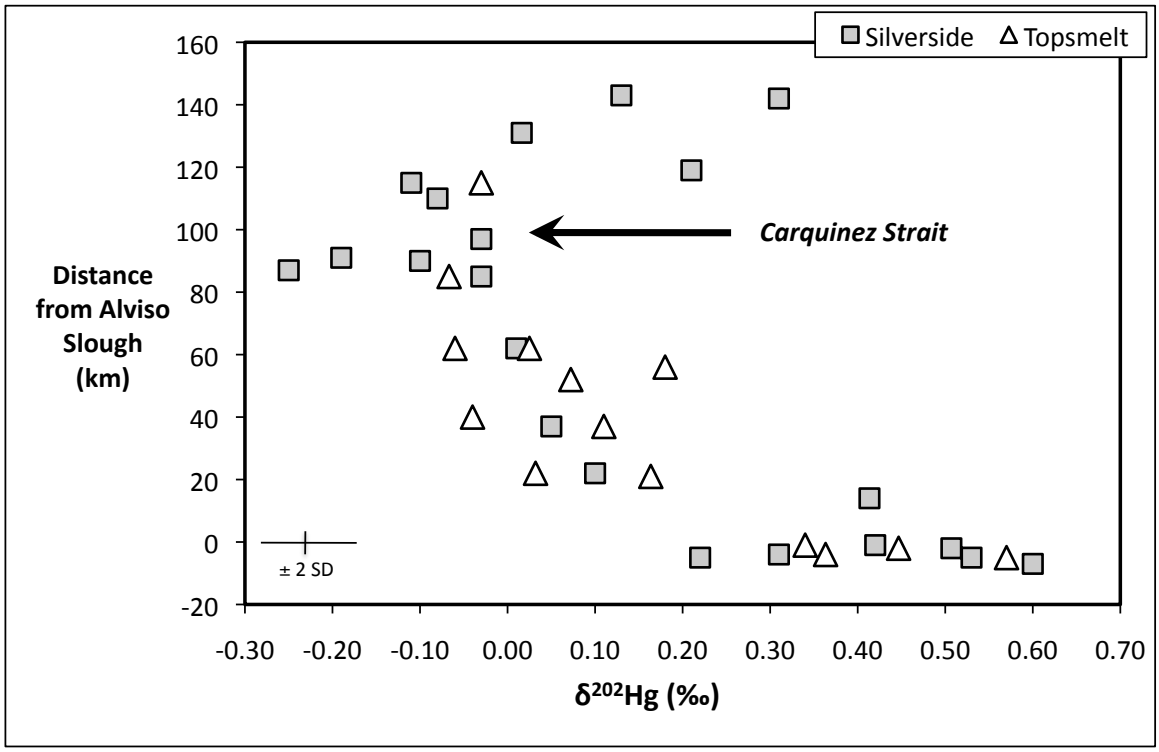

Figure 5.2: Spatial variation of δ^{202}Hg values in San Francisco Bay fish. Silverside and topsmelt δ^{202}Hg values demonstrate a spatial variation, decreasing from Lower South Bay north through San Pablo Bay, and increasing from San Pablo Bay east toward Suisun Bay.

Figure 5.3

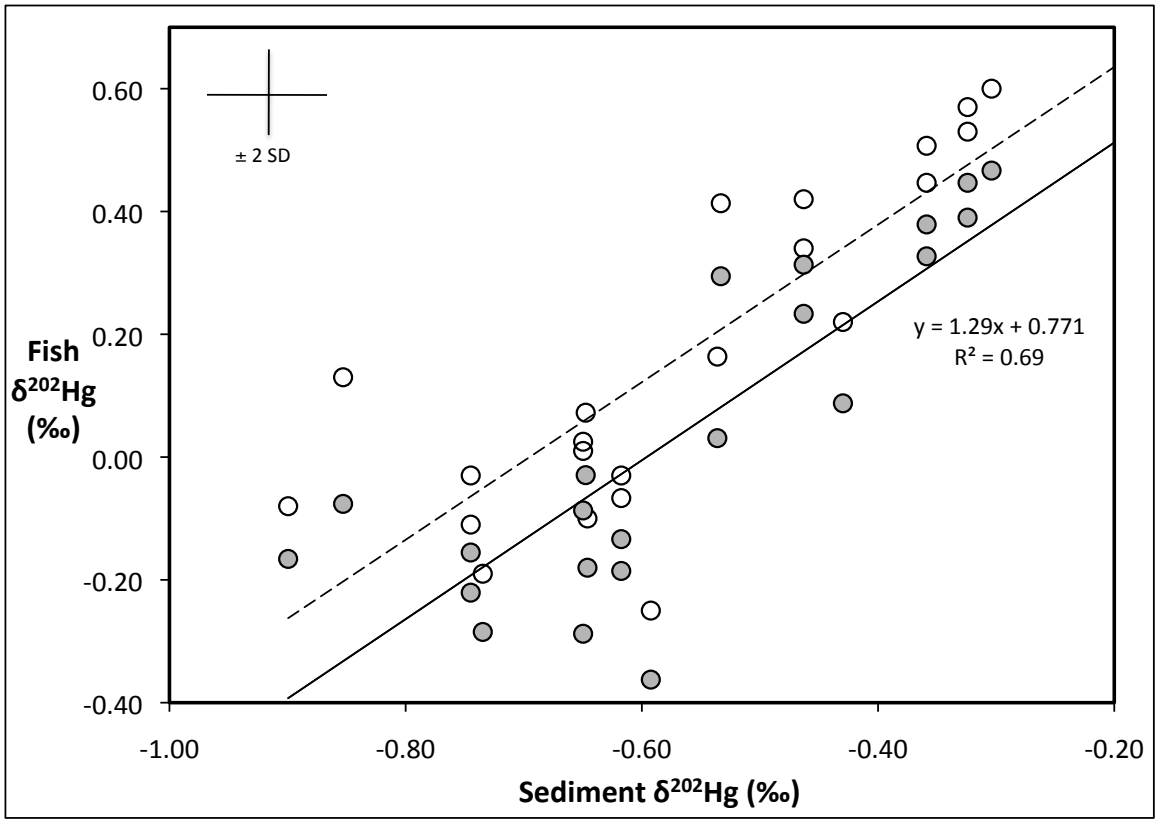

Figure 5.3. Mass-dependent Hg isotope values of sediment (Gehrke et al., 2011) and co-located fish. Open circles represent the δ^{202}Hg values measured in fish; shaded circles represent fish δ^{202}Hg values that have been corrected to remove the inferred effect of photochemical degradation of aqueous MeHg. The average offset between sediment and fish δ^{202}Hg values decreases from 0.73‰ to 0.60‰ with this correction. The dashed line denotes the trend between sediment and fish δ^{202}Hg values and the solid line shows the correlation between sediment and "corrected" fish δ^{202}Hg values.

Supporting Discussion

Fish Species Comparison of Hg Isotope Values

Both silverside and topsmelt were sampled at nine of the 26 fish sampling sites. While the Hg_T concentrations differed between the species, the $\delta^{202}Hg$ values at all nine sites were indistinguishable, with a silverside-topsmelt $\delta^{202}Hg$ value slope of 0.95±0.09 (r^2 = 0.93) (Fig. S5.4a). The $\Delta^{199}Hg$ values for co-located silverside and topsmelt are correlated (slope = 0.67±0.15, r^2 = 0.77; Fig. S5.4b) but display variability beyond analytical uncertainty demonstrating that $\Delta^{199}Hg$ values are more sensitive than $\delta^{202}Hg$ values to subtle differences in species differences in food sources and habitat. Silverside and topsmelt had dramatically different $\Delta^{199}Hg$ values at one site (Pt. Isabel) (CB5; S5.4b). This site is at the mouth of an enclosed wetland, separated from SF Bay open waters by a 300 m man-made channel, creating the potential for the two species to segregate.

Figure S5.1

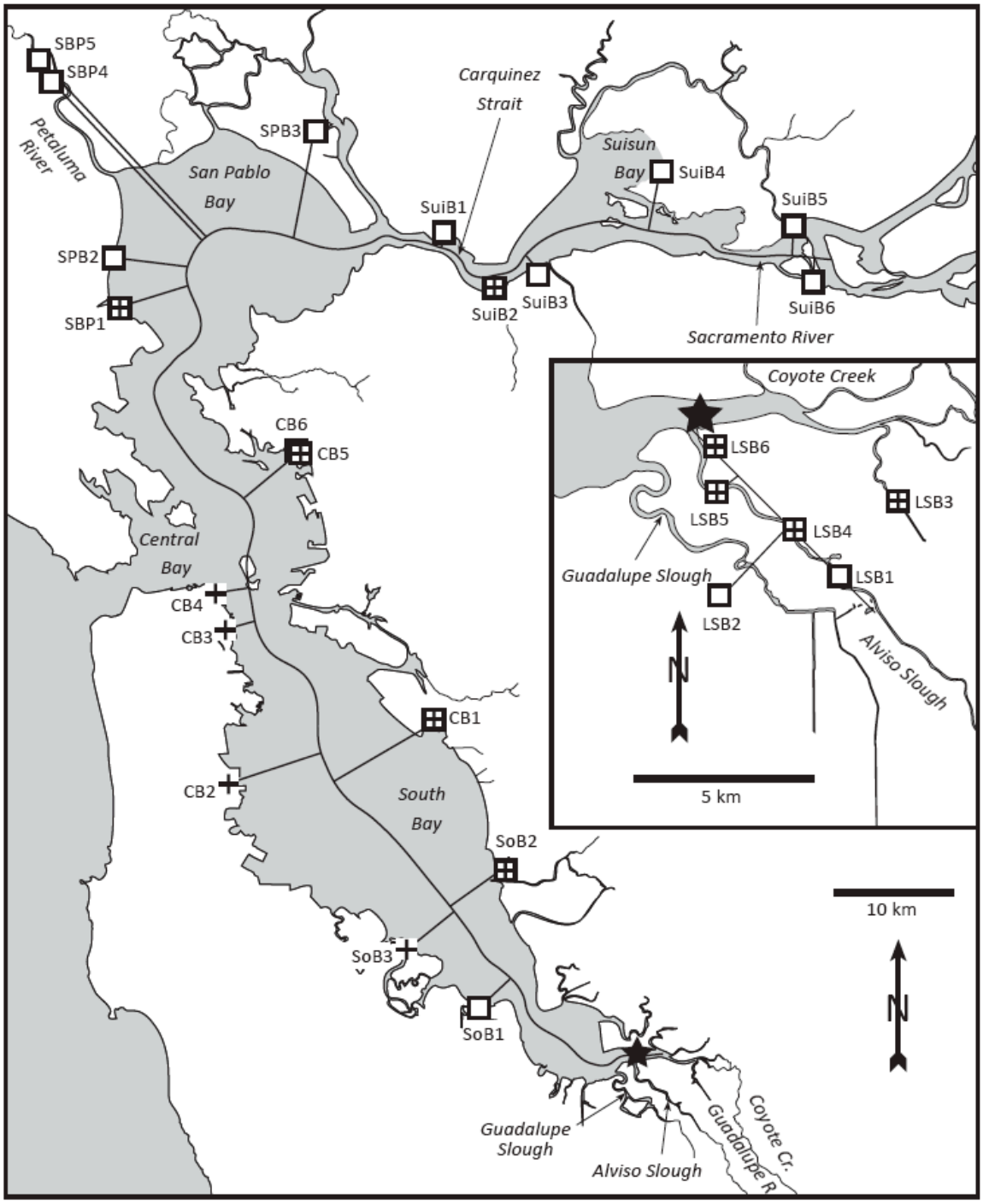

Figure S5.1: Sample locations for composite fish samples analyzed in this study. Open squares denote Mississippi silverside sample locations and plus signs denote topsmelt sample locations.

Figure S5.2

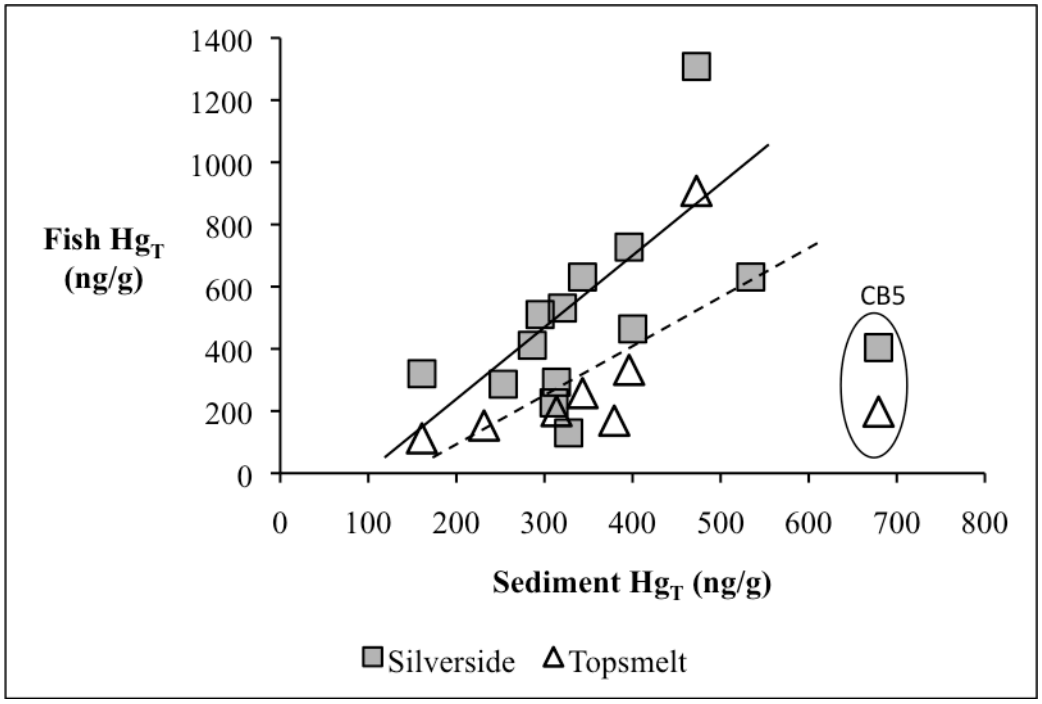

Figure S5.2. Hg_T concentrations of co-located sediments *(1)* and fish. CB5 is an outlier and is from the Central Bay. Lines demonstrate the correlation between sediment Hg_T and silverside (solid, r^2=0.40) or topsmelt (dashed, r^2=0.56) Hg_T. Error bars are within symbols.

Figure S5.3

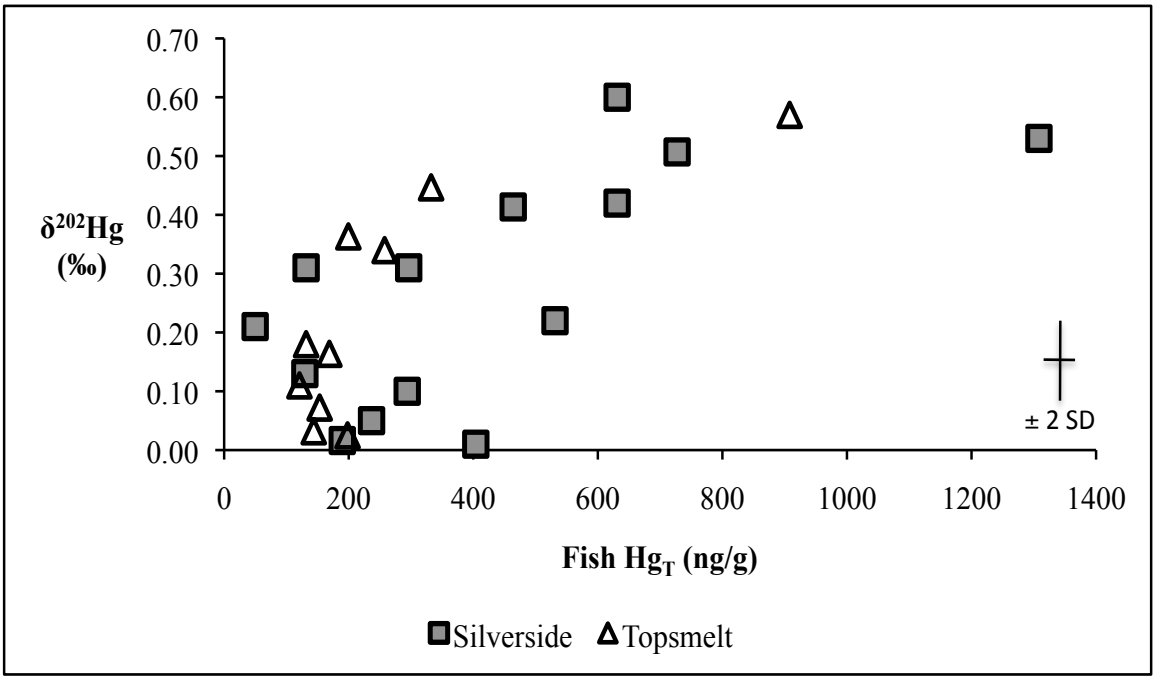

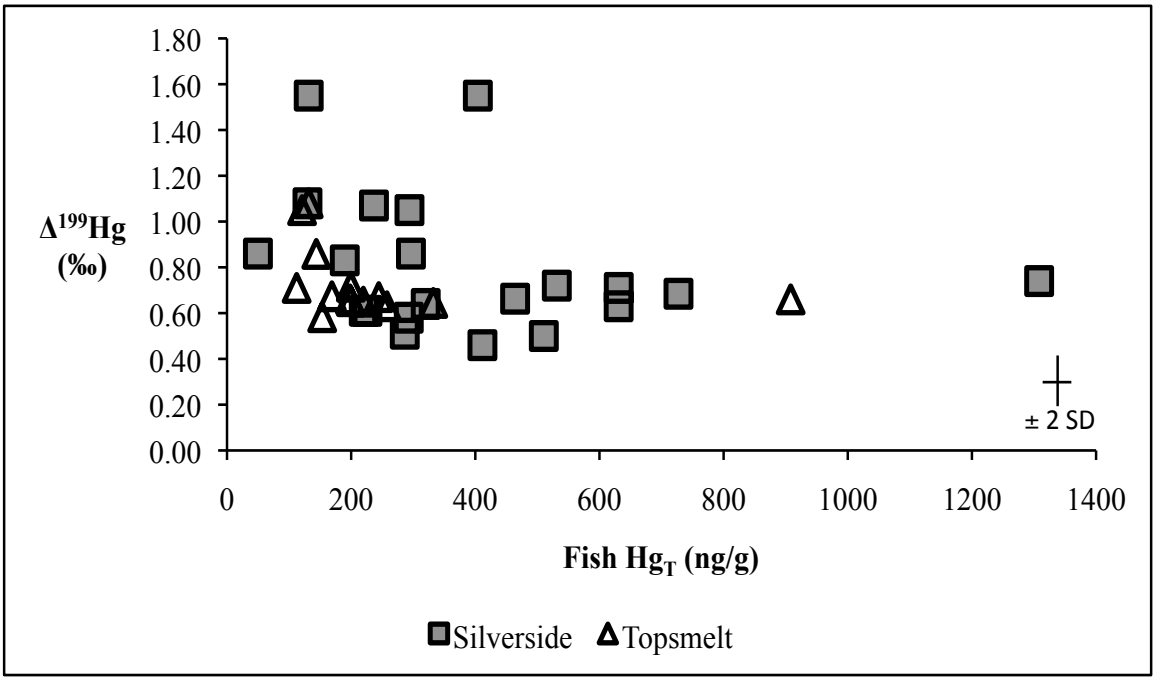

Figure S5.3. Hg isotopic composition versus Hg concentration in fish with (a) δ^{202}Hg values and (b) Δ^{199}Hg values.

Figure S5.4

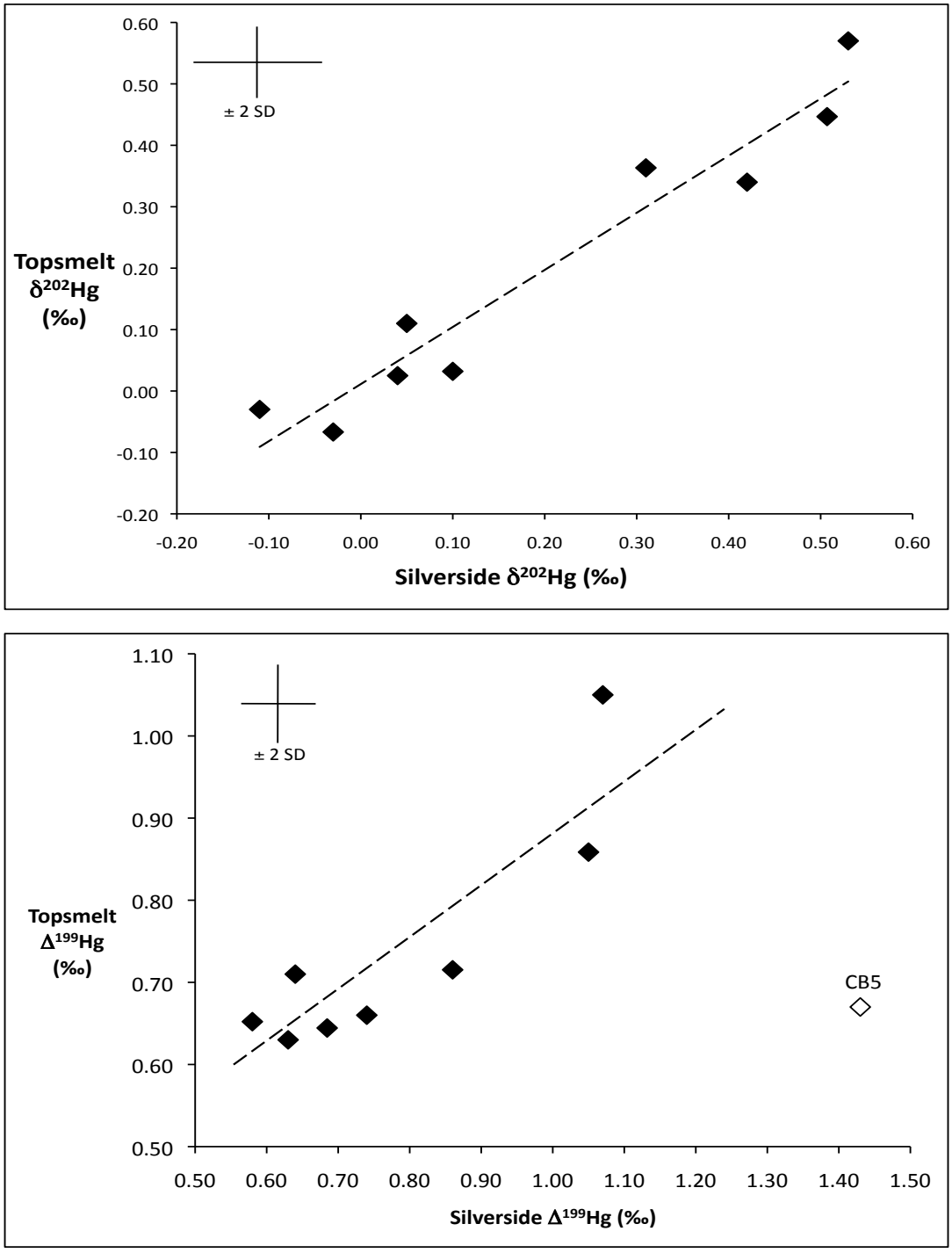

Figure S5.4. Co-located fish species comparison of Hg isotopic composition. Dashed line denotes equal values for the two species. (a) δ^{202}Hg values of MISI and TOSM are highly correlated at all sites. (b) Δ^{199}Hg values of MISI and TOSM are correlated at all sites except CB 5, which is likely due to separated primary habitats (see SI Discussion).

Figure S5.5

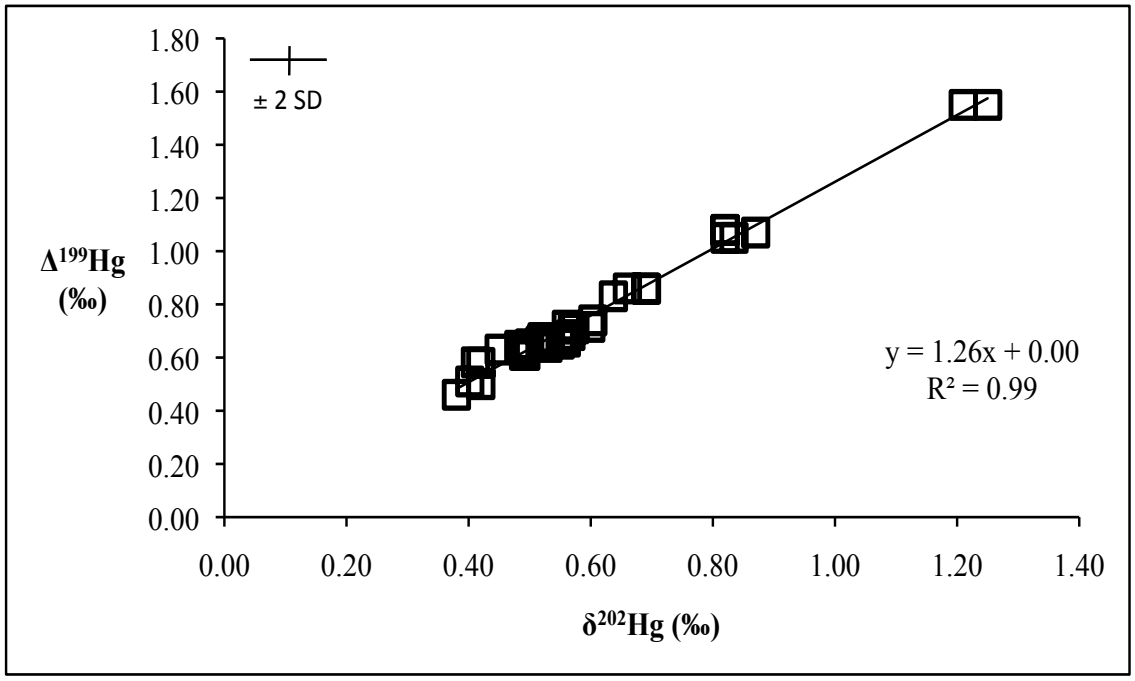

Figure S5.5. Hg mass-independent fractionation in fish. The slope of $\Delta^{199}Hg/\ \Delta^{201}Hg$ (1.26) agrees with laboratory experiments that measured MIF produced upon photochemical degradation of aqueous MeHg (slope ~1.3, see text).

Table S5.1. Locations and analytical data for composite fish samples in SF Bay.

Sample	Latitude °N	Longitude °W	Specie	Hg_T ng/g	$\delta^{202}Hg$ ‰	$\Delta^{201}Hg$ ‰	$\Delta^{199}Hg$ ‰
CB 1 MI	37.71450	-122.19644	MISI	237	0.05	0.87	1.07
CB 5 MI	37.90464	-122.31968	MISI	404	0.01	1.25	1.55
LSB 1 MI	37.42573	-121.97913	MISI	631	0.60	0.57	0.71
LSB 2 MI	37.42462	-122.01393	MISI	531	0.22	0.56	0.72
LSB 3 MI	37.44369	-121.96106	MISI	296	0.31	0.66	0.86
LSB 4 MI	37.43828	-121.99234	MISI	1308	0.53	0.60	0.74
LSB 5 MI	37.44734	-122.01969	MISI	727	0.51	0.57	0.68
LSB 6 MI	37.45945	-122.02044	MISI	631	0.42	0.49	0.63
SoB 1 MI	37.50187	-122.16530	MISI	464	0.41	0.53	0.66
SoB 2 MI	37.59344	-122.14428	MISI	294	0.10	0.83	1.05
SPB 1 MI	38.01427	-122.48989	MISI	293	-0.03	0.42	0.58
SPB 2 MI	38.04816	-122.49760	MISI	226	-0.25	0.49	0.61
SPB 3 MI	38.13725	-122.31639	MISI	220	-0.03	0.49	0.61
SPB 4 MI	38.18311	-122.56256	MISI	411	-0.10	0.38	0.46
SPB 5 MI	38.20891	-122.57894	MISI	510	-0.19	0.42	0.50
SuiB 1 MI	38.06389	-122.19282	MISI	286	-0.08	0.40	0.51
SuiB 2 MI	38.02117	-122.14076	MISI	320	-0.11	0.53	0.64
SuiB 3 MI	38.02554	-122.10174	MISI	50	0.21	0.69	0.86
SuiB 5 MI	38.07170	-121.86864	MISI	132	0.31	1.21	1.55
SuiB 6 MI	38.02476	-121.84384	MISI	130	0.13	0.82	1.08
SuiB 4 MI	38.11617	-121.98523	MISI	190	0.02	0.64	0.83
CB 1 TO	37.71450	-122.19644	TOSM	121	0.11	0.82	1.05
CB 2 TO	37.66090	-122.38198	TOSM	220	-0.04	0.50	0.65
CB 3 TO	37.77092	-122.39819	TOSM	153	0.07	0.41	0.58
CB 4 TO	37.80361	-122.40078	TOSM	132	0.18	0.82	1.08
CB 5 TO	37.90464	-122.31968	TOSM	198	0.03	0.56	0.66
CB 6 TO	37.90429	-122.32320	TOSM	244	-0.06	0.55	0.67
LSB 3 TO	37.44369	-121.96106	TOSM	199	0.36	0.60	0.72
LSB 4 TO	37.43828	-121.99234	TOSM	908	0.57	0.52	0.66
LSB 5 TO	37.44734	-122.01969	TOSM	332	0.45	0.48	0.64
LSB 6 TO	37.45945	-122.02044	TOSM	258	0.34	0.45	0.63
SoB 2 TO	37.59344	-122.14428	TOSM	144	0.03	0.69	0.86
SoB 3 TO	37.53267	-122.23210	TOSM	169	0.16	0.52	0.67
SPB 1 TO	38.01427	-122.48989	TOSM	200	-0.07	0.55	0.65
SuiB2 TO	38.02117	-122.14076	TOSM	112	-0.03	0.57	0.71

MISI=Mississippi silverside, TOSM=topsmelTable S5.2. Isotopic measurements of standard reference materials and sample replicates.

Table S5.2 Hg concentration and Hg isotopic composition of replicate combustions of standards and samples.

Sample	Hg_T ng/g	Recovery %	$\delta^{202}Hg$ ‰	$\Delta^{201}Hg$ ‰	$\Delta^{199}Hg$ ‰
Standards					
DOLT-2	1891	95	-0.62	0.62	0.73
	2109	106	-0.51	0.59	0.73
	2264	114	-0.53	0.58	0.74
Avg	2088	105	-0.55	0.60	0.74
1 SD	187	9	0.06	0.02	0.01
ERMCE 464	4716	90	0.65	2.02	2.34
	4606	88	0.78	1.93	2.37
	4720	90	0.68	1.88	2.34
Avg	4680	89	0.70	1.94	2.35
1 SD	65	1	0.07	0.07	0.01
Replicates of composite fish samples					
CB5 MI	205		-0.03	0.56	0.67
	192		0.08	0.56	0.65
SPB3 MI	220		-0.03	0.49	0.61
	221		-0.04	0.50	0.62
Replicates of different composite fish samples from the same locations					
SoB3 TO	163		0.19	0.53	0.68
	175		0.14	0.51	0.67
SuiB4 MI	159		0.01	0.71	0.94
	221		0.02	0.57	0.72
LSB3 MI	148		0.33	0.57	0.70
	251		0.40	0.63	0.73

Chapter 6

Mercury deposition through the Paleocene-Eocene Thermal Maximum: Insights from continental shelf and deep marine sediments

Authors: Gretchen E. Gehrke, Joel D. Blum, James C. Zachos

In preparation for Paleoceanography

Abstract

The Paleocene-Eocene Thermal Maximum (PETM) was a rapid and extreme climate excursion coincident with a significant perturbation of the global carbon cycle. We explore the impact of the PETM on Hg cycling through Hg concentration and Hg stable isotope analyses of marine sediments deposited in the late Paleocene and early Eocene epochs. The Hg concentrations in sediments from the North American continental margin (ODP site 174AX) double at the onset of the PETM, from ~15 to ~30 ng/g, and Hg concentrations correlate well with previously published $\delta^{13}C$ and $\delta^{18}O$ values. The Hg concentrations of South Atlantic deep sea sediments (IODP site 1263) also increase, from 7 to 16 ng/g, but the flux of Hg to

sediments may not have changed appreciably. There was a significant shift in Hg isotopic composition of deep sea sediments through the P-E boundary. Through the PETM, sediment δ^{202}Hg values shifted from -4.5‰ to -0.3‰, and sediment Δ^{199}Hg concurrently shifted from 0.14‰ to 0.38‰. These Hg isotope shifts suggest an appreciable perturbation of the Hg isotope systematics through the PETM, but the exact cause for this is unknown.

1. Introduction

During the gradual warming of the early Cenozoic Era, Earth experienced several rapid, intense global warming events in the late Paleocene and Eocene epochs known as "hyperthermals." The most extreme hyperthermal was the Paleocene-Eocene Thermal Maximum (PETM) during which sea surface temperatures increased by 5-9°C (Zachos et al., 2006), deep-sea temperatures increased by 4-5°C (Thomas et al., 2002), ocean pH decreased (Pearson and Palmer, 2000; Zachos et al., 2005), and benthic and pelagic foraminifera experienced mass extinction (Thomas, 1998). The climate alteration is marked in marine and terrestrial sediments by a negative carbon isotope excursion of >2.5‰ (Cui et al., 2011; John et al., 2008; Schouten et al., 2007; Zachos et al., 2005), which is preceded by an abrupt carbonate dissolution horizon in deep-sea sediments (Zachos et al., 2005). The global carbon isotope excursion and deep-sea carbonate dissolution horizons indicate a substantial perturbation to the global carbon cycle concluding the Paleocene, which likely resulted from a massive input of carbon dioxide (CO_2) to the ocean (see reviews Higgins and Schrag, 2006; Zachos et al., 2010). The source of

that carbon is widely debated, with leading hypotheses including the oxidation of seafloor methane hydrates (Dickens et al., 1997), global conflagration of peatlands (Kurtz et al., 2003; Secord et al., 2010), or dessication of an epicontinental seaway (see review in Higgins and Schrag, 2006). The mass of carbon estimated to have been injected into the ocean ranges from 2000 to 7000 Pg depending on the carbon isotopic composition of the proposed source (Panchuk et al., 2008), and the duration of carbon injection is estimated to have lasted 10-30 ky (Rohl et al., 2007; Sluijs et al., 2007; Zachos et al., 2006). Recent studies have suggested that at least two events involving carbon release are required to produce the sediment geochemistry observed through the PETM (Carozza et al., 2011; Pagani et al., 2006a; Zeebe et al., 2009). The global recovery of the carbon cycle likely involved significant terrestrial weathering (Panchuk et al., 2008) and carbon sequestration in the terrestrial biosphere (Bowen and Zachos, 2010). Though the sequence of events and underlying cause(s) of the carbon cycle perturbation(s) are as yet unclear, the PETM does record an extreme global warming.

Mercury actively cycles among the atmosphere, oceans and land surfaces, so global changes in atmospheric and marine chemistry are likely to affect the Hg cycle. Changes in terrestrial weathering are also likely to influence the Hg cycle since surface soils and terrestrial sediments comprise the largest reservoir of Hg in the actively cycling environment (Mason and Sheu, 2002). With elevated global temperatures and a more energetic hydrologic cycle (Pagani et al., 2006b), we speculate that Hg evaporation from the surface ocean into the lower atmosphere accelerated, atmospheric Hg deposition to surface environments through

precipitation increased, and Hg transport from surface soils and sediments to the ocean increased (due to higher rates of terrestrial weathering). Alternatively, increased ocean acidity (Zachos et al., 2005) could have promoted more oxidating conditions that facilitated stronger marine retention of aqueous Hg and slowed Hg exchange between the ocean and atmosphere. In addition to rates of Hg exchange being altered, the primary source of Hg to the marine environment also could have changed if the massive source of carbon released at the PETM also released Hg.

To gain insight into changes that occurred in the Hg cycle through the PETM, Hg concentrations and Hg isotopic compositions were analyzed in marine sedimentary sequences that encompass the P-E boundary. Analysis of Hg isotopes has been used to successfully distinguish, identify, and trace different sources of Hg into the environment (Carignan et al., 2009; Estrade et al., 2011; Foucher et al., 2009; Gehrke et al., 2011a; Gehrke et al., 2011c), and to identify photochemical processes influencing Hg cycling (Bergquist and Blum, 2009; Senn et al., 2010). Since it is likely that marine sediments record the Hg isotopic composition of marine Hg (Gehrke et al., 2009), we suggest that marine sediments deposited through the PETM will reflect changes to the composition of marine Hg through that interval, and elucidate the effects of the PETM on global Hg cycling. We analyzed Hg in well-studied cores from the North American continental shelf (ODP site 174AX, Bass River, NJ) and South Atlantic Ocean (IODP sites 1263 and 1262, Walvis Ridge) to explore marine Hg isotope records through the PETM.

2. Materials and Methods

2.1 Sample Locations

Sediment samples from ODP Leg 174AX in Bass River, NJ (39°36'42"N 74°26'12"W) were obtained from the Rutgers University Core Repository. Detailed sampling notes and initial reports were compiled (Miller et al., 1998), and on the basis of this and subsequent data, it was proposed that the Bass River core site was located on the continental shelf at a paleo-depth of ~100 m (Cramer et al., 1999). Sediments from ODP Leg 208 collected at sites 1262 (27°12'51"S 1°34'37"E) and 1263 (28°32'1"S 2°46'46"E) along Walvis Ridge were obtained from the IODP Bremen Core Repository. Sampling notes and initial reports were compiled (Zachos et al., 2004). Tectonic reconstructions suggest that sites 1262 and 1263 were at paleo-depths of 2600 m and 1500 m, respectively (Zachos et al., 2005).

2.2 Hg concentration analysis

Sediments were freeze-dried and homogenized using a boron-carbide mortar and pestle. Powdered sediments were analyzed for Hg concentrations using a Nippon Instruments MA-2000 Hg analyzer using previously described methods (Biswas et al., 2008). The quantification limit for this method during analysis of the Bass River sediments was 0.030 ng Hg, corresponding to ~1.5 ng/g Hg. The Bass River sediment Hg concentrations reported are 3-point averages of measured sediment Hg concentrations that integrate 30-100 cm of sediment. Initial measured Hg concentrations and 3-point averages are provided in Table S6.1. During analysis of the Walvis Ridge sediments, the quantification limit was 0.024 ng Hg, corresponding to ~1 ng/g Hg. Replicate analyses of marine sediment SRM MESS-3

and MAG-1 indicate recovery of greater than 95%, and replicate analyses of in-house standards indicate method reproducibility within ± 8%.

2.3 Hg isotope analysis

Sediment Hg isotope analyses were measured using a Nu Instrument multi-collector inductively coupled mass spectrometer (MC-ICPMS) using modifications of previously described methods (Blum and Bergquist, 2007; Gehrke et al., 2011a). Briefly, 2-3 g splits of homogenized samples were combusted in a two-stage furnace where the first furnace ramped to 750°C and the second furnace was held at 1000°C to ensure complete combustion of organic matter. Volatilized Hg was entrained in a gas stream of air and O_2 and trapped in a 24 mL oxidizing solution of 1% $KMnO_4$. To further concentrate samples, between two and eight 24 mL traps were reduced by $SnCl_2$ in the presence of H_2SO_4 and purged using a modified automated Nippon Instruments sampler into an 8 g trap of 1% $KMnO_4$ to reach a final Hg concentration of 5 ng/g. Analysis of SRMs MESS-3 (NRC-CNRC, Beaufort Sea marine sediment) and MAG-1 (USGS, Gulf of Maine marine sediment) demonstrated greater than 96% recovery through this process. For measurement on the MC-ICPMS, samples, in-house standard UM-Almadén, and NIST-3133 were matched for Hg concentration and solution matrix. Solutions were neutralized with NH_2OH, and samples were reduced online by $SnCl_2$. Evolved Hg gas was entrained in a continuous Ar flow, and separated using a frosted-tip phase separator, and introduced to the plasma along with aerosol Tl (NIST 997). Instrumental mass-bias and drift were monitored using the internal Tl standard and sample-standard bracketing with NIST 3133. On-peak

zero corrections also were applied. Mass-dependent Hg isotope compositions are reported as δ^{202}Hg in permil (‰) notation and calculated as (Blum and Bergquist, 2007):

$$\delta^{202}Hg = 1000*([(^{202}Hg/^{198}Hg)_{sample}]/[(^{202}Hg/^{198}Hg)_{3133}]-1).$$

Mass-independent Hg isotope compositions are reported as Δ^{199}Hg and Δ^{201}Hg in permil (‰) notation and calculated as (Bergquist and Blum, 2007):

$$\Delta^{199}Hg = \delta^{199}Hg_{measured} - (\delta^{202}Hg_{measured}*0.252)$$

$$\Delta^{201}Hg = \delta^{201}Hg_{measured} - (\delta^{202}Hg_{measured}*0.752).$$

Replicate analyses of the in-house standard UM-Almadén demonstrated analytical precision within ±0.10‰ (2 SD) for δ^{202}Hg, and ±0.10‰ (2 SD) for Δ^{199}Hg. Analysis of a procedural replicate had less precision, ±0.15‰ (1 SD) for δ^{202}Hg, ±0.03‰ (1 SD) for Δ^{199}Hg, and ±0.02‰ (1 SD) for Δ^{201}Hg.

3. Results and Discussion

3.1 Hg concentrations in continental shelf sediments

The Hg concentration in continental shelf sediments sampled in the Bass River, NJ core (ODP site 174AX) increased substantially during the PETM. Sediments deposited for more than 300 kyr preceding the P-E boundary (Cramer et al., 1999) had Hg concentrations of 16 ± 2 ng/g (Figure 6.1, Table 6.1). At the onset of the PETM, Hg concentrations increased to 31 ng/g and then decreased to pre-PETM values over 300 kyr (Figure 6.1, Table 6.1), based on sediment ages from Cramer et al. (1999). The Hg concentration increase is coincident with previously published δ^{13}C values (John et al., 2008) (Figure 6.1), suggesting that the C cycle

perturbation and the Hg perturbation were simultaneous. Sediment Hg concentrations are also highly correlated with published $\delta^{18}O$ values (John et al., 2008) ($r^2 = 0.82$) (Figure S6.1) through the ~600 kyr period analyzed, which suggests that global temperature may be an important influence on Hg cycling.

In response to rapid warming, it has been suggested that the global hydrologic cycle accelerated (Pagani et al., 2006b) and terrestrial weathering in certain regions increased (Schmitz and Pujalte, 2007). At Bass River, amplified terrestrial weathering likely contributed to an estimated 5-fold increase in sedimentation rates from 30-100 kyr after the onset of the PETM (John et al., 2008). Since sediment Hg concentrations doubled at the onset of the PETM and the sedimentation rate increased by a factor of 5, the flux of Hg to continental shelf sediments at Bass River may have increased by an order of magnitude and remained elevated above the pre-PETM Hg flux for at least 100 kyr. Sediment total organic carbon (TOC) percentage also increased following the PETM (John et al., 2008), and was likely a vehicle for Hg deposition to those sediments (Gehrke et al., 2009).

3.2 Hg concentrations in deep sea sediments

Marine sediments on Walvis Ridge had low Hg concentrations through the P-E interval. At the deepest site on Walvis Ridge (IODP site 1262) with a paleo-depth of 2600 m (Zachos et al., 2005), Hg concentrations prior to the onset of the PETM were below the quantification limit (QL = 0.024 ng; ≈ 1 ng/g), increased to 2 ng/g in the clay layer at the height of the PETM, and gradually decreased below the quantification limit after ~120 kyr (ages in Zachos et al., 2010). In the shallowest

core obtained from Walvis Ridge (IODP site 1263) at a paleo-depth of 1500 m (Zachos et al., 2005), the Hg concentration in a sediment sample preceding the PETM was 7 ng/g, and Hg concentrations increased to 16 ng/g in clay layer sediments at the height of the PETM (Table 6.1). Following the P-E boundary, Hg concentrations decreased to pre-PETM values over ~ 170 kyr (Table 6.1) (ages in Rohl et al., 2007). The observed changes in sediment Hg concentrations through the PETM interval likely reflect carbonate dissolution and subsequent sedimentation rather than enhanced Hg deposition. While detailed sedimentation rates are not well constrained, general estimates of the PETM interval suggest that sedimentation rates at Walvis Ridge site 1263 decreased from ~2cm/kyr to less than 1 cm/kyr in the clay layer, and then increased to 3 cm/kyr in the 100 kyr following the PETM (Rohl et al., 2007), which would suggest that changes in Hg flux were not appreciable.

Regardless of any changes in Hg flux to Walvis Ridge sites 1262 or 1263 through the PETM, sediments at site 1263 maintained higher Hg concentrations than any Hg concentrations observed in sediments from site 1262. Since the two marine cores are in a restricted geographic area, the supply of Hg to surface waters was likely the same for both cores. However, it has been proposed that, at a paleo-depth of 1500 m, site 1263 was situated such that the sediment-water interface was in the oxygen minimum zone, while at a paleo-depth of 2600 m, site 1262 was below the oxygen minimum zone, with more oxic bottom waters (Chun et al., 2010). Thus, organic matter deposition and preservation, and associated Hg deposition and retention, were likely greater at site 1263. Total carbon analysis on sediments from

the mid-Paleocene and the mid-Eocene suggest low TOC values, ~0.1%, at both sites 1262 and 1263 (Zachos et al., 2004) throughout these two epochs, but TOC was not measured in sediments during the PETM interval and a detailed comparison between the two cores has not been performed.

3.3 Hg isotopes in deep sea sediments

3.3.1 Mass-dependent Hg fractionation in Walvis Ridge sediments

The Hg isotopic compositions of sediments at site 1263 show a significant shift through the PETM. Sediment deposited prior to the PETM has a δ^{202}Hg value of -4.51‰ (Figure 6.2, Table 6.2). This is the lowest δ^{202}Hg value observed in sediments, and the lowest δ^{202}Hg value published to date. However, more negative δ^{202}Hg values of ~-5 to -6‰ were recently reported for a few terrestrial mosses (Sonke et al., 2011). Over ~20-40 kyr through the PETM (Rohl et al., 2007), Walvis Ridge sediments δ^{202}Hg values abruptly shift from -4.51 to -0.34‰ (Figure 6.2, Table 6.2), which is the largest range of δ^{202}Hg values published for any one environmental media (e.g. sediments, soils, peats, precipitation). For ~80 kyr following the PETM, sediment δ^{202}Hg values gradually decline from -0.34 to -1.04‰ (Figure 6.2, Table 6.2). Post-PETM sediments analyzed in this study are within the range of previously published sediment δ^{202}Hg values, which range only from -0.2 to -2.5‰ (Foucher et al., 2009; Gehrke et al., 2011a; Gehrke et al., 2009). Pre-Industrial Era marine sediment δ^{202}Hg values have a much narrower reported range, between -1.34 and -0.61‰ (Gehrke et al., 2009; Gehrke et al., 2011b), which is almost exactly the same range as for the post-PETM sediments analyzed in this

study. Thus, it is possible that the very low δ^{202}Hg value (-4.51‰) observed in sediment preceding the PETM marks an excursion in marine Hg isotopic composition.

3.3.2 Possible causes of the shift in sediment Hg isotopes through the PETM

The observed shift in marine sediment δ^{202}Hg values across the PETM suggests that a perturbation to the Hg isotope system occurred at that time. If mid-Paleocene sediment δ^{202}Hg values are similar to the post-PETM δ^{202}Hg values and the low δ^{202}Hg value (-4.51‰) observed at 335.85 mcd at Walvis Ridge site 1263 is a negative isotopic excursion (rather than the standard marine Hg isotopic composition in the Paleocene), then it is possible that an event preceding the carbon isotope excursion altered the Hg isotope composition of the ocean. It has recently been proposed that substantial global warming occurred prior to the observed CIE, which possibly emanated from the hot, arid climate igniting massive peat fires (Secord et al., 2010). Peats have been reported to have δ^{202}Hg values ranging from -1 to -3‰ (Biswas et al., 2008), but recently, certain terrestrial mosses (that are pre-cursors to peats)were reported to have δ^{202}Hg values as low as -6‰ (Sonke et al., 2011). Fires have been shown to effectively release organic-bound Hg from soils (Biswas et al., 2007), thus conflagration of peatlands could be a low δ^{202}Hg value source. Alternatively, if Walvis Ridge sediment δ^{202}Hg values were low throughout the Paleocene and the shift to -0.34‰ through the clay layer of the PETM marks a positive isotope excursion, it is more likely that there was a mantle-derived source of Hg released to the environment. Volcanic plumes have been reported to have

$\delta^{202}Hg$ = -0.11‰ in volcanic plumes (Zambardi et al., 2009). However, recent studies of the carbon cycle through the PETM have not supported mantle-derived sources of carbon to cause the CIE. While the causes of the carbon cycle perturbation through the PETM are still widely debated, it is possible that more detailed evaluation of the Hg cycle perturbation will contribute valuable insight to global dynamics through the PETM.

3.3.3 Mass-independent Hg fractionation in Walvis Ridge sediments

Sediments also exhibit a shift in MIF through the PETM. Sediment deposited prior to the PETM has $\Delta^{199}Hg$ = 0.14‰ and $\Delta^{201}Hg$ = 0.07‰ (Figure 6.2, Table 6.2), which is similar to that observed in other marine sediments (Gehrke et al., 2009; Gehrke et al., 2011b). Through the PETM, sediment $\Delta^{199}Hg$ and $\Delta^{201}Hg$ values increase, peaking at 0.38‰ and 0.31‰, respectively, approximately 50 kyr after the onset of the PETM (Figure 6.2, Table 6.2). Sediment $\Delta^{199}Hg$ and $\Delta^{201}Hg$ values remain high ($\Delta^{199}Hg$ = 0.31 ± 0.01‰, $\Delta^{201}Hg$ = 0.26 ± 0.05‰) for at least 80 kyr. These are the highest $\Delta^{199}Hg$ and $\Delta^{201}Hg$ values reported in sediments, and are more than twice as high as those observed in Pleistocene Mediterranean Sea sediments (Gehrke et al., 2009) or Holocene Baltic Sea sediments (Gehrke et al., 2011b). Significant MIF has only been reported to be imparted during photochemical reduction of Hg species (Bergquist and Blum, 2007; Blum, 2011) and elevated $\Delta^{199}Hg$ and $\Delta^{201}Hg$ values in marine sediments likely reflect higher degrees of photochemical cycling of Hg in surface waters. By applying the empirical relationship between photochemical Hg reduction and resultant aqueous Hg MIF

that was observed by Bergquist and Blum (2007), we estimate that 15-20% of aqueous Hg was photochemically reduced from surface waters during the 80 kyr following the P-E boundary, whereas only ~5% was photochemically reduced prior to the onset of the PETM. One possible explanation for the elevation in MIF is that photochemical Hg cycling was promoted by a longer residence time of Hg in the upper ocean. Studies of the hydrologic cycle through the PETM and Eocene have suggested that ocean circulation decreased following the initiation of the PETM (Bice and Marotzke, 2002) and a more stagnant water column developed; elevated Δ^{199}Hg and Δ^{201}Hg values in sediments deposited following the PETM is consistent with this hypothesis.

4. Conclusions and Recommendations for Future Work

The Hg concentrations and Hg isotope compositions of continental shelf and open ocean sediments shifted significantly through the PETM. Coincident with the carbon isotope excursion (CIE), Hg concentrations in the continental shelf Bass River (NJ) core doubled from a baseline 16 ng/g to 32 ng/g. In open ocean sediments at Walvis Ridge site 1263, δ^{202}Hg values shifted from an unprecedentedly low -4.51‰ to -0.34‰ through the clay layer marking the PETM, exhibiting the largest range of δ^{202}Hg values reported in sediments or other media.

To evaluate the causes of the shift in Hg isotope compositions of Walvis Ridge sediments through the PETM, it is necessary to establish a baseline from which to compare the shifting Hg isotope composition. Early- and mid-Paleocene Walvis Ridge sediments should be characterized for Hg isotope composition. Additionally,

continental shelf sediments at Bass River, NJ and elsewhere, and terrestrial sediments such as on Spitsbergen (Core BH9-05) encompassing the PETM should be analyzed for Hg isotope composition. By characterizing sediments deposited in a variety of environments, it would be possible to assess the geographic extent and nature of the perturbations to the Hg cycle.

Acknowledgements

The authors would like to than the Consortium for Ocean Leadership for funding through the Schlanger Fellowship for graduate students, and the IODP and Bremen Core Repository for excellent preservation and archival sampling of cores. We would also like to thank Marcus Johnson for indefatigable laboratory maintenance and operation.

References:

Bergquist, B. A. and Blum, J. D., 2007. Mass-dependent and -independent fractionation of Hg isotopes by photoreduction in aquatic systems. *Science* **318**, 417-420.

Bergquist, B. A. and Blum, J. D., 2009. The Odds and Evens of Mercury Isotopes: Applications of Mass-Dependent and Mass-Independent Isotope Fractionation. *Elements* **5**, 353-357.

Bice, K. L. and Marotzke, J., 2002. Could changing ocean circulation have destabilized methane hydrate at the Paleocene/Eocene boundary? *Paleoceanography* **17**, pp.12.

Biswas, A., Blum, J. D., Bergquist, B. A., Keeler, G. J., and Xie, Z. Q., 2008. Natural Mercury Isotope Variation in Coal Deposits and Organic Soils. *Environmental Science & Technology* **42**, 8303-8309.

Biswas, A., Blum, J. D., Klaue, B., and Keeler, G. J., 2007. Release of mercury from Rocky Mountain forest fires. *Global Biogeochemical Cycles* **21**, pp.13.

Blum, J. D., 2011. Applications of Stable Mercury Isotopes to Biogeochemistry, in: Baskaran, M. (Ed.), *Handbook of Environmental Isotope Geochemistry*, 1st ed. Springer, p 229.

Blum, J. D. and Bergquist, B. A., 2007. Reporting of variations in the natural isotopic composition of mercury. *Analytical and Bioanalytical Chemistry* **388**, 353-359.

Bowen, G. J. and Zachos, J. C., 2010. Rapid carbon sequestration at the termination of the Palaeocene-Eocene Thermal Maximum. *Nature Geoscience* **3**, 866-869.

Carignan, J., Estrade, N., Sonke, J. E., and Donard, O. F. X., 2009. Odd Isotope Deficits in Atmospheric Hg Measured in Lichens. *Environmental Science & Technology* **43**, 5660-5664.

Carozza, D. A., Mysak, L. A., and Schmidt, G. A., 2011. Methane and environmental change during the Paleocene-Eocene thermal maximum (PETM): Modeling the PETM onset as a two-stage event. *Geophysical Research Letters* **38**, pp.5.

Chun, C. O. J., Delaney, M. L., and Zachos, J. C., 2010. Paleoredox changes across the Paleocene-Eocene thermal maximum, Walvis Ridge (ODP Sites 1262, 1263, and 1266): Evidence from Mn and U enrichment factors. *Paleoceanography* **25**, PA4202.

Cramer, B. S., Aubry, M., Miller, K. G., Olsson, R. K., Wright, J. D., and Kent, D. V., 1999. An exceptional chronologic, isotopic, and clay mineralogic record of the latest Paleocene thermal maximum, Bass River, NJ, ODP 174AX. *Bulletin de la Societe Geologique de France* **170**, 883-897.

Cui, Y., Kump, L. R., Ridgwell, A. J., Charles, A. J., Junium, C. K., Diefendorf, A. F., Freeman, K. H., Urban, N. M., and Harding, I. C., 2011. Slow release of fossil carbon during the Palaeocene-Eocene Thermal Maximum. *Nature Geoscience* **4**, 481-485.

Dickens, G. R., Castillo, M. M., and Walker, J. C. G., 1997. A blast of gas in the latest Paleocene: Simulating first-order effects of massive dissociation of oceanic methane hydrate. *Geology* **25**, 259-262.

Estrade, N., Carignan, J., and Donard, O. F. X., 2011. Tracing and Quantifying Anthropogenic Mercury Sources in Soils of Northern France Using Isotopic Signatures. *Environmental Science & Technology* **45**, 1235-1242.

Foucher, D., Ogrinc, N., and Hintelmann, H., 2009. Tracing Mercury Contamination from the Idrija Mining Region (Slovenia) to the Gulf of Trieste Using Hg Isotope Ratio Measurements. *Environmental Science & Technology* **43**, 33-39.

Gehrke, G. E., Blum, J. D., and Marvin-DiPasquale, M., 2011a. Sources of mercury to San Francisco Bay surface sediment as revealed by mercury stable isotopes. *Geochimica Et Cosmochimica Acta* **75**, 691-705.

Gehrke, G. E., Blum, J. D., and Meyers, P. A., 2009. The geochemical behavior and isotopic composition of Hg in a mid-Pleistocene western Mediterranean sapropel. *Geochimica Et Cosmochimica Acta* **73**, 1651-1665.

Gehrke, G. E., Blum, J. D., and Slomp, C. P., 2011b. Mercury Concentration and Isotopic Composition in Modern and Pre-Industrial Baltic Sea Sediments. *Chemical Geology* ***submitted***.

Gehrke, G. E., Blum, J. D., Slotton, D. G., and Greenfield, B. K., 2011c. Mercury Isotopes Link Mercury in San Francisco Bay Forage Fish to Surface Sediments. *Environmental Science & Technology*, **45**, 1264-1270.

Higgins, J. A. and Schrag, D. P., 2006. Beyond methane: Towards a theory for the Paleocene-Eocene Thermal Maximum. *Earth and Planetary Science Letters* **245**, 523-537.

John, C. M., Bohaty, S. M., Zachos, J. C., Sluijs, A., Gibbs, S., Brinkhuis, H., and Bralower, T. J., 2008. North American continental margin records of the Paleocene-Eocene thermal maximum: Implications for global carbon and hydrological cycling. *Paleoceanography* **23**, pp.20.

Kurtz, A. C., Kump, L. R., Arthur, M. A., Zachos, J. C., and Paytan, A., 2003. Early Cenozoic decoupling of the global carbon and sulfur cycles. *Paleoceanography* **18**, pp.14.

Mason, R. P. and Sheu, G. R., 2002. Role of the ocean in the global mercury cycle. *Global Biogeochemical Cycles* **16**, pp.16.

Miller, K. G., Sugarman, P. J., Browning, J. V., Olsson, R. K., Pekar, S. F., Reilly, T. J., Cramer, B. S., Aubry, M., Lawrence, R. P., Curran, J., Stewart, M., Metzger, J. M., Feigenson, M. D., Brenner, G. J., and Dalton, R. F., 1998. Bass River Site Report. *Proceedings of the Ocean Drilling Program, Initial Reports* **174AX**, 5-43.

Pagani, M., Caldeira, K., Archer, D., and Zachos, J. C., 2006a. An ancient carbon mystery. *Science* **314**, 1556-1557.

Pagani, M., Pedentchouk, N., Huber, M., Sluijs, A., Schouten, S., Brinkhuis, H., Sinninghe Damste, J. S., Dickens, G. R., and Expedition, S., 2006b. Arctic hydrology during global warming at the Palaeocene/Eocene thermal maximum. *Nature* **442**, 671-675.

Panchuk, K., Ridgwell, A., and Kump, L. R., 2008. Sedimentary response to Paleocene-Eocene Thermal Maximum carbon release: A model-data comparison. *Geology* **36**, 315-318.

Pearson, P. N. and Palmer, M. R., 2000. Atmospheric carbon dioxide concentrations over the past 60 million years. *Nature* **406**, 695-699.

Rohl, U., Westerhold, T., Bralower, T. J., and Zachos, J. C., 2007. On the duration of the Paleocene-Eocene thermal maximum (PETM). *Geochemistry Geophysics Geosystems* **8**, pp.13.

Schmitz, B. and Pujalte, V., 2007. Abrupt increase in seasonal extreme precipitation at the Paleocene-Eocene boundary. *Geology* **35**, 215-218.

Schouten, S., Woltering, M., Rijpstra, W. I. C., Sluijs, A., Brinkhuis, H., and Damste, J. S. S., 2007. The Paleocene-Eocene carbon isotope excursion in higher plant organic matter: Differential fractionation of angiosperms and conifers in the Arctic. *Earth and Planetary Science Letters* **258**, 581-592.

Secord, R., Gingerich, P. D., Lohmann, K. C., and MacLeod, K. G., 2010. Continental warming preceding the Palaeocene-Eocene thermal maximum. *Nature* **467**, 955-958.

Senn, D. B., Chesney, E. J., Blum, J. D., Bank, M. S., Maage, A., and Shine, J. P., 2010. Stable Isotope (N, C, Hg) Study of Methylmercury Sources and Trophic Transfer in the Northern Gulf of Mexico. *Environmental Science & Technology* **44**, 1630-1637.

Sluijs, A., Brinkhuis, H., Schouten, S., Bohaty, S. M., John, C. M., Zachos, J. C., Reichart, G. J., Damste, J. S. S., Crouch, E. M., and Dickens, G. R., 2007. Environmental precursors to rapid light carbon injection at the Palaeocene/Eocene boundary. *Nature* **450**, 1218-U5.

Sonke, J. E., Pokrovsky, O., and Shevchenko, V., 2011. Mercury stable isotopic compositions of lichens and mosses from the Russian (sub-)Arctic*10th*

International Conference on Mercury as a Global Pollutant, Halifax, Nova Scotia, Canada.

Thomas, D. J., Zachos, J. C., Bralower, T. J., Thomas, E., and Bohaty, S., 2002. Warming the fuel for the fire: Evidence for the thermal dissociation of methane hydrate during the Paleocene-Eocene thermal maximum. *Geology* **30**, 1067-1070.

Thomas, E., 1998. Biogeography of the Late Paleocene benthic foraminiferal extinction. *Late Paleocene-Early Eocene Climatic and Biotic Events in the Marine and Terrestrial Records*, 214-243.

Zachos, J. C., Kroon, D., and Blum, P., 2004. Early Cenozoic Extreme Climates: The Walvis Ridge Transect Sites 1262-1267. *Proceedings of the Ocean Drilling Program, Initial Reports* **208**.

Zachos, J. C., McCarren, H., Murphy, B., Rohl, U., and Westerhold, T., 2010. Tempo and scale of late Paleocene and early Eocene carbon isotope cycles: Implications for the origin of hyperthermals. *Earth and Planetary Science Letters* **299**, 242-249.

Zachos, J. C., Rohl, U., Schellenberg, S. A., Sluijs, A., Hodell, D. A., Kelly, D. C., Thomas, E., Nicolo, M., Raffi, I., Lourens, L. J., McCarren, H., and Kroon, D., 2005. Rapid acidification of the ocean during the Paleocene-Eocene thermal maximum. *Science* **308**, 1611-1615.

Zachos, J. C., Schouten, S., Bohaty, S., Quattlebaum, T., Sluijs, A., Brinkhuis, H., Gibbs, S. J., and Bralower, T. J., 2006. Extreme warming of mid-latitude coastal ocean during the Paleocene-Eocene Thermal Maximum: Inferences from TEX86 and isotope data. *Geology* **34**, 737-740.

Zambardi, T., Sonke, J. E., Toutain, J. P., Sortino, F., and Shinohara, H., 2009. Mercury emissions and stable isotopic compositions at Vulcano Island (Italy). *Earth and Planetary Science Letters* **277**, 236-243.

Zeebe, R. E., Zachos, J. C., and Dickens, G. R., 2009. Carbon dioxide forcing alone insufficient to explain Palaeocene-Eocene Thermal Maximum warming. *Nature Geoscience* **2**, 576-580.

Figure 6.1:

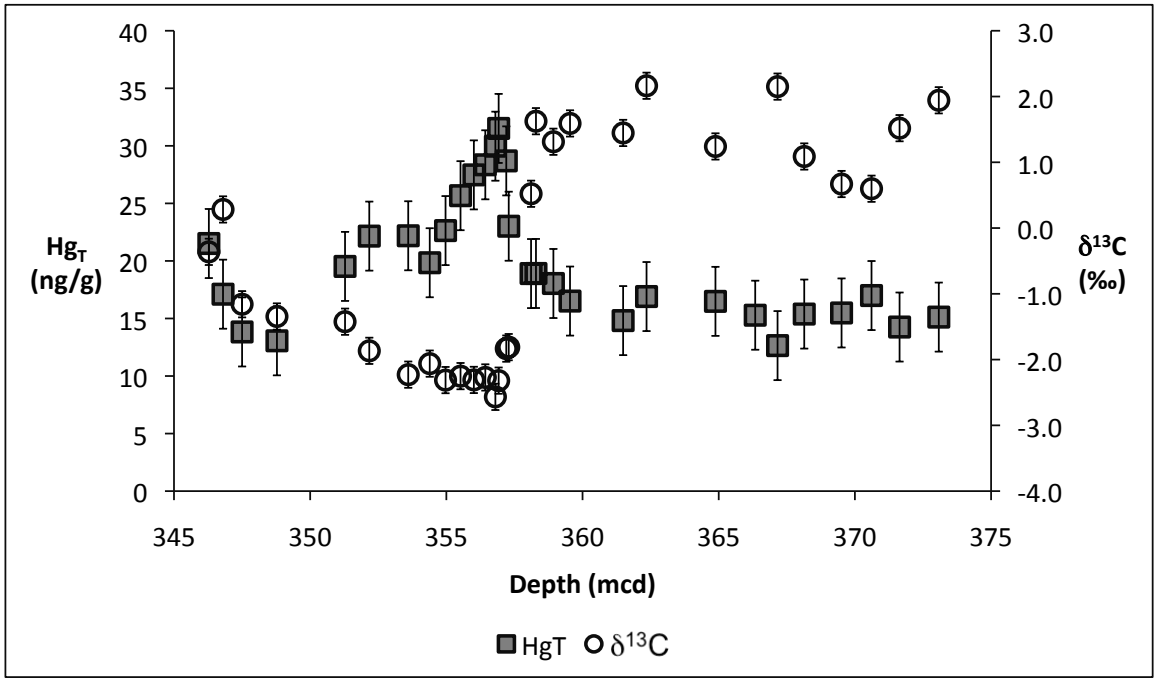

Figure 6.1: Sediment depth profile of Hg concentration (ng/g) and $\delta^{13}C$ (‰) (JOHN et al., 2008) in Bass River core (ODP site 174AX). Reported Hg concentrations are the 3-point running average of measured values and integrate between 30 and 100 cm, with more detailed intervals through the PETM. The peak in Hg concentration is coincident with the carbon isotope excursion (CIE).

Figure 6.2:

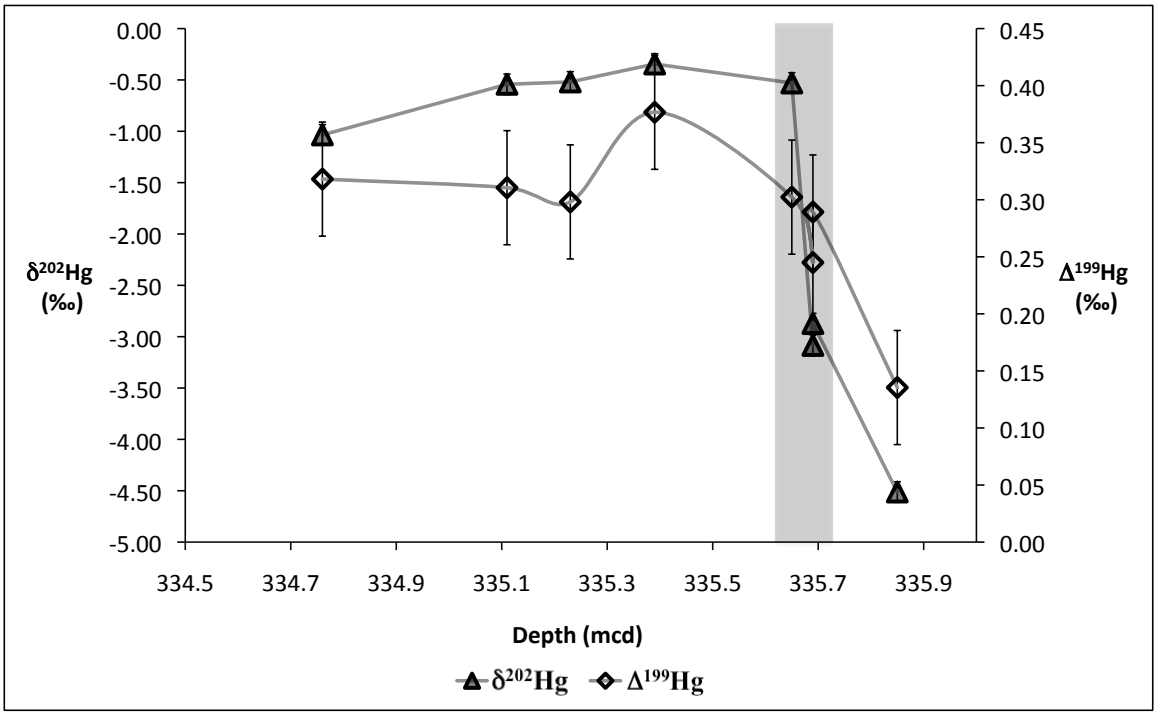

Figure 6.2: Hg isotopic compositions of sediments in Walvis Ridge (IODP site 1263) through the PETM. Filled triangles represent δ^{202}Hg and open diamonds represent Δ^{199}Hg values. The shaded rectangle represents the clay layer at the P-E boundary.

Table 6.1: Hg concentrations and C isotopes in Bass River (ODP site 174AX) and Walvis Ridge (ODP sites 1262 and 1263)

ODP site 174AX			ODP site 1262			ODP site 1263		
Depth (mcd)	**$\delta^{13}C$ (‰)***	**Hg_T (ng/g)‡**	**Depth (mcd)**	**$\delta^{13}C$ (‰)#**	**Hg_T (ng/g)**	**Depth (mcd)**	**$\delta^{13}C$ (‰)#**	**Hg_T (ng/g)**
345.16	-0.32		138.14	-	1.06	333.15	-	3.29
346.28	-0.36	21.51	139.19	-	BDL	333.76	-	2.06
346.80	0.28	17.11	139.41	-	BQL	334.56	1.13	2.10
347.50	-1.16	13.83	139.72	-	0.97	334.76	0.22	7.99
348.78	-1.34	13.06	139.84	0.23	1.62	335.11	-0.77	8.27
351.28	-1.42	19.52	139.92	0.26	1.56	335.23	-0.87	4.81
352.17	-1.87	22.16	140.00	IC	1.72	335.39	-0.45	7.52
353.60	-2.23	22.19	140.04	IC	2.05	335.65	0.68	13.6
354.39	-2.06	19.84	140.12	IC	1.40	335.69	0.20	16.2
354.97	-2.31	22.64	140.16	2.21	BQL	335.85	2.10	6.68
355.52	-2.25	25.67	141.12	-	1.02			
356.01	-2.31	27.48						
356.43	-2.27	28.35						
356.80	-2.57	29.97						
356.92	-2.32	31.51						
357.20	-1.83	28.69						
357.29	-1.81	23.02						
358.11	0.52	18.90						
358.29	1.62	18.91						
358.93	1.31	18.04						
359.54	1.59	16.51						
361.49	1.45	14.82						
362.35	2.16	16.91						
364.88	1.24	16.49						
366.34	-	15.28						
367.16	2.15	12.64						
368.14	1.09	15.38						
369.51	0.67	15.48						
370.61	0.60	16.99						
371.64	1.52	14.26						
373.08	1.94	15.12						
374.39	1.86	21.51						
345.16	-0.32	17.11						
346.28	-0.36	13.83						
346.80	0.28	13.06						
347.50	-1.16	19.52						
348.78	-1.34	22.16						
351.28	-1.42	22.19						
352.17	-1.87							

* values published in JOHN et al. (2008)

‡ 3-pt running averages of measured Hg_T; BQL = below quantification limit (~1 ng/g)

values published in ZACHOS et al. (2005)

Table 6.2: Hg isotope composition and concentration in Walvis Ridge site 1263

Depth (mcd)	Age since PEB (kyr)*	Hg_T (ng/g)	$\delta^{202}Hg$ (‰)	$\Delta^{199}Hg$ (‰)	$\Delta^{199}Hg$ (‰)
334.76	153	7.99	-1.04	0.28	0.32
335.11	71	8.27	-0.54	0.24	0.31
335.23	42	4.81	-0.52	0.18	0.30
335.39	22	7.52	-0.34	0.31	0.38
335.65	5	13.56	-0.53	0.30	0.30
335.69	0	16.20	-3.09	0.12	0.24
335.69	*0*	*16.20*	*-2.87*	*0.15*	*0.29*
335.85	-15	6.68	-4.51	0.07	0.14

* ages approximated from those published in ROHL et al. (2007)
PEB = Paleocene-Eocene Boundary
Italicized row represents a replicate sample processing

Table S6.1. Hg concentrations in Bass River (ODP site 174AX)

Depth (mcd)	**$\delta^{13}C$ (‰)***	**Hg_T (ng/g)**	**Hg_T (3-pt avg) (ng/g)**
345.16	-0.32	23.0	
346.28	-0.36	21.8	21.5
346.80	0.28	19.8	17.1
347.50	-1.16	9.8	13.8
348.78	-1.34	11.9	13.1
351.28	-1.42	17.5	19.5
352.17	-1.87	29.2	22.2
353.60	-2.23	19.8	22.2
354.39	-2.06	17.6	19.8
354.97	-2.31	22.2	22.6
355.52	-2.25	28.2	25.7
356.01	-2.31	26.7	27.5
356.43	-2.27	27.6	28.4
356.80	-2.57	30.8	30.0
356.92	-2.32	31.5	31.5
357.20	-1.83	32.2	28.7
357.29	-1.81	22.4	23.0
358.11	0.52	14.5	18.9
358.29	1.62	19.9	18.9
358.93	1.31	22.4	18.0
359.54	1.59	11.9	16.5
361.49	1.45	15.3	14.8
362.35	2.16	17.3	16.9
364.88	1.24	18.1	16.5
366.34	-	14.0	15.3
367.16	2.15	13.7	12.6
368.14	1.09	10.2	15.4
369.51	0.67	22.2	15.5
370.61	0.60	14.0	17.0
371.64	1.52	14.8	14.3
373.08	1.94	14.0	15.1
374.39	1.86	16.6	

* values from (JOHN et al., 2008)

Figure S6.1:

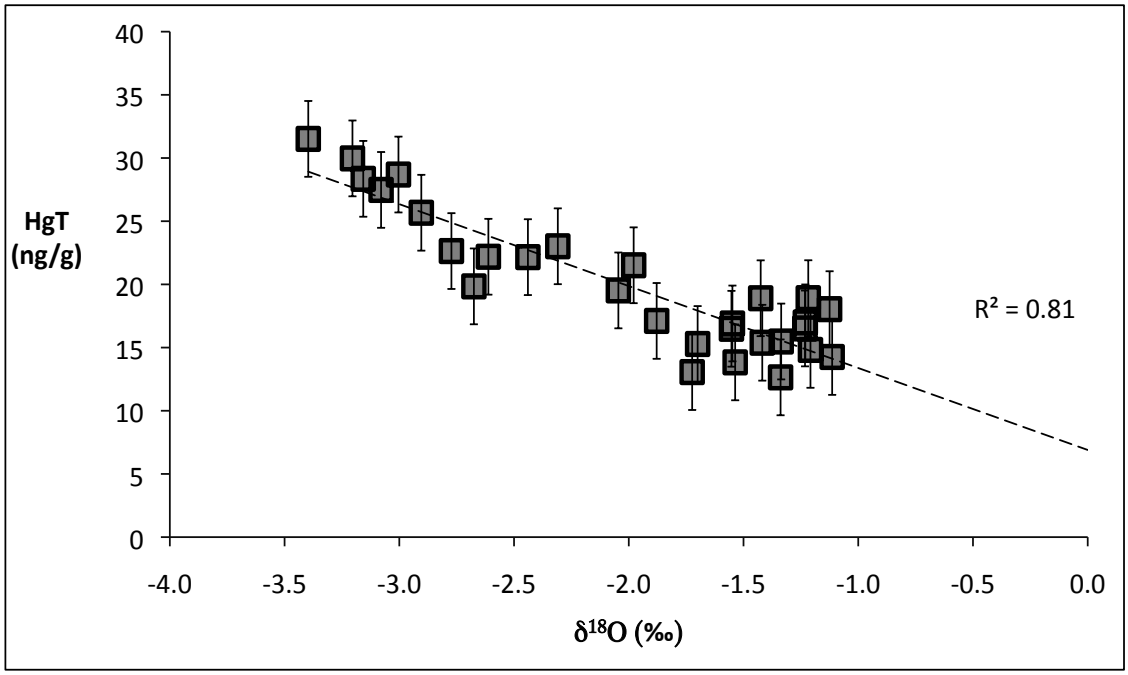

Figure S6.1: Hg concentrations and published $\delta^{18}O$ values (JOHN et al., 2008). Data presented in 3-point running averages of measured values.

Chapter 7

Conclusions

The research described in this dissertation explores the behavior of Hg in the marine environment. Utilizing the novel technique of Hg stable isotope analysis, this research elucidates biogeochemical influences on marine Hg cycling and anthropogenic impacts on that cycle. Correlations between Hg and other trace metal concentrations through a sapropel sequence suggests that Hg was transported to depth in association with organic matter, and demonstrates that accelerated primary productivity rates could promote amplified marine Hg deposition (Chapter 2, Gehrke et al., 2009). Since changes in water column chemistry were shown to substantially influence marine Hg deposition, it is inferred that Hg concentration enrichments were insufficient to identify the influence of additional Hg sources. Through Hg isotope analyses, it is possible to discern the effects of ambient water column chemistry and recent Hg inputs. A significant change in Hg isotopic composition between pre-Industrial and modern sediments illustrates that recent anthropogenic Hg inputs did present a substantial additional source of Hg to the Baltic Sea, which was accumulated in Baltic Sea sediments (Chapter 3, Gehrke et al., 2011b).

Focusing on a region known to be contaminated with anthropogenic Hg, research in this dissertation demonstrates that the legacy of historic mining activities continues to contribute Hg to SF Bay surface sediments (Chapter 4, Gehrke et al., 2011a), even though decades have passed since the majority of those mines were in operation. A spatial gradient in sediment Hg isotopic composition through SF Bay demonstrates that Hg emanating from historic placer Au mining operations was a chief source of Hg entering SF Bay through northern tributaries and Hg leaching from waste products associated with old Hg mines was a principal source of Hg entering through southern tributaries to SF Bay. The Hg in surface sediments is shown to be the dominant source of Hg to the aquatic food web in SF Bay (Chapter 5, Gehrke et al., 2011c), as the Hg isotopic composition of biosentinal fish paralleled that of surface sediments. A consistent offset between the Hg isotope ratios in sediments and co-located fish also shows that the incorporation of sediment-derived Hg into the foodweb was mediated by additional biotic and/or abiotic processes (Chapter 5, Gehrke et al., 2011c).

After utilizing Hg isotope compositions to discern sources of Hg and processes mediating Hg cycling in the modern marine environment, research in this dissertation applies Hg isotope analyses to investigate Hg cycling under appreciably different global conditions through the Paleocene-Eocene boundary (Chapter 6). The lowest δ^{202}Hg values ever observed in marine sediments preceded the Paleocene-Eocene Thermal Maximum (PETM). Through the PETM, the largest shift in Hg isotope composition observed in a single environmental medium occurred. These data indicate a considerable perturbation to the global Hg cycle during this

era. To better resolve the nature of that perturbation, this dissertation recommends further work characterizing the Hg isotopic compositions of sediments during the Paleocene epoch.

Through the successful application of Hg isotope analyses to marine and tidal sediments in paleo- and modern environments, and modern fish, this dissertation clarifies several outstanding questions and demonstrates the utility of Hg isotope analyses. Concurrently, several new questions have been raised concerning macroscale Hg dynamics as well as Hg isotope systematics. With specific regard to topics explored in this dissertation, two primary research questions remain unanswered.

One pressing question uncovered in this dissertation is what caused the perturbation in the Hg isotopic composition of sediments during the PETM? To gain more insight into Hg cycling in the late Paleocene and early Eocene, two research projects would be essential. First, it would be necessary to determine the Hg isotopic compositions of deep sea sediments (specifically at IODP site 1263) through the early and mid-Paleocene in order to understand the nature and timing of the Hg perturbation. It would also be vital to determine the Hg isotopic compositions of continental shelf sediments (specifically IODP site 174AX) through the PETM in order to compare them with deep sea sediments. Additionally, it would be useful to characterize the Hg concentrations and Hg isotope compositions of a terrestrial core through the PETM (such as BH9-05) to glean insight to terrestrial-marine dynamics and thus global Hg cycling.

A second, and perhaps more fruitful, research direction stemming from questions raised in this dissertation may be the relationship between sediment Hg and fish Hg. What are the causes of the observed Hg isotope fractionation between sediments and fish, and what processes primarily mediate the incorporation of Hg from sediments into the food web? As demonstrated in Chapter 5 (Gehrke et al., 2011c), there is a consistent offset between the isotopic composition of Hg in sediments and co-located small fish in SF Bay, but that offset became more complex in the northeastern reaches of SF Bay. More extensively exploring the sediment-fish Hg isotopic relationship in Suisun Bay and northern wetlands, and exploration of co-located sediments and fish in other estuaries and lakes would be useful to understand the persistence of this relationship. Moreover, the mechanistic causes of the sediment-fish Hg isotope offset would be of fundamental importance to discern, especially to promote ecological protection. Laboratory experiments investigating Hg isotopic effects of microbial methylation, of MeHg-laden sediment suspension, or of MeHg uptake by plankton could be useful.

With an underlying goal of protecting human and environmental health from Hg contamination, Hg isotopic studies have been and will continue to be highly informative. This dissertation provides a framework for exploration of Hg sources to marine sediments through time and space, and provides a basis for further investigation into the relationship between Hg in sediments and the Hg incorporated into the aquatic food web.

References:

Gehrke, G. E., Blum, J. D., and Marvin-DiPasquale, M., 2011a. Sources of mercury to San Francisco Bay surface sediment as revealed by mercury stable isotopes. *Geochimica Et Cosmochimica Acta* **75**, 691-705.

Gehrke, G. E., Blum, J. D., and Meyers, P. A., 2009. The geochemical behavior and isotopic composition of Hg in a mid-Pleistocene western Mediterranean sapropel. *Geochimica Et Cosmochimica Acta* **73**, 1651-1665.

Gehrke, G. E., Blum, J. D., and Slomp, C. P., 2011b. Mercury Concentration and Isotopic Composition in Modern and Pre-Industrial Baltic Sea Sediments. *Chemical Geology* ***submitted***.

Gehrke, G. E., Blum, J. D., Slotton, D. G., and Greenfield, B. K., 2011c. Mercury Isotopes Link Mercury in San Francisco Bay Forage Fish to Surface Sediments. *Environmental Science & Technology* **45**, 1264-1270.